The impacts of irrigation to the hydrological processes in the unsaturated zone beneath almond grove orchards

By

Sangita Dandekhya

Thesis
Submitted to Flinders University
for the degree of

Master of Science Groundwater Hydrology

Flinders University
2 December 2019

CONTENTS

LIST OF FIGURES

LIST OF TABLES

SUMMARY

This study is a part of an ongoing research project that is investigating the hydrological processes within the unsaturated zone of irrigated almond orchards. One of the key processes to understand is root zone drainage (RZD) which subsequently affects the total recharge to the regional groundwater aquifer system and potential salinisation of the Murray River. The field research was conducted at an irrigated almond orchard, located near Boundary Bend, Victoria, Australia. Two near-surface geophysical methods, electrical resistivity tomography (ERT) and terrain conductivity frequency domain electromagnetic induction (FDEM) surveys were used to understand the subsurface geology of the study area. Water levels in both the perched aquifer and regional aquifer systems were monitored to examine the hydraulic behaviour and perching of the shallow water table. The monitoring of the shallow drainage systems enabled estimation of the volume of water that was being captured from the perched aquifer. The comparison of the 2D resistivity profiles from the ERT surveys with stratigraphic and lithological logs confirmed the occurrence, depth and thickness of alluvial material (13 m thick) and Blanchetown Clay Formation (10 m thick) below the land surface. The terrain conductivity surveys also confirmed the continuity of the Alluvial Formation and Blanchetown Clay throughout the study area. This clay layer acts as a semi-confining layer and thereby intercepts the downward transport of RZD, resulting in a perched aquifer condition. Water level monitoring showed a decreasing hydraulic gradient of both the regional aquifer system and the shallow perched aquifer towards the Murray River. The watertable in the perched aquifer is approximately 2m above the regional water table. The monitoring of inflow in nine shallow drainage pits over four months from late April to early September 2019 was used to calculate the total volume of water (885 m^3) that was perched over the clayey formation in this time period. Averaging this volume over the year, the rate of RZD is calculated to be around 0.80 mm/yr. However, the rate of RZD is far lower than the irrigation rate (1000 mm/yr), which suggests high efficiency use of irrigation water by almond trees or some RZD directly recharging the aquifer that is bypassing the shallow drainage pits. In summary, the RZD is contributing to the formation of shallow perched aquifer conditions over the alluvial clay layer in the study area, which limits the total recharge to the regional water table. Nevertheless, further study is deemed necessary to quantify the total recharge under irrigated agriculture and its implications to salinisation of the nearby Murray River.

Keywords: irrigation, root zone drainage, clay layer, perched aquifer, groundwater recharge, geophysics, resistivity, frequency domain electromagnetic induction, salinity

DEDICATION

I would like to dedicate this thesis to people who believe in me…

DECLARATION

I certify that this thesis does not incorporate without acknowledgment any material previously submitted for a degree or diploma in any university; and that to the best of my knowledge and belief it does not contain any material previously published or written by another person except where due reference is made in the text.

Signed: **Sangita Dandekhya**

Date: 02/12/2019

ACKNOWLEDGEMENTS

Firstly, I would like to acknowledge DFAT for awarding me this Australia Awards Scholarship to pursue this Master of Science in Groundwater Hydrology at Flinders University. I greatly acknowledge NCGRT & Flinders University for granting me the opportunity to conduct my major research on the ongoing project in the study area.

Most of all, I would like to express my earnest gratitude to my principal supervisor, Professor Peter Cook and co-supervisors Associate Professor, Huade Guan for their untiring support, consistent encouragement and inspirational guidance. I am grateful for all the time they have devoted to our consultations, their patience and knowledge they shared with me throughout the research without which this research wouldn't be possible. I truly feel fortunate enough to have them as my supervisors and working with them was truly an honour and experience of a lifetime for me.

I am thankful to my course coordinator, Dr. Ilka Wallis not only for her warm and approachable gestures towards me but also for her efforts to connect me with Professor Peter Cook and with this research project.

I am thankful to Mr. Nicholas White for all your help and support during my field research works and for driving me always to and from Adelaide to Victoria during field visits. Special sincere thanks to Dr. Eddie Banks for all his efforts and guidance to execute geophysical field surveys (ERT & CMD-Explorer), and for teaching me so many geophysical data analysis software.

Finally, I would like to express my gratitude to my parents, family members, friends, and most importantly to my husband, Anup Shrestha, for always believing in me more than I do myself, and for his constant encouragement, support and boosting me up when I feel low.

Sangita Dandekhya

1. INTRODUCTION

1.1 Background

Land use change and water management practices across the Murray Basin have resulted in widespread salinisation of land and water resources (Brown & Stephenson 1991), which is one of the major environmental problems in the Murray Basin (Evans & Kellett 1989). The salinisation not only transformed the fertile agricultural land to marshy saline wasteland but also led to waterlogging of the soil zone, thereby inundating the root zone and killing the vegetation. In addition, salinisation increased the groundwater salinity as well as the salinity concentrations in the Murray River in South Australia (Brown & Stephenson 1991).

In the early 20th century, native vegetation was extensively cleared for agricultural development and the cultivation of shallow-rooted food crops. This change in land management practices consequently induced a high rate of infiltration/ root zone drainage (RZD) within the soil (unsaturated zone), which then led to increased recharge, to the regional aquifer systems in an arid and semi-arid region of the Murray Basin (Brown & Stephenson 1991; Evans & Kellett 1989). RZD, also known as 'deep drainage', refers to the volume of water, which flows down past the root zone of the crop (Newman et al. 2009). Similarly, recharge is referred to the hydrological process in which water moves from the unsaturated root zone towards the regional saturated geological material (groundwater aquifer system) (Newman et al. 2009). A study conducted by Jolly et al. (1989) on hydrological changes in the unsaturated zone under dryland agriculture reported an increase in the recharge rate from 0.08 mm/yr before clearing, to 45mm/yr after clearing the native vegetation. Likewise, the study by (Allison et al. 1990) showed that the groundwater recharge rate has increased by two orders of magnitude after removal of native vegetation in the semi-arid region of South Australia. This process has led to an increasing rise in the groundwater table elevations in the basin.

The development of irrigated agriculture along the Murray River has also been linked to further increases in RZD (Newman et al. 2009). The RZD under irrigated agriculture is estimated to be around 10% of the irrigated water (Newman et al. 2009). The irrigation and drainage management plan for the irrigated almond grove orchards in the Murray Basin has estimated an irrigation requirement of 3978 million litres annually for total irrigation area of 286 hectares (Sluggett et al. 2007). RZD rate is assumed to be approximately 140 mm/yr under the irrigated almond grove orchards which is equivalent to one-tenth the volume of irrigation water. Similarly, Heaney, Beare

and Bell (2001) have estimated the RZD rate of around 200 mm/yr under irrigated horticulture, dominantly consisting of citrus tree plantations, along the Murray River in the Riverland of South Australia.

Therefore, it is clear that RZD under irrigated agriculture is much higher in comparison to RZD in dryland agriculture. This increase in RZD is likely to increase the net recharge to the groundwater system, which results in a rise in the watertable as well as a greater likelihood of shallow perched water table conditions. It is apparent that both the increased rate of recharge and rate of rise in the watertable is likely to be much higher under irrigated agriculture than under dryland agriculture due to a higher RZD rate.

The Murray River is the only natural outlet of salt out of the Murray Basin (Evans & Kellett 1989). Therefore, the rise in the local and regional watertable due to irrigated farming is expected to increase the saline groundwater discharge to the Murray River, which not only increases the flow rate of the river but also increases the salinity concentrations.

1.2 Problem Statement

An increase in recharge to the aquifer system was anticipated in the study area following the increase in RZD as recharge is usually assumed to be equal to RZD (Newman et al. 2009). Previous studies reported the existence of a discontinuous, heavy, thick clay layer in the near surface underneath the Murray Basin, which acts as an aquitard and thus, likely to impede the flow of RZD thereby leading to perching of RZD. The rate of irrigated RZD is assumed to be 10-15%, although the actual rate of RZD under irrigated agriculture is yet to be quantified (Newman et al. 2009). Consequently, the interception of RZD over the Blanchetown Clay Formation is likely to reduce the total recharge to the saturated Parilla Sands aquifer, which is expected to reduce the groundwater discharge and salt load to the Murray River (Allison et al. 1990). However, the formation of shallow perched water tables can cause waterlogging and salinisation of fertile agricultural land, which reduces agricultural productivity.

This research examines the hydrological process in the unsaturated zone under irrigated almonds and the impact on RZD. We examine firstly whether such clay layer exists underneath the study area. Secondly, we estimate the rate and volume of RZD intercepted by such clay unit if it exists.

1.3 Research Objectives

The main objective of this research was to understand the impact of irrigation on groundwater systems, focusing on the hydrological processes in the unsaturated zone, which influence the flow of root zone drainage under irrigated almond grove orchards adjacent to the Murray River.

The specific aims of the study were to:

i. examine whether the perching of the shallow unconfined aquifer occurs underneath irrigated almonds by using near surface geophysical techniques to map the stratigraphy/ geology, and to examine the presence, thickness, and continuity of clay units, and change in water content in the unsaturated zone.
ii. evaluate the groundwater levels in the shallow and regional groundwater aquifer systems and how the aquifers respond to root zone drainage and increased recharge as a result of irrigation.
iii. estimate the root zone drainage rate and the volume of drainage water that is being captured by the shallow drainage system in the study area.

1.4 Organisation and structure of the thesis

The thesis report has been structured into five chapters as follows: Chapter 1: Provides an overview of the research, including the background to the research problem, and the research objectives. Chapter 2: is a literature review of the research problem, which includes a review of previous studies in the research area to understand the overall positioning of the research problem in the present context. Chapter 3: describes the study area. Chapter 4: describes the different research methods used in this research study. Chapter 5: presents the results and discussion and includes the analysis and interpretation of the data collected. Chapter 6: summarises the findings from the study and the research outcomes.

2 LITERATURE REVIEW

2.1 Salinisation and its types

Salinisation is the process of the accumulation of salts in land and water sources to concentrations such that it has an impact on the natural environment and ecosystem. There are two types of salinisation, namely, natural and anthropogenic. Natural salinisation, also known as primary salinisation, is the hydrological processes involved in the formation of salt lakes. Naturally, primary salinisation occurs in a closed basin with continuous accumulation of the salts contained in rainwater and through the leakage of salts from the natural ecosystem (Williams 2001). In contrast, anthropogenic salinisation, also known as secondary salinisation, is the hydrological changes that have occurred as the result of human activities, which cause an increase in the salt content of the natural water bodies such as lakes, rivers, and groundwater (Williams 2001).

In particular, anthropogenic salinisation is increasing, which has significant undesirable and usually permanent effects on the natural environment. However, salinisation is not only the problem of the present-day as it was reported in different countries in the past. For instance, back 4,500 years ago, the salinisation problem was believed to affect Mesopotamian agriculture (Jacobsen & Adams 1958). The clearing of land for agriculture and irrigated agriculture has caused salinisation issues predominantly, not only in semi-arid regions of the world (Han et al. 2017) but also in Australia (Peck, Thomas & Williamson 1983).

Moreover, one-third of the irrigated agricultural land in the world has been affected by salinisation by the 1960s (Reeve & Fireman 1967), which has increased to 34-47% by 1980s (FAO 1990). It is also a significant issue in many other dryland countries with a semi-arid climate where it has severely impacted land and water resources (Ghassemi 1995; Peck, Thomas & Williamson 1983).

In Australia, salinisation is one of the major environmental concerns (Jenkin 1981). Dryland agriculture is dominant in the Murray Basin. The agriculture which relies on the natural rain for irrigation (rainfed agriculture) is known as dryland agriculture. Earlier studies in the 1980s have forecasted six times increase in the area of the land affected by salinisation in Australia in the next few decades. In addition, Australia and some other countries also experience dryland salinity problems which are the salinisation of the non-irrigated agricultural land (Peck, Thomas & Williamson 1983) especially in the semi-arid and arid regions where the mean yearly rainfall range from 25 to 500 mm. Likewise, the Mallee region of the Murray Basin has widespread irrigated agriculture and likely to cause salinity risk from the irrigated farming practiced in there. Therefore,

this region is predicted to increase additional 75% salt load to the Murray River by 2050 (Newman et al. 2009).

2.2 Worldwide costs of salinity

Salinisation has multidimensional impacts on the social, economic and environmental sectors. Dryland salinisation deteriorates the fertility of the agricultural land and thereby reducing the area of productive agricultural land (Hillman 1981). Similarly, land clearing for agriculture and irrigated agriculture has increased the recharge and leakage of the stored salts from the soil into the water resources in the semi-arid regions globally, which has resulted in current land and water salinisation and waterlogging problems (Han et al. 2017).

In Australia, salinisation has caused the loss of agricultural production worth more than around AUD $73 million yearly (1 USD= 1 AUD) and, additional AUD $132 million per year from the loss of water resources and infrastructure cost (Williams 2001). Similarly, Barnett (1990) studied the financial loss of both the river and land salinisation in the western Murray Basin in South Australia and Victoria. The study estimated the financial cost of salinisation at a community level to be nearly $1.4 million annually, which is predicted to increase $4.7 million annually over the next 50 years (Barnett 1990).

2.3 Murray Basin Agricultural and Hydrological Importance

According to Crabb and Milligan (1997), agricultural land covers 80% of the catchment area of the Murray-Darling Basin which generates nearly $10 billion dollars annually and is 41% of Australia's gross agricultural production. Only 2% of the agricultural land is irrigated, however, the irrigated agriculture generates about 40% of the Basin's total production (Newman & Goss 2000). The Murray Basin has developed as economically the most important agricultural regions in Australia over the past 100 years (Brown & Stephenson 1991) however, groundwater-related salinisation of its landscapes and river systems threatens the economy and natural environments (Brown & Stephenson 1991).

The Murray River is the longest river in Australia (Allison et al. 1990), is 2590 km long which drains the inland side of the south-eastern Australian highlands (Stephenson 1986). In particular, the Murray River along with its tributaries drains around one-seventh of the land area of Australia (Allison et al. 1990) and is estimated that there are 4600 million megalitres (ML) of groundwater storage in the Murray Basin aquifers but only two-thirds of which is useful to humans (Evans &

Kellett 1989). The irrigation water use in this catchment accounts for 80% of the national total (Peck, Thomas & Williamson 1983).

2.4 Murray Basin Climate

The Murray Basin is characterised by a semi-arid climate, however, the climate varies extensively even within the catchment boundary (Brown & Stephenson 1991; Stephenson 1986). The average annual rainfall is low and ranges from 250-300 mm/yr (Allison & Hughes 1983). According to the Bureau of Meteorology, a median annual rainfall of 500 mm is reported over the Murray Basin (Brown & Stephenson 1991). Rainfall is dominant during summer in the north-western region of basin, while most of the rainfall occurs during winter in the southern area of basin (Brown & Stephenson 1991; Stephenson 1986). The distribution of median annual rainfall and average annual evaporation over the Murray-Darling Basin is shown in **Figure 2-1.**

Annual evaporation of 2400 mm was reported in the Murray Basin in 1975 by the Bureau of Meteorology (Brown & Stephenson 1991). Thus, evaporation is higher across the whole basin such that average evaporation is many times higher than the average rainfall (Brown & Stephenson 1991).

Image removed due to copyright restriction

Figure 2-1: (a) Distribution of median annual rainfall (mm) and, (b) average annual evaporation (mm). Data from the Bureau of Meteorology, Australia; adapted from Stephenson (1986).

2.5 Overview of Murray Basin Geology

The Murray Basin is a closed low-lying saucer-shaped intracratonic groundwater basin containing thin flat-lying Cainozoic sediments **(Figure 2-2).** It covers an area of 300000 km^2 of western New South Wales, northwest Victoria, and southeast South Australia (Brown & Stephenson 1991) with maximum sediments thickness of 600 m and a majority of the area has a thickness of 300 m (Allison et al. 1990; Stephenson 1986). In addition, it extends nearly 850 km from east to west and 750 km from north to south (Brown & Stephenson 1991). This groundwater basin comprises of numerous regional groundwater systems within 200-600 m of Cainozoic unconsolidated sediments and sedimentary rocks underneath (Brown & Stephenson 1991; Evans & Kellett 1989).

Image removed due to copyright restriction

Figure 2-2: Map of the Murray Basin (Saintilan & Overton 2010)

The comprehensive geological study of the Murray Basin was conducted by Brown and Stephenson (1991) and hydrogeological study by (Evans & Kellett 1989), which is referred here to understand the hydrogeology of the basin. According to Evans and Kellett (1989), the regional aquifers of the Murray Basin can be put into three discrete provinces namely

i. the Riverine Province (eastern and southern),
ii. the Mallee-Limestone Province (southwestern) and
iii. the Scotia Province (north-western) as shown in **Figure 2-3**.

Similarly, there are four major regional aquifers in the Murray Basin namely,

i. the Renmark Group aquifer system,
ii. Murray Group aquifers system,
iii. Pliocene Sands aquifer and
iv. Shepparton Formation aquifer **(Figure 2-4**) (Evans & Kellett 1989).

The details of these aquifers are discussed in detail in the Hydrogeology of the Murray Basin (Evans & Kellett 1989). The study area is situated near the boundary between River and Mallee Provinces. The following section illustrates the geological characteristic of the Murray Basin in reference to the three provinces of the basin **(Figure 2-3).**

Riverine Province:

The Riverine province lies beneath the Riverine plain and the eastern Mallee region in New South Wales and Victoria **(Figure 2-3).** This province includes the geological layers the uppermost layer of Shepparton Formation, followed by the Pliocene Sands layer that is underlaid by the next layer of the Renmark Group Formation **(Figure 2-4).** The average thickness of the formation under the Riverine plain is about 250 m. And the groundwater dominantly flows from east to west direction.

Mallee-Limestone Province:

The Mallee- Limestone province lies in Victoria and South Australia **(Figure 2-3).** The major geological formations in this province is the Murray Group limestone aquifer, Lower Renmark Group, Pliocene Sands, Loxton-Parilla Sands (**Figure 2-4).** The Murray Group limestone aquifer in this province is confined by Geera Clay in the east. The Murray Basin has a maximum thickness of 600m in this formation at the Paringa Embayment, however, the average thickness of this

formation is around 300-350 m. The regional groundwater flow direction in this province is towards north and west directions.

Scotia Province:

The Scotia Province is located in South Australia and New South Wales (Evans & Kellett 1989) **(Figure 2-3).** This province is characterised by the presence of several active groundwater discharge zones where the groundwater flows dominantly from the north towards the Murray River, which is the only discharge conduit for the groundwater flow and moving the salt out of the basin (Evans & Kellett 1989). This province has a substantial thickness of all three low-permeability units (mid-tertiary low-permeability layer, upper confining layer and lower confining layer). The Blanchetown Clay occurs as a confining bed and underlies the Loxton-Parilla Sands aquifer.

.

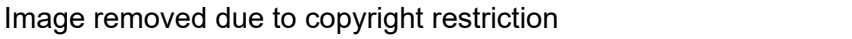

Figure 2-3 Depth to the basement (relative to sea level) showing the broad structural elements of the basin, and their relationship to the three main provinces (Evans & Kellett 1989)

Image removed due to copyright restriction

Figure 2-4 Simplified stratigraphic section plotted against geological time periods adapted from (Evans & Kellett 1989)

2.6 Lake Bungunnia

Lake Bungunnia, a Plio-Pleistocene mega lake, is considered to exist 1.7 Ma between 2.5 Ma and 0.7 Ma covering a large area in the western Murray Basin, Australia (Bowler 1980). The potential extent of Lake Bungunnia is shown in **Figure 2-5.**

According to (Firman 1965, 1973), the Blanchetown Clay and the overlying Bungunnia Limestone are the sedimentary units that were deposited in Lake Bungunnia. The Blanchetown Clay is a fluvio-lacustrine unit that is usually either greenish grey, red-brown or variegated sandy clay with many local variations in lithology (Stephenson 1986). The Blanchetown Clay's thickness varies from a few meters generally up to 20m (Stephenson 1986). This clay formation is widespread all over the Riverland region of South Australia and the Sunraysia region of New South Wales and Victoria (Newman et al. 2009).

The Blanchetown Clay plays a vital role in hydrogeology of the study area because this thick clay layer acts as an imperfect aquitard where it is likely to forms perched water table/ aquifer over it (Barrett et al. 2002). However, the distribution of the Blanchetown Clay is naturally intermittent all

over the western Murray Basin, representing topographic irregularities at the time of deposition, combined with the effects of later erosion (Stephenson 1986). It is because the Lake Bungunnia fragmented down into a number of disconnected lakes during the time of its final disappearance from the region (Bowler 1980). For example, the salt lakes in the Western Murray Basin are considered as the remnants of the Bungunnia Lake (Stephenson 1986). In contrast, the topmost Blanchetown Clay is usually gypsiferous in the areas without Bungunnia Limestone, which is resulted due to the drying up and disintegration of the Lake Bungunnia (Stephenson 1986). Subsequently, a layer of younger aeolian and fluvial sediments was overlaid on the top of the Blanchetown Clay and Bungunnia Limestone. This aeolian sediment layer has a thickness commonly of 5m and, greater than 20 m in some dunes (Stephenson 1986).

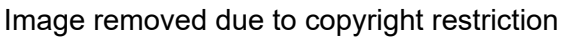

Figure 2-5 Murray Basin (geological) showing the extent of Lake Bungunnia as proposed by (Bowler 1980)

2.7 Overview of Murray Basin Hydrogeology

The hydrogeology of the Murray Basin plays a significant role in the recharge rate and salinity concentration spatial distribution within the basin. Notably, most of the salinisation problems are interrelated to the groundwater, therefore it is essential to understand the regional hydrogeology and groundwater flow systems of the basin for addressing the problem (Evans & Kellett 1989).

The Murray Basin functions as a closed groundwater system (Evans & Kellett 1989) due to its geology such that the water can outflow from basin either as evaporation or in the form of leakage from the basin towards the Murray River, which is the only natural drainage for both the water and salt particularly in the southwestern Murray Basin (Allison et al. 1990; Evans & Kellett 1989)**.** The following section illustrates the hydrogeological characteristics of the major aquifers and aquitards of the Murray Basin **(Figure 2-3, Figure 2-4 & Table 2-1).**

1. **Renmark Group aquifer system**

Renmark Group Aquifer is a basal confined aquifer that comprised of lower to mid-Tertiary Fluvial clay, silt, sand and minor gravel with a ubiquitous carbonaceous deposit (**Figure 2-4**).

Riverine province: The Renmark Group aquifers in the Riverine province is further divided into the Upper, Mid and Lower Renmark Group aquifers. The Geera Clay layer in the central-western Riverine Plain acts as geological interruption (aquitard layer) which has a prominent influence on water pressure distribution and the hydrochemistry of groundwater in the Renmark Group aquifers (Evans & Kellett 1989). In addition to acting as a barrier against through flow across the aquifers, the Geera Clay layer acts as a source of salts that diffuse downward into the lower Renmark Group aquifer (Evans & Kellett 1989).

The groundwater predominantly flows from east to west direction. Horizontal hydraulic conductivity in the Renmark Group aquifers ranges from 10-30 m/day in the eastern side to 1-5 m/day towards the western Riverine Plain.

Mallee-Limestone Province: Only the Lower Renmark Group aquifer is present in the Mallee-Limestone province. The groundwater flows upward from the Lower Renmark Group aquifer and is generally north-westerly and westerly through overlying confining mid-tertiary sediments into the Murray Group Limestone aquifer near the Murray River. The hydraulic conductivity of the aquifer is equal to that of the Lower Renmark Group aquifer in the Riverine province.

Aquitard: mid-Tertiary low-permeability barrier

The mid-Tertiary low-permeability geological formation comprised of Winnambool Formation, Geera Clay, and Ettrick Formation forms an effective aquitard to the Renmark Group (**Figure 2-4**). The Geera Clay indicates the largest amount of the marine transgression in the Late Oligocene-Miocene into the Murray Basin. This mid-Tertiary low-permeability geological formation spreads in an arc about 100 km wide through the centre of the basin which acts as an aquitard which impedes the through-flow of water between Renmark Group aquifers system (upper, mid and lower Renmark aquifer) **(Figure 2-4)** (Evans & Kellett 1989). Likewise, this low permeability clay (a composite of the Winnambool Formation & Geera Clay) function as a barrier to lateral throughflow in the Renmark Group aquifers and overlying Pliocene Sands (Evans & Kellett 1989). The upper part of the Geera Clay acts as a sink for salts, while the lower part of Geera Clay acts as a source of salt. The horizontal hydraulic conductivity of the Geera Clay is $4*10^{-4}$ m/day and vertical hydraulic conductivity $2*10^{-5}$ m/day.

2. Murray Group aquifer system

The Murray Group aquifers are the widely exploited regional aquifers in the Murray Basin. They are comprised of middle Tertiary marine limestone and calcarenite. The groundwater supplies are extensively extracted for irrigation and water supplies. This aquifer overlies the lower confining layer and is confined by the mid-Tertiary low-permeability barrier on the eastern side. Likewise, the upper half of the Murray Group aquifers in the eastern side is confined by the upper confining layer whereas the western side is overlaid by the Loxton-Parilla sands of the Pliocene Sands aquifer (**Figure 2-4**).

The Murray River is located at the northern hydrogeological boundary of the Murray Group aquifer in the Mallee-Limestone province (Evans & Kellett 1989).

Lower Confining layer: Aquitard

Mallee- Limestone Province: The lower confining layer separates the Renmark Group aquifer and the Murray Group Aquifer in the Mallee- Limestone Province. It comprises of Ettrick Formation clay and marl extending over a large area of the Mallee-Limestone Province. The thickness of this confining layer is nearly 20-30 m in the northeast and 10 m in the southwest (Barnett, 1983) as cited in **(Evans & Kellett 1989)**. The hydraulic properties of the lower confining layer are like that of Geera Clay of the mid-tertiary low-permeability barrier.

Upper Confining layer: Aquitard

The upper confining layer comprised of clay and silt of the Bookpurnong Beds which is underlaid by Winnambool Formation clay and marl along the eastern boundary (**Figure 2-4**). It confines the eastern half of the Murray Group Limestone aquifer in the Mallee-Limestone province. This confining layer has a thickness of around 30-40 m in the northeastern side of the province, which gets thinner to the west. The vertical hydraulic conductivity ranges from $5*10^{-4}$ to $1*10^{-4}$ m/day (Lawrence 1975). The groundwater chemistry of this layer showed the characteristics of the underlying Murray Group Limestone, which specifies the saturation of this layer is from below and not from the overlying Pliocene Sands aquifer.

3. Pliocene Sands aquifer

Riverine Province: Pliocene Sands aquifer lies completely under the Riverine province and is hydraulically continuous with the upper Renmark Group aquifer. Towards the western Riverine Plain, the Calivil Formation is overlain laterally by the Loxton-Parilla Sands. The thickness of both is equal to around 60m of fine to medium sand with minor clay and silt. The Calivil Formation of the Pliocene aquifer is mostly confined or semi-confined by low-permeability basal clays of the overlying Shepparton Formation. The Loxton-Parilla Sands of the Pliocene Sands aquifers form the major water table (unconfined) aquifer in the western part of the Riverine province. However, the Loxton-Parilla Sands of this aquifer is confined by the overlying Blanchetown Clay in some places. The Loxton-Parilla Sands overlie the Geera Clay/ Winnambool Formation (the mid-Tertiary low-permeability barrier) over most of the Riverine province, except a narrow strip where they directly located over the upper Renmark Group aquifer. Major recharge to the Loxton-Parilla Sands occurs by infiltration of local rainfall. The groundwater flows usually westward in the Riverine province in the Pliocene Sands aquifer.

Mallee-Limestone province: The Pliocene sands aquifer in the Mallee-Limestone province is usually unconfined and is comprised of the Loxton-Parilla Sands. The recharge in the Pliocene Sands aquifer in this province is a downward flow of rainfall in most of the area. The groundwater flow direction is the same as in the Murray Group aquifer and the Renmark Group Aquifer of this province. The water table in the Pliocene Sands aquifer matches the potentiometric surface in the Murray Group and discharges to the Murray River upstream of Overland corner (Figure 2-3).

4. Shepparton Formation aquifer

The Shepparton Formation occupies the topmost layer of the Cainozoic Murray Basin sequence in the Riverine Plain (**Figure 2-4**). This Formation includes heterogeneous fluvio-lacustrine sediments with clay, silt, and sand, of Pliocene to Quaternary age. This unit is likely to have problems associated with waterlogging and soil deterioration as this unit is highly irrigated. The Shepparton Formation is classified into upper and lower units in Victoria. The hydraulic conductivity of the Shepparton Formation ranges between 2-3 m/day. Direct rainfall is the source of recharge to the Shepparton Formation aquifer.

Table 2-1: Hydrogeology of the Murray Basin

Province	**Riverine Province**	**Mallee-Limestone Province**	**Scotia Province**
Geological Formation	i. Shepparton Formation ii. Pliocene Sands (Mostly Calivil Formation sediments) iii. Renmark Group (upper, mid & lower Renmark aquifer)	i. Pliocene Sands Aquifer ii. Murray group limestone iii. Geera Clay/ Winnambool Formation (Tertiary sediments (Marine) iv. Renmark Group	i. Pliocene Sands Aquifer ii. Murray group limestone iii. Geera Clay/ Winnambool Formation (Tertiary sediments (Marine) iv. Renmark Group
Thickness	Approx. 250m • 400 m thick in the east of the Murrayville Fault • 250 m on the Pinnaroo Block to the west	Around 300-350 m	
Flow direction	The dominant flow in all aquifers is from east to west	The regional groundwater flow direction in all aquifers toward north-west and west	
Renmark Group Aquifers System	i. Upper Renmark Group Aquifer ii. Middle Renmark Group Aquifer iii. Lower Renmark Group Aquifer	i. Lower Renmark Group Aquifer	i. Upper Renmark Group Aquifer ii. Middle Renmark Group Aquifer iii. Lower Renmark Group Aquifer

Aquitard	Mid-Tertiary low-permeability barrier (Geera Clay/ Winnambool Formation)	• At bottom of the Murray aquifer= Lower confining layer (Ettrick Formation Clay) at the bottom • Eastward= Mid-Tertiary low-permeability barrier (Geera clay) • Eastern Upper half= upper confining layer • Western upper half= Loxton-Parilla Sands of the Pliocene Sands aquifer	• At bottom of the Murray aquifer= Lower confining layer (Ettrick Formation Clay) at the bottom • Mid-Tertiary low-permeability barrier (Geera clay) • upper confining layer
Murray Group Aquifers System	N/A	Murray Group Aquifer	Murray Group Aquifer • less developed in Scotia province
Pliocene Sands Aquifer		Pliocene Sands Aquifer	Pliocene Sands Aquifer • Loxton-Parilla sands

2.8 Land use Change in Murray Basin

Agriculture and human intervention have caused drastic and significant alterations in the vegetation of the Murray Basin in the early 20th century (Brown & Stephenson 1991). The deep-rooted native vegetation from the majority of the area in the southern half of the basin has been removed and substituted with shallow-rooted crops like wheat and other grain cultivation, as well as extensive northern areas for grazing (Brown & Stephenson 1991). Likewise, the areas along the major rivers as Murray River have been cleared for orchards, vineyards, rice fields, and other cultivation and has been developed major irrigation areas adjacent to rivers (Brown & Stephenson 1991). The highest percentage of the irrigated lands of the Murray Basin lies within the Riverine province in the southern and eastern regions of the basin (Evans & Kellett 1989).

2.9 Effects of Clearing on RZD

The extensive land clearance and agricultural development disrupt the hydrologic equilibrium of the basin (Evans & Kellett 1989). The schematic diagram in **Figure2-6** illustrates the effects of clearing on the hydrological equilibrium in the Murray Basin.

Before illustrating the effects of clearing, it is important to understand that the hydrological terms namely, Root Zone Drainage (RZD) and recharge. RZD is the net downward flux of water from surface to immediately below the root zone in the unsaturated zone (Newman et al. 2009), while, recharge is the total flow of water from the unsaturated zone to the regional water table (Newman et al. 2009; Scanlon, Healy & Cook 2002). It is assumed that recharge is usually assumed to be equal to RZD (Newman et al. 2009). However, recharge may not be equal to RZD due to the presence of the discontinuous, heavy, thick clay layer in the near surface underneath the Murray Basin which was reported in earlier studies. The clay acts as aquitard which impede the transport of RZD resulting in perching of RZD. In this case, recharge can be less than RZD.

Before Clearing: Deep-rooted native Mallee is dominantly present in the western half of the Murray Basin which played a key role in maintaining the balance cyclic pattern in the salts concentration from rainfall by transpiring out the pure water such that the salt-rich water is left behind to leach downward below the root zone (Newman & Goss 2000). Most of the basin area was forested and therefore, the total recharge into the basin was much less in comparison to the recharge through the cleared area (Evans & Kellett 1989). Moreover, the prevalence of an arid climate with an occurrence of the very low rainfall and the consumptive uses of the nearly all rainfall by the native vegetation and, slow groundwater flow pattern impeded thorough flushing of the accumulated salts (Newman & Goss 2000). Moreover, both RZD and recharge underneath the native vegetation were very low as this vegetation species cut-off a significant quantity of runoff from infiltrating down the soil (Allison et al. 1990; Jolly et al. 1989). In addition, the salt cycle of the basin was balanced such that the saline groundwater flows into the river was slow and in equilibrium.

After Clearing: agricultural development in the early 20th century triggered a widespread extensive clearing of deep-rooted native vegetation and replacement by shallow-rooted agricultural and food crops in the Murray Basin. Following the long-term land use change, there was an increase in the overall amount of downward flux of water due to a drastic increase in RZD and eventually recharge to the underlying basin aquifers. The effects of this clearing can be

explained in a two-time scale namely, the effect shortly after clearing and long-term effects of vegetation clearance.

Shortly after clearing: There was an overall increase in RZD shortly after clearing. The consumptive water use of the shallow-rooted food is relatively less in comparison to the native vegetation which means lower crop-water demand and lower capacity of crops to use all the rainfall, unlike native vegetation. In other words, the shallow-rooted agricultural crops and grasses transpire a smaller quantity of water in comparison to the transpiration by the deep-rooted native vegetation. This smaller crop water requirement for shallow-rooted food crops caused a higher amount of water to flow downwards into the ground thereby increasing the effective infiltration/ RZD into the soil (Jolly et al. 1989; Newman & Goss 2000). The increased drainage gradually flows down towards the water table. At this stage, the groundwater recharge rate remains constant as excess drainage takes some time to reach the water table.

The long-term effect of clearing: Eventually, the excess drainage and inflow of rainwater progressively fill the shallow aquifers, increasing water pressure and leading to an overall rise in groundwater table (Newman & Goss 2000). Moreover, the clearing of land since European settlement mainly in the recharge zones has increased the infiltration into the ground thereby increasing the water pressure (Evans & Kellett 1989). This significant increase in rate of infiltration and recharge rate not only disrupt the existing long-term hydrological process and cycles but have also ultimately resulted in the development of the various secondary salinisation problems as water logging in the low-lying areas which lead to land salinisation, and groundwater salinisation and river salinisation in the Murray Basin (Evans & Kellett 1989).

Image removed due to copyright restriction

Figure 2-6 Schematic diagram illustrating the effect of clearing on hydrological equilibrium (Cook et al. 1996)

2.10 RZD and Recharge under Dryland Agriculture

Various studies have been conducted in the different regions of the Murray Basin to evaluate the change in RZD and recharge rate under dryland agriculture (Allison et al. 1990). The significant increase in recharge was reported, however, each study reported a variable rate of recharge as each study was conducted in a different region of the basin. The recharge was estimated to increase from 0.04-0.09 mm/yr under native vegetation (Allison et al. 1990; Allison & Hughes 1983) to around 3-40 mm/yr under dryland agriculture (Allison et al. 1990; Allison & Hughes 1983).

2.11 Time Lag Between RZD and Recharge in Dryland Agriculture

The change in the recharge rate following the landuse change was further complicated by the time lags associated with the hydraulic response of aquifers to these changes in the hydrological processes (Han et al. 2017). In general, time lag refers to the time required for RZD to flow through the unsaturated zone to the aquifer (Newman et al. 2009). The time lag is also referred to as response time and is the length of time required for the groundwater system to change from an initial condition to a new steady-state (Cook et al. 2003).

According to (Allison et al. 1990; Cook et al. 2003), time lag is related to the depth to the water table (D) (thickness of the unsaturated zone), recharge rate or drainage rate (R), the initial and final drainage rates, the initial water content (θ_{dry}), the final water content (θ_{wet}), and the soil hydraulic properties as shown in **Equation-2.1.**

$$\boldsymbol{Time\ lag, t_L} = \frac{\boldsymbol{D}*\boldsymbol{\theta_{wet}}}{\boldsymbol{R}} * \frac{\theta_{wet}-\theta_{dry}}{\theta_{wet}} = \frac{\boldsymbol{D}*(\theta_{wet}-\theta_{dry})}{\boldsymbol{R}}$$ …… **Equation-2.1** (Allison et al. 1990; Jolly et al. 1989)

Where, t_L = time lag

D= depth to the water table

θ_{wet} = final (new) water content of the soil in equilibrium with the new drainage rate

θ_{dry} = initial water content of the soil under the initial drainage rate

R= recharge rate

The time lag between the RZD under dryland agriculture and groundwater recharge is calculated **(Table-2-2)** using **Equation-2.1** for different values of depth to the water table. The time lag calculation for different value of depth to water table considered the initial water content of the soil under native vegetation, θ_{dry} = 0.06, which increased by 0.06 such that water content under dryland agriculture, θ_{wet} = 0.12, and the increased recharge rate, R= 20 mm/yr under dryland agriculture.

Based on the calculated recharge rates, it requires 30 years for RZD to recharge to the groundwater table at 10m **(Table-2-2)**. In contrast, when the water table at a depth greater than 70 m, the same RZD rate requires 210 years to reach the water table. Therefore, the time lag between the RZD and groundwater recharge has a direct correlation with the depth to the aquifer along with the recharge rate or RZD rate and water content.

Table 2-2: Calculation of time lag between the RZD under dryland agriculture and groundwater recharge

Depth to WT, (m)	Water content in solute front = water content above pressure front (Range= 8%-12%)	Water content below pressure front = initial water content of soil (Range= 4%-6%)	Recharge Rate, (mm/yr)	Time Lag, (years)
D	θ_{wet}	θ_{dry}	R	t_L
10	0.12	0.06	20	30
15	0.12	0.06	20	45
25	0.12	0.06	20	75
30	0.12	0.06	20	90
40	0.12	0.06	20	120
55	0.12	0.06	20	165
70	0.12	0.06	20	210

2.12 Time Lag Between Recharge and Groundwater Discharge to River

The time lag between an increase in groundwater recharge and an increase in groundwater discharge (or increase in river discharge) is related to the distance between the recharge and the discharge areas, and the hydraulic diffusivity (transmissivity and specific yield) of the aquifer (Cook et al. 2003). This timelag between increase in aquifer recharge and aquifer discharge is mathematically shown in Equation-2.2 below.

$$\tau = \frac{S_y * L^2}{T} = \frac{L^2}{D_h} \quad \text{..... Equation-2.2}$$

Where τ = system response time or critical time (T)

T= transmissivity (L^2/T) = K* h

K= hydraulic conductivity (L/T)

h = saturated thickness of unconfined or confined aquifer (L)

S_y = specific yield for unconfined aquifer or storativity for the confined aquifer (dimensionless)

L= domain length

$D_h = T/S_y$ = **hydraulic diffusivity** of the sediments/ aquifer (L^2/T) (Jazaei, Simpson & Clement 2014)

Cook et al. (2003) conducted a study to calculate time lag between the recharge and discharge of aquifer which indicated that an increase in groundwater discharge following an increase in recharge is a function of time (**Figure 2-7)**. The study by Cook et al. (2003) has considered 1 km width parallel to the river which drains the aquifer and estimated an increase in groundwater discharge of 10 m^2/yr for an increase in groundwater recharge of 10 mm/yr, considering aquifer parameters as hydraulic conductivity (K=5m/day), storativity (S=0.1), depth of water table (h=50m) and length between aquifer recharge and discharge (L=100 km).

As seen in **Figure 2-7,** the time lag between an increase in recharge and groundwater discharge to the river is very much influenced by the distance between the aquifer and the river. It means that the time lag increases with an increase in distance between the location recharging the aquifer and the point of discharge from the aquifer. However, the same recharge has no significant impact on groundwater discharge rate to the river as the recharge occurred over longer distance (more than 20 km) from the river for 200 years and more**.**

Likewise, the earlier study by (Heaney, Beare & Bell 2001) in the Mallee of Murray Basin is aligned to an aforementioned result which states that due to the flat topography and subsequent low hydrological pressure, the equilibrium response time rises speedily with the lateral distance the water flows in the Mallee.

Effect of timelag in River salinisation

The groundwater adjacent to the river is saline in the Murray Basin. The rising water table following an increase in recharge also causes increased hydraulic gradients towards the Murray River. This results in an increase in saline groundwater discharge into the river (Cook et al. 2003).

In the context of dryland agriculture, the salinisation process takes a long time to develop under dryland agriculture because the unsaturated zone over much of the area is thick (up to 50 m), and also groundwater flow paths towards the river are long (up to 200 km) (Cook et al. 2003).

Image removed due to copyright restriction

Figure 2-7 Increase in groundwater discharge as a function of time for increase in aquifer recharge for specific aquifer parameter (Cook et al. 2003). The recharge on 1 km width parallel to the river is assumed at different distance as represented by different curves. The aquifer parameters considered in this figure are recharge rate of 10 mm/yr at time t=0, transmissivity (T= 250 m^2/day), storativity (S=0.1) and distance between groundwater recharge and discharge (L= 100 km).

2.13 Increase in Salinity due to Dryland Agriculture

The increase in dryland recharge not only increases the salinity of the groundwater but also consequently leads to the land and river salinisation because these components are constantly interacting with each other in the basin.

Land Salinisation: Increase in water pressure following an increase in RZD and recharge after clearing of land in the semi-arid region of the Murray Basin cause soil salinisation and water-logging of low-lying area (Allison & Hughes 1983), because of the subsequent rise in water table which ultimately transports the natural salt to the soil's surface (Newman & Goss 2000). The

salinity audit reported an increase of ten times in the area of land affected by salinisation due to dryland agriculture in the coming 50 years (Newman & Goss 2000). The land salinisation problem was reported in Southern Australia in the area where the original initial groundwater table is comparatively near the land surface (Allison et al. 1990). Land salinisation and water-logging have a devastating impact on vegetation in the low-lying areas (Allison & Hughes 1983).

River Salinisation: The outflow of the saline groundwater from the basin to the Murray River, consequently increase the salinity level of the Murray River (Williams 2001). As the dissolved salt in so increased, infiltration and recharge are transported and accumulated thereby increasing the salt load of the river. In fact, an increase of 84% in the salinity level of the River Murray was estimated from 1938 to 1981 AD (Peck, Thomas & Williamson 1983). The ten times increase in the area of salinisation is expected to double the rate of salt mobilisation from 5 million tonnes per year to 10 million tonnes per year in the dryland agricultural area by 2100 (MDBMC 1999).

The salinity level of the Murray River is non-uniform both in space and time. The salinity level of the upstream reaches of the river is low (<100 uS/cm). The salinity is relatively higher in the downstream reaches of the Murray River (as shown in **Figure 2-8)** given the increased drainage and groundwater discharge from the irrigation areas towards the downstream reaches along the length of the Murray River (Morton & Cunningham 1985; Newman & Goss 2000). Allison et al. (1990) studied the impact of this increased recharge flux on the salinity of the Murray River using groundwater modelling which estimated an increase of salinity up to 1μS/cm per year within the next 50 years **(Figure 2-9).**

In addition, the stream salinisation exhibits temporal variation such that the level of stream salinity is relatively higher during the low flow season. Salinity levels at Morgan are forecasted to rise roughly 50% over the next 50 years (2050) and that in some tributary streams the salinity levels could disqualify agriculture and urban use (Newman & Goss 2000).

Even the source of salt varies along the river from upstream to downstream. The salinity at the upstream of the Murray River is accounted to the natural weathering of rocks which resulted in roughly stable and consistently dispersed salinity in the upstream of the river. In the context of the downstream of the Murray River, the inflow of the saline groundwater into the river is the major source of salt load (Morton & Cunningham 1985; Newman & Goss 2000).

Image removed due to copyright restriction

Figure 2-8 Median river salinity, 1978-1986.After Mackay et al. (1988). River distances are from the River Murray Commission (1984). Cited in (Allison et al. 1990)

Image removed due to copyright restriction

Figure 2-9 Salinity level forecasted in the two monitoring levels along the Murray River. (Allison et al. 1990)

2.14 Effects of Irrigation on RZD

Irrigated agriculture occurs along the floodplain of Murray Basin following the clearing of native vegetation which changes the overall RZD **(Figure 2-11).** The overall RZD and recharge in the irrigated areas are comparatively higher than in the dryland semi-arid agricultural land as irrigation return flow from the irrigated land account to the significantly high additional recharge in the area (Scanlon, Healy & Cook 2002).

Annually, around 10 megalitres per hectare of water are irrigated in horticulture which is comparable to 1000 mm of precipitation (Heaney, Beare & Bell 2001). Considering an irrigation

efficiency of 80%, the total annual recharge under irrigated crops is equivalent to 200 mm of groundwater recharge (Heaney, Beare & Bell 2001) which is much higher compared to the total annual recharge of 45mm under dryland agriculture.

Image removed due to copyright restriction

Figure 2-10: The Mallee Irrigation region (Newman et al. 2009)

Soil Structure: Hydrogeology /soil structure also affects recharge rates. In the case of the presence Blanchetown Clay, the RZD is inhibited through this low-permeability geological layer into the groundwater system. According to (Watkins & Waclawik 1996), the highest rate of infiltration through the Blanchetown Clay is expected to be around 100 mm/yr.

Pathway of RZD: In addition to the rate of RZD, it is important to account the RZD pathway to the river (Newman et al. 2009) because it eventually affects the total recharge in the basin. The hydrological processes in the irrigated agricultural land are schematically represented in **Figure 2-11.**

In the first pathway, the recharge into the regional groundwater is directly from the RZD such that the groundwater mounds (build vertically initially and flow laterally afterward) are formed which generates groundwater gradients that force water flow towards the river and its floodplain (Newman et al. 2009). This process of generating a lateral flow within the regional aquifer requires several years to several decades to reach equilibrium (Newman et al. 2009).

In the second type of RZD pathway, a shallow perched groundwater on the top of the relatively impermeable layers with an inflow of RZD (**Figure 2-11).** This leads to interflow, lateral flow along with the perching layer, such that water flows toward the landscape which is not associated with major aquifer discharge. Moreover, the rate of flow is higher in interflow than in recharge. It is likely that RZD to flow to the surface water through interflow without affecting regional groundwater. The interflow is likely either to be drained by the drainage system or can be evaporated from the 'inland' discharge sinks. It is important to note in this RZD pathway that the regional saline water is not mobilised (Newman et al. 2009).

Image removed due to copyright restriction

Figure 2-11: Graphical representation of hydrological processes in an irrigated Mallee farming setting © Aquaterra. (Adapted from (Newman et al. 2009))

2.15 RZD and Recharge Rates under Irrigation

It is difficult to estimate the RZD due to the lack of a direct method of RZD measurement. In addition, the RZD estimated by each method are different. Thus, Newman et al. (2009) conducted a study to come up with the methods of RZD drainage as earlier there was not a direct approach for estimating RZD.

The RZD of 5-15% is estimated by the regional based estimation of RZD (Newman et al. 2009). However, the RZD is estimated to vary from <0.5- 100% by point-based RZD estimation methods (Newman et al. 2009).

Usually, 10% of the traded water for irrigation is considered as recharge in groundwater models for the Basin Salinity Management Strategy (BSMS). However, it does not account for the crops, irrigation systems, soils or source water salinity as critical issues. Similarly, in some cases, the groundwater model used formulated RZD values or derived RZD estimates based upon calibration processes (Newman et al. 2009).

Thus, this highlights the importance of this research which has one of its goals to measure the RZD rate under irrigation.

2.16 Time Lag Between Irrigation RZD and Recharge

The time lag between the irrigation RZD and groundwater recharge is calculated **(Table 2-3)** using the same formula (**Equation-2**). It is considered that the irrigated agriculture is practiced over the cleared land which has been in a condition of dryland agriculture for a while. Therefore, the initial water content, θ_{dry} is considered to be that of the dryland agriculture which is equal to 0.12 (θ_{dry} = 0.12). In addition, the water content is assumed to increase to 0.25 (θ_{wet} = 0.25) due to irrigation. Besides that, the irrigation recharge of 200 mm/yr is considered. According to (Heaney, Beare & Bell 2001), groundwater recharge equal to 200 mm/yr irrigated agriculture when the irrigation efficiency is 80%.

The calculated time lag for different depths to water table under irrigated agriculture indicated the hydraulic response time increase with an increase in depth of water table **(Table 2-3).** Based on timelag calculated in **Table 2-3** at different depth of water table for constant recharge rate of 200mm/yr, it requires 7 years for RZD to recharge groundwater table at 10m depth whereas it requires 46 years for same RZD to recharge water table at depth of 70m.

Therefore, given the considerable increase in RZD, the time lag between the RZD and groundwater recharge under irrigated agriculture is considerably less in comparison to the time lag between the RZD and recharge under the dryland agriculture.

Table 2-3: Time Lag between the irrigation RZD and groundwater recharge under irrigated agriculture

Depth to WT, (m)	Water content in solute front = water content above pressure front (Range= 20%-25%)	Water content below pressure front = initial water content of soil (Range= 8%-12%)	Recharge Rate, (mm/yr)	Time Lag, (years)
D	θ_{wet}	θ_{dry}	R	t_L
10	0.25	0.12	200	7
15	0.25	0.12	200	10
25	0.25	0.12	200	16
30	0.25	0.12	200	20
40	0.25	0.12	200	26
55	0.25	0.12	200	36
70	0.25	0.12	200	46

2.17 Time Lag Between Increase in Irrigation Recharge and Increase in River discharge

In the context of the Murray Basin, the irrigated agriculture is predominantly along the Murray River **(Figure 2-11),** therefore, a hydraulic response is rapid in comparison to the inland dryland agriculture by virtue of the proximity to the Murray River. As mentioned already **Figure 2-7** showed the relationship between past recharge to discharge to the river as a function of the distance from the river. The nearest distance to the river, the least is the time lag (or hydraulic response time) between the irrigation recharge and river discharge.

Due to the relatively shorter time lag between recharge and discharge in the irrigated agriculture along the Murray River, both the rate of discharge and overall salinity of the Murray River is expected to rapidly increase in response to the increase in drainage under the irrigated

agriculture. Therefore, the increase in recharge in the near floodplain of the river means higher groundwater discharge to the river.

2.18 Increase in Salinity in Murray River due to Irrigation

Irrigation causes building up of salts in the crop's root zone because the river water containing some salts is applied in irrigation such that the salts are stored at the root zone following the removal of water via evapotranspiration (Newman et al. 2009). Around 96000 hectares of irrigated land of the Murray Basin clearly exhibited the possible salinisation in the mid-1980s which is expected to increase over 500,000 hectares of irrigated land in the coming years (Newman & Goss 2000). In fact, Mallee region of the Murray Basin is a major region of future salinity risk from irrigation (Newman et al. 2009). Irrigation is currently diverting nearly 2 million tonnes of salts annually (Newman & Goss 2000). Moreover, it is forecasted that the irrigation practices in this region will produce around 75 percent of the extra salt load to the river by 2050 (Newman et al. 2009).

2.19 Methods of RZD Estimation

The RZD drainage is often considered equivalent to recharge but the time lag of many years is very likely (Newman et al. 2009). Therefore, the RZD estimated at the crop's root zone is often under- or overestimate of the actual water table recharge because RZD is not always guaranteed to be equal to the recharge. For instance, the removal of water below the root zone through drainage pipes which reduces the total recharge to the aquifer. Likewise, perching of water transport and store water elsewhere and reduce the overall recharge (Newman et al. 2009).

As a consequence, the recharge has increased and salinisation has developed in some regions over decades whereas, in other places especially in the Mallee, the recharge has yet to meaningfully impact the deep, regional water tables (Newman & Goss 2000). Therefore, this uncertainty associated with the RZD estimation indicates the uncertainty in assessing the irrigated salinity impact in the Murray Basin (Newman et al. 2009).

The numerous methods have been developed for RZD estimation which can be classified as point-based and regional-based measurements (Newman et al. 2009).

Point-based measurement of RZD comprises of lysimetry, measured water balance, Darcy's law, capacitance probes, zero flux plane, artificial tracers, and natural tracers (chloride mass balance). Lysimeters provide the direct measurement of RZD however, this method is not used in the Mallee

Irrigation region so far. Measured water balance is a commonly used method in estimating RZD in Mallee Irrigation Region and the estimated RZD ranges from around 5 -30% (Newman et al. 2009). Likewise, the RZD measurement by Darcy's Law has relatively high uncertainty as it is dependent on the soil hydraulic conductivity which is spatially highly variable. The estimate of RZD is measured with the use of representative soil hydraulic conductivity data for the Mallee region such that estimated RZD ranges from 24 to 100 % for the Mallee region. Capacitance probes measure point-based in-situ soil moisture content. A network of 7500 capacitance probes in Australia has measured RZD around 17-23%.

Similarly**,** regional-based measurement methods of RZD constitutes of drainage system monitoring, remote sensing, district scale crop, and water use surveys (GIS), assumed water use efficiency, agronomic and soil physics models, groundwater models, salt loads to the river. The drainage system monitoring method of RZD measurement estimated RZD to be around 15% of irrigation water applied. Similarly, the district scale crop and water use surveys calculate the water balance at the district level to estimate the RZD is calculated to be around 15% of irrigation water. However, the reliability of the estimate of RZD from the water balance method is low. Similarly, RZD is estimated to be around 15% of the water applied to a crop based on the assumed water use efficiency method. 5-15% RZD is predicted based on various groundwater models (Newman et al. 2009).

2.20 Methods of Recharge Estimation

The rate, timing, and location of recharge are significant in areas of groundwater hydrology (Cartwright et al. 2017; Healy, R. W. 2010). However, the recharge is often difficult to quantify and, generally, the least understood because of its extensive spatial and temporal variability (Healy, R. W. 2010). Various methods are employed to estimate and understand the process of recharge like tracers (natural tracers, chloride mass balance method), physical techniques, numerical modelling and so on (Healy, R. W. 2010; Scanlon, Healy & Cook 2002). Though, it is often difficult to identify which methods of recharge measurement are reliable over the other because recharge rate and its timing are influenced by the climate, geomorphology and, geology of the area (Scanlon, Healy & Cook 2002). Hence, various factors must be considered while choosing the method for recharge measurement (Scanlon, Healy & Cook 2002). This section focuses on the process and techniques used in measuring these processes.

There are various methods used to estimate recharge estimation based on the three hydrologic zones namely, surface water, unsaturated zone and saturated zone **(Table 2-4)** (Scanlon, Healy

& Cook 2002). The methods of recharge estimation are broadly divided into three namely, physical methods, tracers methods and numerical modelling approach (Scanlon, Healy & Cook 2002).

Table 2-4: Various methods of recharge estimation in three hydrologic zones

Surface water	Unsaturated zone	Saturated zone
Physical 1. Channel-water budget 2. Seepage meters 3. Baseflow Discharge	Physical 1. Lysimeters 2. Zero-flux plane 3. Darcy's law	Physical 1. Water-table fluctuation method 2. Darcy's law
Tracers 1. Heat Tracer 2. Isotopic Tracers	Tracers 1. Applied tracers 2. Historical tracers 3. Environmental tracers	Tracers 1. Groundwater dating 2. Environmental tracers-chloride
Numerical Modelling	Numerical Modelling	Numerical Modelling

Tracer Techniques of Recharge Estimation

Various tracers are used in recharge estimation such as heat tracers, isotope tracers, environmental tracers, applied tracers, historical tracers, groundwater dating tracers and so on. Heat tracers are used in estimating infiltration from ephemeral surface-water resources (Lapham 1989). Stable isotopes of oxygen and hydrogen help to determine the source of groundwater recharge, however, it is not easy to quantify the recharge rate (Scanlon, Healy & Cook 2002). The frequently used applied tracers are bromide, tritium and visible dyes (Athavale & Rangarajan 1988; Scanlon, Healy & Cook 2002). In addition, Allison and Hughes (1983) also used time-series monitoring of the concentration of tritium in the soil underneath native vegetation to understand the mechanism of soil water movement into the soil. Frequently used tracers in recharge estimation are radioactive tracers, especially ^{14}C, ^{3}H, ^{36}Cl, and the noble gases, (Cartwright et al. 2017). Historical tracers that are in the environment following the anthropogenic activities in earlier days as contaminant spills, atmospheric nuclear testing (^{3}H and ^{36}Cl).

The environmental tracers as chloride (Cl) are widely used in estimating the recharge over the range of timescale from a few years to numerous hundred thousand years, which helps in understanding the long-term and recent pattern in groundwater systems (Cartwright et al. 2017). Likewise, a number of studies used natural solute tracers to deduce groundwater recharge rates by estimating vertical soil water flux below the root zone (Jolly et al. 1989). These environmental tracers are often preferred over other methods in recharge estimate as it involves the direct field measurement, and can provide an estimate of recharge which integrates a range of time scales (De Vries, Selaolo & Beekman 2000; Nativ et al. 1995).

The Chloride mass balance method is one of the most widely used tracer-based methods to estimate the groundwater recharge in the world (Crosbie, RS et al. 2018; Han et al. 2017) both in the saturated and unsaturated zones (Scanlon, Healy & Cook 2002). It is widely used globally for recharge estimation because it can be used in many climatic zones and cost-effective as it involves only the measurement of chloride in groundwater and rainfall (Crosbie, RS et al. 2018). (Allison & Hughes 1983) used the chloride concentration of soil in the unsaturated zone to estimate the increase in RZD and recharge after the long-term landuse change in the semi-arid Southern Australia of Murray Basin. It measures recharge at a point scale which is upscaled to estimate the groundwater recharge at the regional scale (Crosbie, RS et al. 2018).

Measurement of chloride concentration is preferred over other tracers as tritium in the area with a low recharge rate (Allison & Hughes 1983). The study by (Allison & Hughes 1983) used various chemical tracers to quantify the change in recharge following the long-term landuse change in the semi-arid South-eastern Australia of the Murray Basin.

Physically-based techniques

In addition to the use of tracers, there are several physically-based methods of recharge estimation namely, water table fluctuation (WTF) method, channel-water budget, seepage meters, baseflow discharge, zero-flux plane, Darcy's law, monitoring of matric suction, lysimeters, and water budget approaches (Han et al. 2017; Scanlon, Healy & Cook 2002).

Lysimetry is used especially to measure drainage/recharge of water following the root zone, however, this method is a very costly and invasive technique and gives only locally applicable estimates (Allison, Gee & Tyler 1994). In addition, the limitation associated with this method is the same as that with monitoring of matric potential.

Zero Flux Plane is the physical technique in which recharge is measured by comparing the change in soil-water storage below the zero-flux plane (ZFP). The ZFP denotes the plane where the vertical hydraulic gradient is zero (Scanlon, Healy & Cook 2002).

The **WTF methods** calculate recharge based on rainfall-induced seasonal fluctuation of groundwater levels and the aquifer's specific yield (Healy, Richard W & Cook 2002).

Likewise, **matric potentials monitoring method** is useful in unsaturated zones to demarcate recharge processes associated with interannual climate variability and land use/land cover changes (Scanlon et al., 2005) and could be expanded to (semi-) arid regions globally (Scanlon et al. 2006). However, the difficulty in upscaling of recharge estimate and instrumental difficulties is the major limitation associated with this method of recharge estimate (Han et al. 2017).

In the **Water balance method** of recharge estimation, the recharge is calculated based on other water balance terms as precipitation, surface runoff, evapotranspiration, and groundwater flow. Therefore, this method of calculating recharge is based on residual approach. The accuracy of recharge calculation is depended on the accuracy in the measurement of other parameters, therefore this method is often considered to be of relatively low accuracy especially in the semi-arid region where the recharge is very low in comparison to other parameters (Scanlon, Healy & Cook 2002). Moreover, this method is applicable over a wide range of space and time scales (Scanlon, Healy & Cook 2002).

The precision of the recharge measurement is dependent on the accuracy of the measurement of other components in the water balance equation of the basin. It is because of a minor deviation of the measurements of other parameters from the actual measurement likely cause comparatively higher inaccuracies in recharge estimation (Scanlon, Healy & Cook 2002). The practicality of this method is also questioned especially in the arid and semi-arid regions (Scanlon, Healy & Cook 2002).

The recharge estimated by all the above methods was compared by (Crosbie, R et al. 2010) in a specific region in South Australia. The study found that i) WTF method gives a small spatial scale estimate of gross recharge at an annual scale; ii) The CMB and the WB methods estimate net recharge (gross recharge minus ET from the water table) and iii) the WTF method estimated the highest magnitude of recharge on large spatial scales, followed by CMB, and the WB method.

However, each technique provides recharge estimates over varying space and time scales (Scanlon, Healy & Cook 2002).

3 STUDY AREA

The study is located on the Alma Almonds Orchard property, which covers an area around 326 ha and is in the Parish of Yungera, Boundary Bend, Victoria. Geographically, this orchard is situated south of the Murray Valley Highway and nearly 9 km west of the Boundary Bend Township. The study area is bounded by Murray Valley Highway in the north, Cameron Lane in the east and Paul Lane in the west, and a strip of native vegetation in the south **(Figure 3-1).** The highest elevation in the study area is 67.5 m AHD in the north-east and the lowest elevation is 53 m AHD in the southwest (Sluggett et al. 2007). The Murray River is located 500 m to the north of the Alma Almonds Orchards (Hoban and Daamen (2007).

Figure 3-1: Location Map of the study area.

3.1 Geology and Hydrogeology of the Study Area

The geology of the study area includes the Quaternary Woorinen Formation, Alluvium (Channel sand), Blanchetown Clay and Parilla Sands (Hoban & Daamen 2007; Sluggett et al. 2007). Details of each of these major formations are described further in the following four sub-sections. Stratigraphic details and associated hydrogeological data from bores in the vicinity of the study

area were collated from the Victorian Government's groundwater data portal (Visualising Victoria's Groundwater.) to create two north-south cross sections (**Figure 3-3 & Figure 3-4).** The transect N-S comprises eight state bores and has a total length of around 19 km in the north-south direction. Likewise, transect 1-1' is nearly 12 km and contains four states bores **(Figure 3-2).**

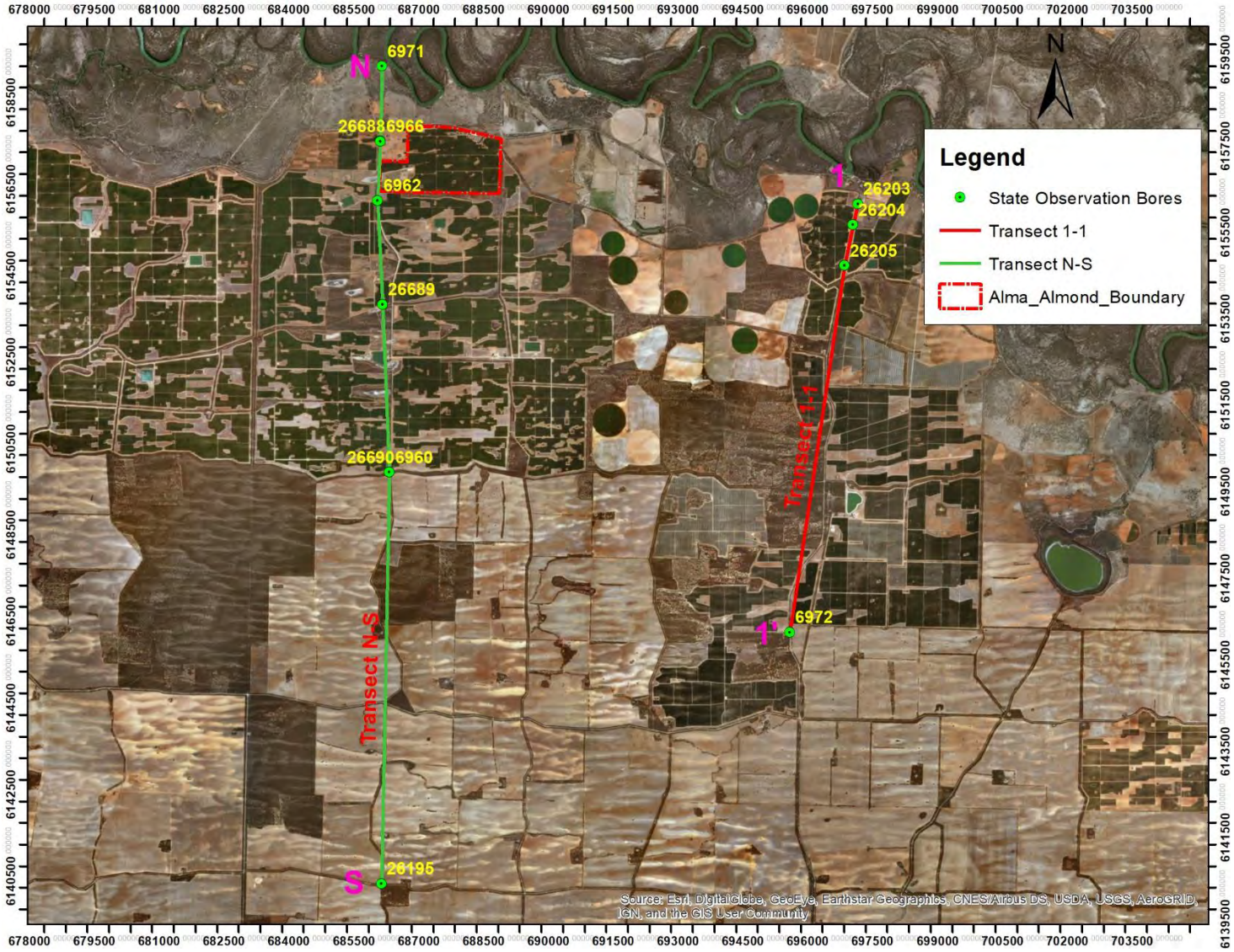

Figure 3-2: Location of transect N-S and 1-1' that were used to create cross sections of the geology and stratigraphy. State observation bores also shown.

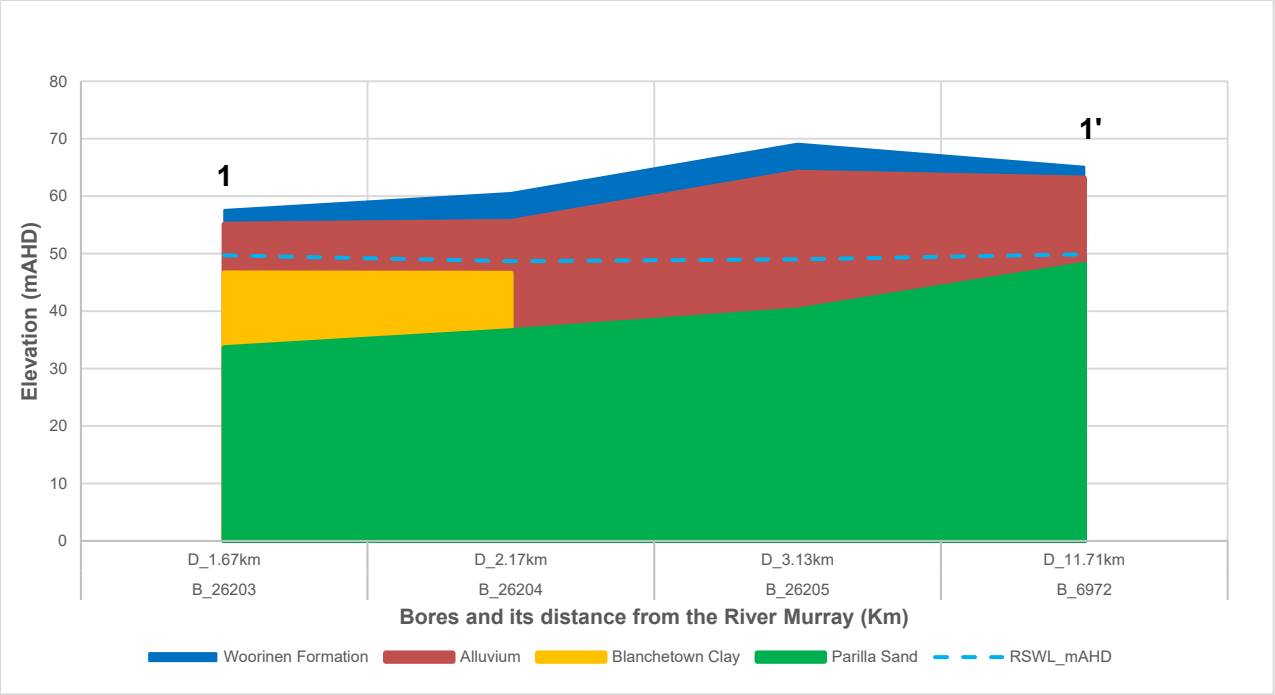

Figure 3-3: Cross section of the stratigraphy along transect 1-1'. The average RSWL of the Parilla Sands aquifer is also shown. The horizontal axis is not in scale.

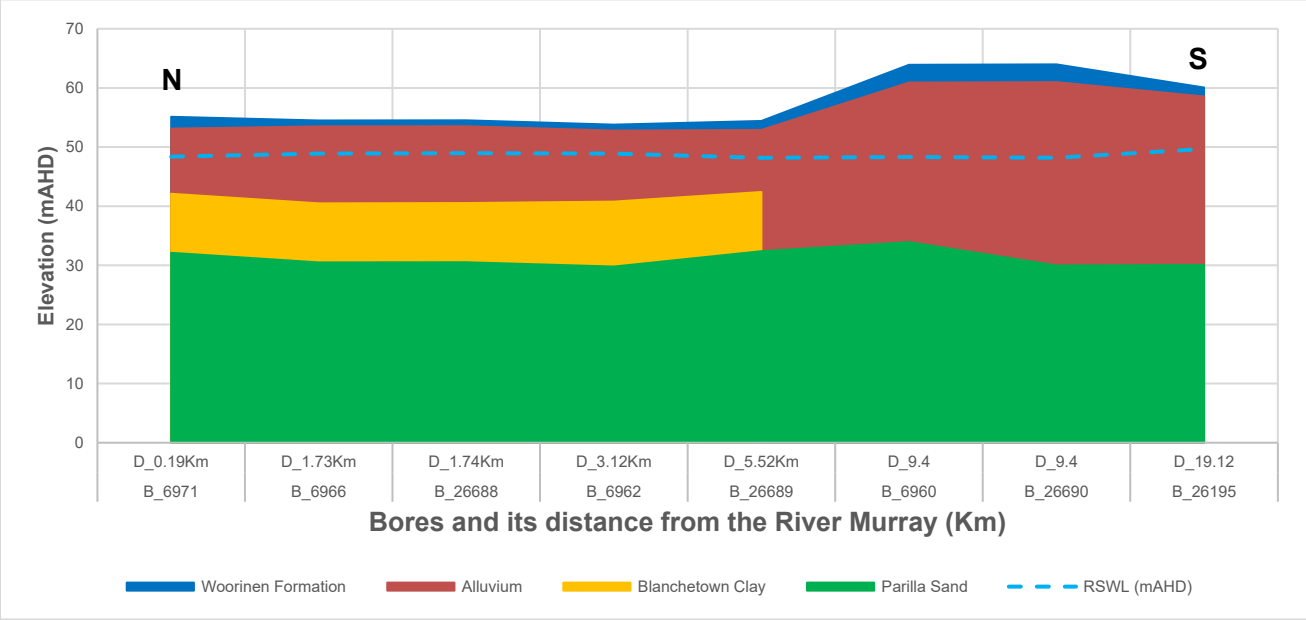

Figure 3-4: Cross section of the stratigraphy along transect N-S. The average RSWL of the Parilla Sands aquifer is also shown. The horizontal axis is not in scale.

3.1.1 Woorinen Formation/ Lowan Sands

The Quaternary Woorinen Formation, the topmost geological layer, forms the land's surface and ranges in thickness from 1 to 5 metres with a maximum thickness of 6 metres. The Woorinen Formation is characterised by remnant sand dunes which are created by the wind-blown (aeolian) deposits trending in the east to west orientation thereby resulting in the undulating topography in the region. This formation is dominantly sand and mostly free draining. The Woorinen Formation is underlaid by the Alluvium (Hoban & Daamen 2007).

3.1.2 Alluvium and Channel Sands Aquifer

Below the Woorinen Formation and overlying the Blanchetown Clay and the Parilla Sands Aquifer is an alluvial deposit, referred to as the Alluvium and Channel Sands. This alluvial material was deposited within the Murray Trench (up to 3.5 km wide just south of the study area), which was formed by the scouring and erosion in the past by the ancestral Murray River (Hoban & Daamen 2007). The alluvial sediment deposits in the Murray Trench are comprised of two geological units, namely, the Coonambidgal Formation and the Monoman Formation. The Coonambidgal Formation is a floodplain layer of 3-8 m thickness and consists of clays and silts, which act as a semi-confining layer over the Channel Sands Aquifer (also known as the Monoman Formation) (Hoban & Daamen 2007; Sluggett et al. 2007). The thickness of the Monoman Formation is between 3 to10 m and gradually increases in thickness away from the river inland (Figure 3-3 & Figure 3-4). It is comprised of medium to coarse-grained sand and the associated aquifer and the Murray River are hydraulically connected (Hoban & Daamen 2007).

3.1.3 Blanchetown Clay

The Blanchetown Clay underlies the alluvium deposits and overlies the Parilla Sands Formation aquifer. This extensive clay layer, comprised of clay and local silty sands, is absent in some areas where the clay has been eroded, or in structural highs where the clay has not been deposited (Hoban & Daamen 2007). The Blanchetown Clay acts as a semi-confining layer over the Parilla Sands aquifer, which has a thickness ranging from 5 to 7 m and therefore is likely to impede the flow of RZD downwards to the regional Parilla Sands aquifer.

3.1.4 Parilla Sands

The Parilla Sands form the regional aquifer and this layer extends throughout the Sunraysia district (Hoban & Daamen 2007). This formation comprises fine to coarse-grained sand deposited in a marine environment. The Parilla Sands has a variable thickness between 1 to 101 metres. The earlier study by Thorne (1990) reports that the Parilla Sands is usually 40 to 80 metres thick

and mostly occurs at depths ranging from 1 to 70 metres below the surface. This widespread thick layer of the Parilla Sands has a highly undulating surface and acts as the shallowest regional aquifer in the Murray Basin where the groundwater flow is mostly towards the west.

3.2 Depth to the Water Table

The regional water table of the Parilla Sands aquifer is just between 4 m to 10 m below the land surface in the region of the study area as observed in Figure 3-5, which shows the reduced standing water level in the state bores completed in the Parilla Sands aquifer. In addition, Figure 3-3 & Figure 3-4 shows the water table within the alluvium layer.

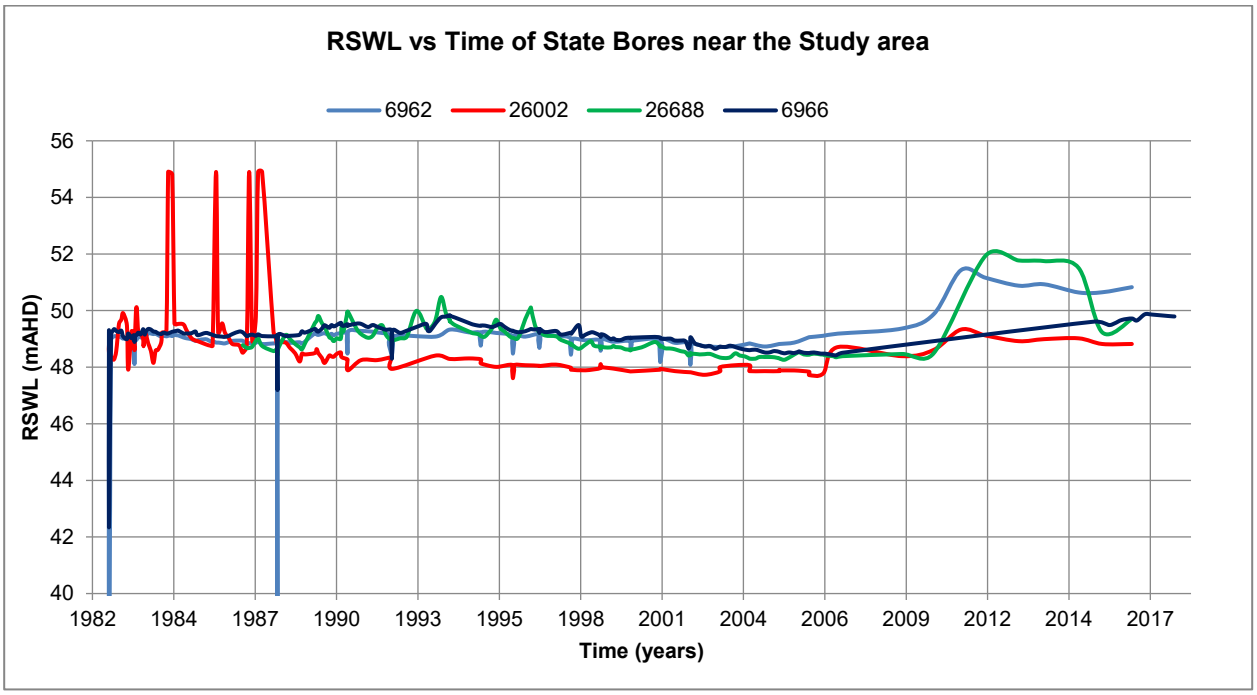

Figure 3-5: Water levels (mAHD) of the regional Parilla Sands aquifer from the State Government observation bores from 1982 to 2017.

3.3 Groundwater Flow Direction

Groundwater in the Murray Basin can only discharge either by evaporation or by leakage into the Murray River itself as the Murray Basin acts as a closed groundwater basin. The hydraulic gradient of both the Alluvium and Channel Sands aquifer and the Parilla Sands aquifer is towards the Murray River (Hoban & Daamen 2007). The land elevation on the northern boundary of the

study area is 6.66m above the water level in the Murray River, which is 47.60 mAHD at Euston Weir.

3.4 Irrigation

Irrigated almond cultivation has been widely developed in the study area where there is an estimated average annual irrigation requirement of approximately 3,978 ML per annum to irrigate a maximum area of 286.18 ha of almonds (Sluggett et al. 2007).

3.5 Justification for the selected Study Area

The study focussed on the Alma Almonds Orchard in Robinvale because it is in close proximity to the Murray River (500m). In addition, irrigated almond farming has recently developed in the study area and the changes to the hydrological processes as a result of irrigation require further investigation

Geologically, Alma Almonds' boundary/ area is prone to drainage hazards. The drainage problem is identified mostly in the area with moderate to slow draining topsoils and/or limestone, which is underlaid by the relatively impermeable Blanchetown Clay (Sluggett et al. 2007). The earlier hydrogeological studies in the study area characterised the Blanchetown Clay as an aquitard which favours the formation of perched water tables in the geological units above (Brown & Stephenson 1991).

Therefore, irrigation development in the study area and the nearby region is likely to increase the risk of future groundwater-related salinity problems on the Murray River due to its close proximity. Increases in the hydraulic head gradient towards the river as a result of the irrigation development and the direct hydraulic connection between the Murray River and the adjacent Alluvium and Channel Sands aquifers also threatens the water quality of the river (Hoban & Daamen 2007).

4 METHODS

4.1 Field Visits and Field Activities

Three field visits were conducted to the site. The first field visit was conducted in late April 2019 to early May 2019 (29 April to 1 May). The major field activities were:

i. Installation of non-vented pressure transducer dataloggers in 7 piezometers, 8 test wells, and 9 drainage pits and installation of two loggers to measure the barometric pressure to correct the non-vented loggers.
ii. Manual measurements of the depth to the water level in all these water monitoring infrastructures using a water level meter.
iii. An accurate survey of the water monitoring infrastructure using a Trimble RTK GPS surveying unit.
iv. Electrical Resistivity Tomography (ERT) surveys along a 475m long transect parallel and beneath one of the N-S almond tree rows within the study area using two electrode configurations (dipole-dipole and Wenner-Schlumberger array with 5m electrode spacing).
v. Frequency domain electromagnetic induction (FDEM) survey using a terrain conductivity meter along four transects parallel to the ERT transect.
vi. Water sampling from drainage pits, piezometers, and test wells to analyse major ions and stable isotopes of water.

The second field visit was undertaken during mid-July 2019 (15 July to 20 July) and included:

i. Repeat the ERT survey. An additional ERT survey was conducted at a higher spatial resolution along a 237.5 m long transect with 2.5m electrode spacing using a dipole-dipole and Wenner-Schlumberger array.
ii. Installation of pressure transducer dataloggers in four state observation bores in the vicinity of the study area.
iii. Water sampling from drainage pits, piezometers, test wells, and state observation bores for subsequent analysis of major ions and stable isotopes of water.
iv. A revised survey using the Trimble RTK GPS surveying unit with a tripod and 4m extension pole to increase accuracy compared with the initial field trip due to interference of the signal by the high density of almond trees.

v. Install weir boxes at the two discharge outlet pipes. In addition, water level dataloggers were installed within the weir boxes and an In-Situ BaroTroll® was installed nearby.
vi. Manual measurements of depth to water in all groundwater monitoring infrastructure.

The last field visit was conducted in the first week of September (2- 6 September 2019). The field activities were:

i. Repeated ERT surveys that were undertaken in the second field trip.
ii. FDEM conductivity survey along nine different transects distributed across the study area.
iii. Manual discharge measurements to calibrate the weir flow rates.
iv. A sampling of the discharge water at the outlet.
v. Manual water level measurements in all groundwater monitoring infrastructure.

4.2 Research Methods

The study used numerous field research methods to understand the hydrological processes in the unsaturated zone that influence the transport of the RZD.

4.2.1 Electrical Resistivity Tomography (ERT) Survey

Electrical Resistivity Tomography (ERT), also known as a direct current (DC) resistivity method, is a geophysical technique used to map the resistivity of subsurface material (Revil et al. 2012; Schlosser 2017). The technique was conducted to map the stratigraphy of the near-surface geology of the study area and to examine the presence of clay, its thickness, and continuity, and to infer the temporal changes in water saturation in the near surface. In addition, time lapse ERT surveys, also known as geophysical monitoring, were employed in different months to estimate the change in apparent resistivity which helps to map temporal variation in water content in the subsurface (Beff et al. 2012). The advantage of resistivity approaches is that they can provide a 2D and 3D picture of the subsurface. Time-series resistivity measurements enable changes in soil moisture to be quantified even without detailed characterisation of sediment properties (which do not change with time). In addition, the DC resistivity method was used to locate the perched water table as this method can be used for both the fresh-water detection and hydrogeological monitoring in saline groundwater environments (Barrett et al. 2002).

4.2.1.1 Limitations of ERT

ERT methods can be used to estimate the spatial soil moisture distribution underneath the subsurface without disturbing the soil profile, however, the measurement of soil moisture

measurement in highly saline environments is challenging due to electrical resistivity being influenced by both the soil moisture content and salt concentration (Brindt, Rahav & Wallach 2019). The other inherent limitation of the resistivity surveying is the difficulty to exactly determine the actual resistivity value of the geological formation (McNeill 1980). Because of such uncertainty, the resistivity surveys are used to examine patterns in resistivity variation either laterally or vertically to outline geological features of interest (McNeill 1980).

4.2.1.2 Transect Selection for ERT surveys

Two transects of different lengths in a north-south orientation were selected to pass through a maximum number of soil types in the study area (Figure 4-1), which have been categorised into seven major soil types (Sluggett et al. 2007). The shorter transect lies within the middle of the longer transect. Almond trees are planted in a north-south orientation and therefore, the ERT transects were also aligned in a north-south orientation to provide easier installation.

Figure 4-1: ERT survey transects and water monitoring infrastructure (piezometers, test wells, drainage pits & state groundwater bores) in the study area. The detail of ERT transects is in Section 4.2.1.2. Drainage pits and outlets are described in section 4.2.3. Test wells, piezometers and state bores are described in Section 4.2.4.

ERT survey is influenced by the spacing of the electrodes, which determine the depth of resistivity measurement and resolution of the resistivity profile (2D cross section). The resistivity survey generates a deeper resistivity profile when the electrode spacing is large. In contrast, the survey produces shallower resistivity profile when electrodes are closely spaced (Schlosser 2017). For the longer transect of 475m length, the 96 electrodes were installed at 5 m spacing while, for the shorter transect of 237.5 m length, the 96 electrodes were installed at 2.5 m spacing **(Figure 4-1).** These two transects of different lengths and electrode spacing were selected to obtain resistivity 2D cross sections of different depth and resolutions in the same place.

4.2.1.3 Electrode configuration and array type for ERT survey

ERT is influenced by the array type (Schlosser 2017). The technique of arranging the current and potential electrodes on the Earth's surface is called a resistivity array (Revil et al. 2012). The choice of the type of array/ electrode configuration for ERT surveys is governed by the type of structure to be mapped, the sensitivity of the resistivity meter, the background noise level, the horizontal data coverage, the depth of investigation and the signal strength (Loke 2000; Revil et al. 2012). The resistivity measurements in the study area were conducted by arranging multiple electrodes in two-electrode configurations, namely, the Dipole-Dipole and Wenner-Schlumberger electrode configuration.

The dipole-dipole array configuration is extra sensitive to lateral changes in soil moisture (Dick et al. 2018) and therefore especially useful for observing differences in resistivity laterally along the profile (Schlosser 2017). Moreover, this array has better horizontal data coverage than the Wenner for 2D surveys. However, this array has a shallower depth of investigation compared to the Wenner array (Loke 2000).

Wenner-Schlumberger is a combination of the Wenner and Schlumberger array. It is sensitive to both horizontal and vertical structures. The signal strength in this array is higher than the dipole-dipole array. However, the Wenner-Schlumberger array is characterised by narrower horizontal data coverage in comparison to the dipole-dipole array (Loke 2000).

4.2.1.4 ERT survey in the study area

A Syscal Pro Switch Box 96 electrical resistivity meter (Iris Instruments) was used to measure the apparent electrical resistivity of the subsurface by injecting an electric current into the ground through two electrodes. The change in potential difference or voltage difference is measured in the other two electrodes between the source and receiver.

ERT surveys with both Dipole-Dipole and Wenner-Schlumberger electrode configurations were conducted along a transect of 475 m long with 96 electrodes at 5m spacing during the first field trip in early May 2019. In the following trip in mid-July 2019, ERT measurements with Dipole-Dipole and Wenner-Schlumberger electrode configurations were repeated on a transect of 475 m long with 96 electrodes at 5m spacing. Additional ERT measurements with Dipole-Dipole and Wenner-Schlumberger electrode configurations were taken with a 2.5 m electrode spacing on a transect of 237.5 m for better resolution of the data. The 2.5m electrode spacing measurements

covered the mid-section of the 5m spacing transect (Figure 4-1). Similarly, the four ERT measurements were repeated like the earlier measurements during early September.

The resistivity data was downloaded from Syscal Pro and later processed in ProSys II and inverted using Res2Dinv software (Loke 2000). The resistivity data was checked and filtered for bad data points/ measurements in Prosys II. The filtered resistivity data was then inverted to generate a two-dimensional apparent resistivity distribution profile along the transect. This was analysed to visualise the stratigraphy and perched water table behaviour in the study area.

In this study, the data from the Wenner-Schlumberger electrode configuration were only analysed and interpreted as the 2D resistivity profile from Wenner-Schlumberger array had fewer bad data points than the dipole-dipole configuration.

4.2.1.5 Time Lapse Resistivity

Time lapse resistivity is a powerful technique used for monitoring change in water content in the vadose zone (Revil et al. 2012). Repeated resistivity measurements at different times allow estimation of temporally variable soil properties such as water content and salinity of pore water from the contribution of temporally stable soil properties (Vereecken et al. 2014). Time lapse resistivity is calculated to estimate the variation in apparent resistivity at two different times and to identify the area with a maximum change in resistivity in the study area. The time lapse resistivity in percentage apparent resistivity variation is calculated as (Equation- 4.1);

apparent resistivity variation (%) = (Rho data file 1- Rho data file 2/ Rho data file 1) *100 **…….Equation 4.1**

The time lapse in apparent resistivity was calculated for two time periods- i. between May and July and ii. between July and September from field resistivity surveys in those months. The resistivity data from the Wenner-Schlumberger array were used for the calculation. For time lapse resistivity calculation between May and July, the resistivity data corresponding to Wenner-Schlumberger array of 445m long transects was used. In the case of calculation of the time lapse resistivity between July and September, the resistivity data for longer transect (445m) and shorter transect (237.5m) were used to generate the time lapse resistivity profile.

4.2.2 Frequency Domain Electromagnetic Induction Conductivity Survey

Frequency domain electromagnetic induction (FDEM) instruments measure apparent electrical conductivity, and this denotes the weighted average of the subsurface electrical conductivity

across a depth range that governed by the distance between the transmitter and receiver coils as well as their orientation (McNeill 1980). Mapping of the conductivity variation at several depths across the study area gives a picture of the geology and its variation across the study area. A terrain conductivity meter (CMD Explorer manufactured by GF Instruments) enabled rapid contactless recording of apparent conductivity across the study area. It was also used to examine the change in the geometry of the shallow perched watertable. Moreover, the representativeness of the transect selected for the resistivity surveys was checked and validated by the conductivity surveys. The CMD-Explorer measures conductivity simultaneously at 6.7m, 4.2m, and 2.2m in the Hi-moment orientation. The instrument was set in continuous measurement mode so that the instrument measures and records conductivity data at 1 second intervals.

The conductivity surveys were conducted along 13 transects of different lengths to map the conductivity variation across the study area. Conductivity surveys were conducted on four transects (T1-May, T2-May, T3-May, and T4-May) in a north-south direction and parallel to ERT transects during early May **(Figure 4-1 & Figure 4-2**). Furthermore, additional surveys were conducted along nine transects distributed across the study area in early September (Figure 4-2). Two transects (T-2 & T-7) were in an east-west orientation.

CMD Data Analysis Process

The data from the CMD-Explorer were downloaded using GF software and analysed by plotting the conductivities at three different depths along the survey transects which were orientated in a north-south and east-west direction.

The land elevations along the transects are also plotted to help visualise the variation in conductivity with topography and to compare transects that have similar conductivity values at the same elevation.

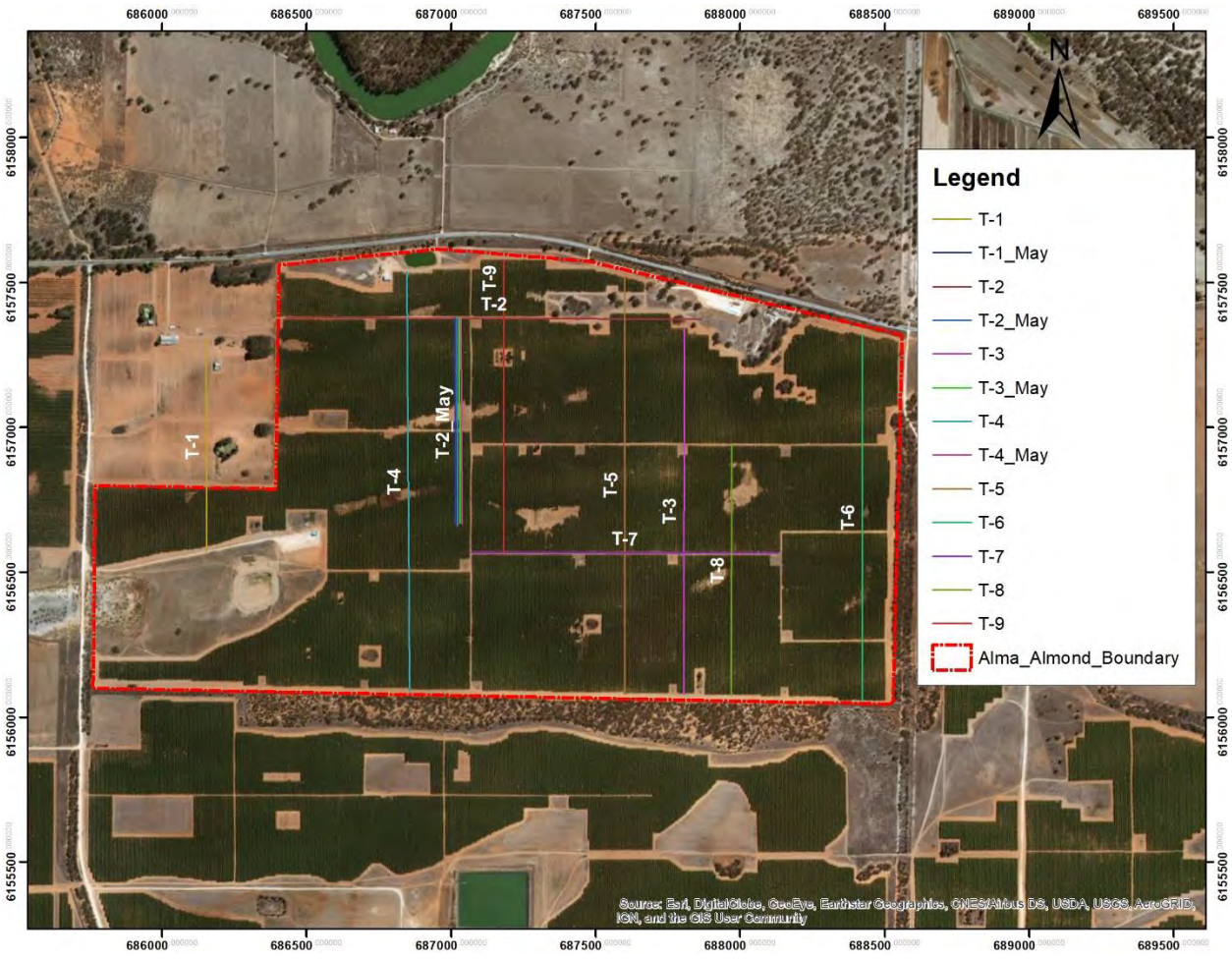

Figure 4-2: North-south and east-west FDEM conductivity survey transect locations over the study area.

4.2.3 Monitoring of the Shallow Drainage Network

This research study used the shallow drainage network across the study area to evaluate the RZD. The tile drainage network drains the excess water accumulated in the subsurface of the study area. The tile drainage is designed such that subsurface pipes drain excess water from a certain plot of land which ultimately flows towards the designated drainage pits under gravity.

There are 12 drainage pits (DP1-DP12) distributed across the study area as shown in **Figure 4-1, Figure 4-4, & Figure 4-6.** The drainage pits are shallow circular pits having a diameter of around 1m and are constructed mostly within the Alluvial Formation. The average depth of these monitored drainage pits is around 4 m, however, the depth ranges from 3 m to 5 m. The drainage

water stored in each drainage pit is pumped out daily to either of two outlet pipes that discharge water to the salt lake in the southwestern corner of the study area.

Pressure transducers/ dataloggers were installed in 9 of the drainage pits at the end of April 2019 to monitor water level fluctuations. The other 2 drainage pits were dry during the study period. The dataloggers record total water pressure in terms of the height of water in drainage pits every 15 minutes from the end of April to early September 2019. Similarly, 2 v-notch weirs were installed at the outlet pipes to measure the total drainage captured across the Alma Almond property **(Figure 4-5)**. Four pressure transducer dataloggers were installed; 2 loggers in each weir, to measure the total water pressure in each weir. Likewise, three In-Situ BaroTroll® barometers were installed across the study area, two at drainage pits and one near the discharge outlet pipes, to measure the barometric pressure and provide the atmospheric correction term to the non-vented dataloggers.

Water Pressure Calculation

The data from the non-vented pressure transducer loggers installed in the water monitoring infrastructure were corrected for barometric pressure to a water pressure head (m) using the following formula (Equation-4.2).

Pressure recorded in logger = Barometric Pressure head (air pressure) + Water Pressure head

$$(h_{logger}) = (h_{air}) + (h_{p,water})$$

Therefore, Water Pressure head ($h_{p,water}$) = h_{logger} - h_{air}---------- Equation-4.2

The water pressure head calculated after barometric correction gives the estimate of the change in water level in the drainage pits, which is plotted against time to visualise the trend in water level stored and pumped out from the pits. Similarly, the water pressure data in the weir is also plotted to observe the trend in total inflow and discharge from the weirs.

Calculation of Volume of RZD

The cumulative volume of RZD was calculated from the sum of the total drainage inflow from the network of shallow drainage pits. **Figure 4-3** shows the trend of drainage inflow and outflow from the shallow drainage pits. The inflow in the drainage pits is represented by the line ascending to a certain level, where the pump is activated to remove the water within the pit and the water level declines with the cycle repeating again. The frequency of the cycle appears to be on a daily basis,

however, it does vary between the different drainage pits as the response is related to the irrigation rate and also rainfall.

The cumulative volume of inflow in a drainage pit within a certain time period is calculated by the sum of inflow into the pit (Δ**h)**. The total cumulative volume of the drainage in the study area is estimated as the sum of inflow in each drainage pits ($\sum\Delta$**h**) as shown in equation-4.3.

$\sum\Delta h = \Delta h_{(DP1)} + \Delta h_{(DP2)} + \Delta h_{(DP3)} + \ldots\ldots + \Delta h_{(DP8)} + \Delta h_{(DP9)}$ ---------- **Equation 4.3**

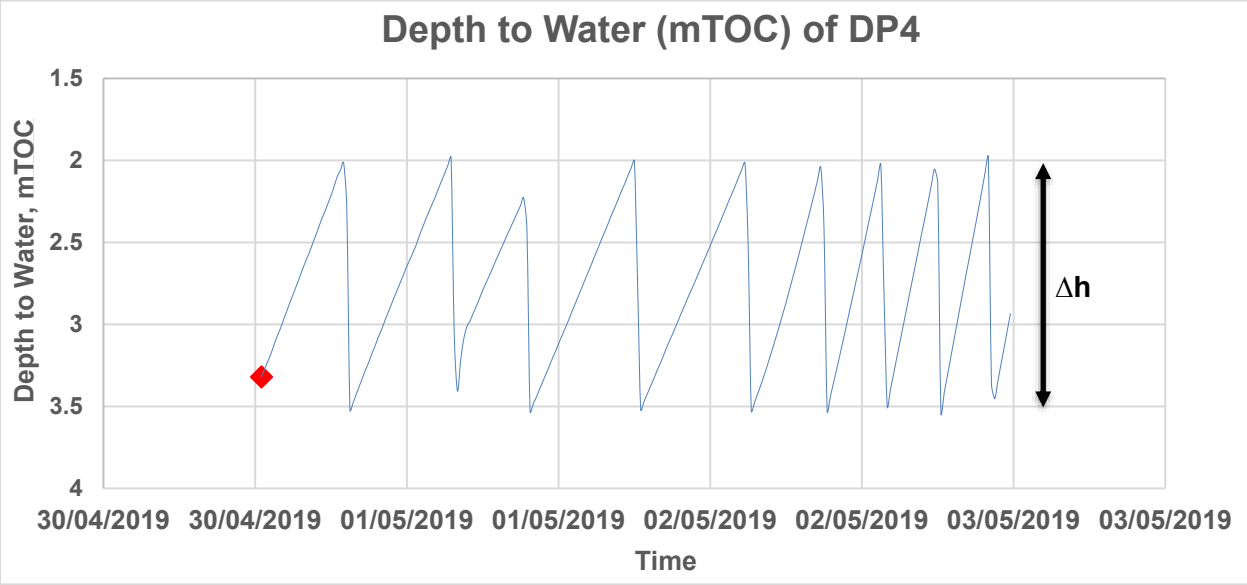

Figure 4-3: The trend in water level change in drainage pit DP4 where inflow to the pit is represented by the ascending line, and pumping out from the pit is showed by the rapidly descending line. The total drainage volume in a drainage pit is as equal to the sum of total inflow. The plot of full dataset for DP4 is in Figure 5-15, Section 5.3.2.

Calculation of RZD Rate

From the calculated total volume of the RZD ($\sum\Delta$**h**) which is equal to the total volume of inflow in drainage pits, the RZD rate in the study area is calculated by diving total RZD by the total study area (A) (Equation 4.4).

RZD rate= $\sum\Delta$**h/ A …… Equation- 4.4**

These cumulative drainage volume and drainage rate over time data are compared with rainfall and irrigation to check the correlation of these changes in water level with rainfall and irrigation. Further, these data help in calculating the total water balance in the study area.

Weir Calibration: The weirs were calibrated using the manual discharge measurement values and water pressure after barometric correction from the pressure transducers. Due to the limited data set, this is only the preliminary calibration of weirs and detailed calibration will be conducted with more manual discharge measurements at a later in this ongoing project. The calibration curve will be used to calculate the total volume of water discharged through the weir.

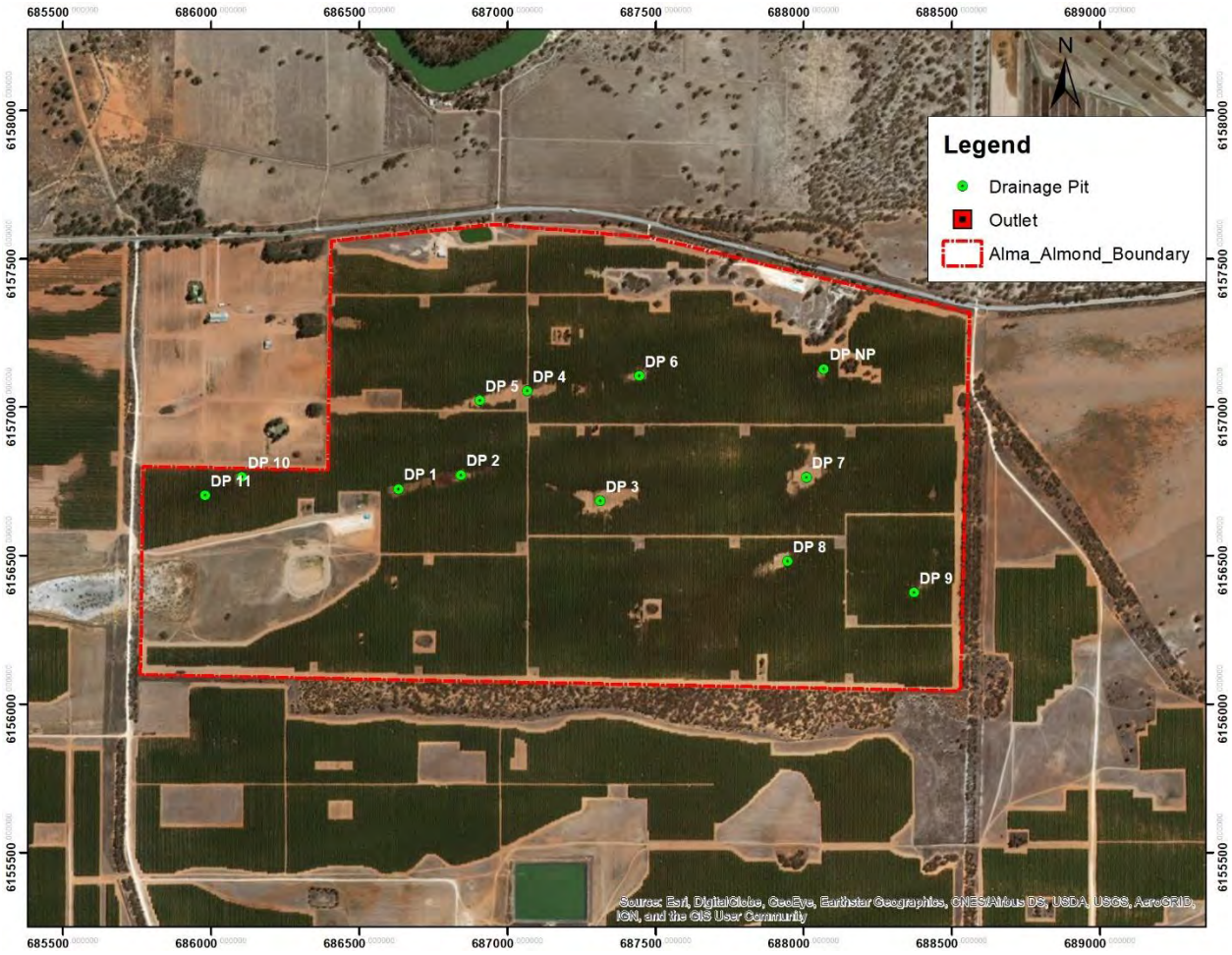

Figure 4-4: Network of shallow drainage pits across the Alma Almonds orchard. The outlet is also shown by a red square with a black square in the middle.

Figure 4-6: One of the shallow drainage pits in the Alma Almond Orchards.

Figure 4-5: Discharge outlet pipes and the installed V-notch weirs as part of the study.

4.2.4 Monitoring Groundwater Levels

The study area comprises various groundwater monitoring infrastructure, screened at different depths in the shallow aquifer system **(Figure 4-1 & Figure 4-7).**

Test wells: There are 8 test wells (T1 to T8) of around 1-2m depth within the Alma Almond property to monitor the groundwater levels of the shallow Woorinen Formation aquifer (thickness of 1 to 2 m) in case of perching. Monitoring of the water level in the test wells is also used to monitor the soil water so as to optimise irrigation efficiency and reduce drainage accessions (Sluggett et al. 2007).

Piezometers: There are 7 piezometers in the study area consisting of 3 shallow (2.5m to 5.5m), and 4 deep (11.5m to 22m). Six of these piezometers (namely-P1s, P1d, P2s, P2d, P3s, & P3d) were located along a north-south transect **(Figure 4-1 & Figure 4-7).** The water level data from these wells were used to identify and monitor the development of perched water level conditions within the Woorinen Formation aquifer and leakage to the Parilla Sands aquifer over time.

Figure 4-7:Bores in transect in the Alma Almond Orchards

The water levels in the 8 test wells and 7 piezometers were monitored by installing pressure transducer data loggers in each of them from May to early September 2019. Pressure loggers were also installed in 4 State Government monitoring bores (6962, 6966, 26002 & 26688), which are located in the vicinity of the study area to monitor the change in the regional water table of the Parilla Sands aquifer. The data loggers (In-Situ LevelTroll® loggers) recorded the groundwater level in 15 minutes intervals from May to early September 2019. The barometric correction is applied to the data measured by the pressure loggers to get the water pressure head. In addition, the groundwater level is measured manually at different times to ensure the accuracy of the recorded value by the pressure loggers.

The hydraulic head in each groundwater structure is calculated as below in Figure 4-8 (Post & Von Asmuth 2013);

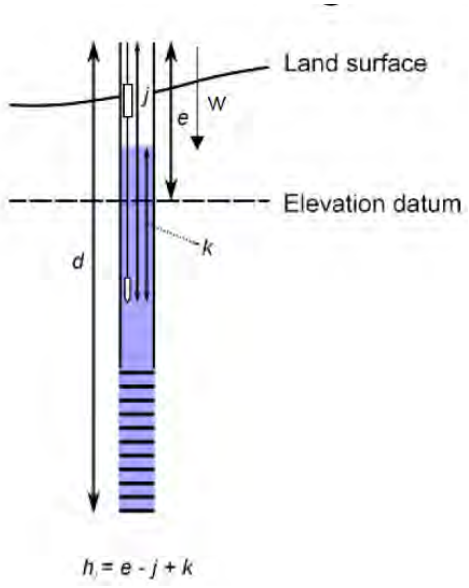

d= well length (from TOC to middle of screen), m

w= Depth to water from TOC, m

e= Height of TOC above datum, mAHD

j= Depth of logger's Sensor below TOC

k= Height of water column above sensor

i. **Method1: hydraulic head** (h, mAHD) = e- w
ii. **Method2:** Hydraulic head (h, mAHD) = e-j+k

Figure 4-8: Schematic representation of measurement in hydraulic head calculation Source: (Post & Von Asmuth 2013)

Perching of RZD: Groundwater level time series data observed within the unsaturated zone (data from test wells and shallow bores) was used to determine whether perched aquifer conditions formed in the shallow Woorinen Formation and also to estimate the drainage rates under irrigated agriculture.

Mapping Hydraulic Gradient: The water levels from the groundwater monitoring infrastructure was used to map hydraulic gradients, vertically and horizontally to understand the direction of the groundwater flow in the study area.

Correlation of change in water level with Rainfall and Irrigation: Rainfall data from the nearest rainfall station at Boundary Bend was downloaded from the Bureau of Meteorology (http://www.bom.gov.au/climate/data/index.shtml) to fill in the gaps in the incomplete rainfall data record from the Alma Almond Orchards farm. Similarly, the irrigation records of the Alma Almonds Orchards were collected for two months from May 2019 and June 2019. The recent data for months from July and August is not available so the irrigation data for the corresponding months from 2018 was used.

4.2.5 Real Time Kinematic Geographical Positioning System (GPS) Survey

A Trimble R10 surveying unit in RTX (satellite mode) was used to measure the location of all water monitoring infrastructure including drainage pits, test wells and bores within the study area**,** and State Government monitoring bores near to the study area **(Figure 4-9 & Appendix-2)**. In addition, the GPS survey was employed to get accurate geographical location data for the ERT and FDEM survey transects.

Figure 4-9: GPS survey

Figure 4-10: Collected groundwater samples

4.2.6 Water Sampling and Natural Tracers Measurements

Water samples were taken from drainage pits, test wells, groundwater bores, drainage outlets, and State Government monitoring bores during early May, mid-July, and early September. The groundwater samples were collected in four separate bottles each for analysing different parameters of water quality (**Figure 4-10).**

Well Purging

Unlike the process of water sample collection from the drainage pits, test wells, and discharge outlets, the groundwater monitoring infrastructure (piezometers and bores) were purged of three wells volumes before sampling to ensure a representative sample. Well purging is the process of taking out of stagnant water collected within the bores and the filter pack before sampling (Environment Protection Authority 2000).

Groundwater Quality Analysis

The subsequent analysis of water samples in the lab gives the measures of EC, pH, major ions and stable isotopes of hydrogen (2H) and Oxygen (18O) composition of water samples in the perched groundwater system and the regional groundwater (**Figure 4-10).** However, only the electrical conductivity and Chloride concentration data from different groundwater structures were used in this study to investigate the different water sources from the monitoring infrastructure.

5 RESULTS & ANALYSIS

This chapter comprises four sections. The first section is the results and data analysis of the ERT survey. The second section is the analysis and interpretation of the FDEM conductivity survey. The third section is an analysis of water level monitoring data from the piezometers within the almond grove orchard and State Government regional groundwater monitoring bores next to the study area. The fourth and final section is analysis of data from the shallow drainage network that has been installed to intercept the root zone drainage and to prevent waterlogging of the unsaturated zone.

5.1 Electrical Resistivity Tomography (ERT) Survey

The ERT survey was conducted in the study area to map the 2D lithology/ geology of the near-surface, and to examine the presence, thickness, and continuity of clay units and change in water content under irrigated Alma Almonds Orchards. The 2D resistivity profiles of the subsurface generated from ERT surveys for the north-south orientated 475 m and 237.5m long transects are shown in **Figure 5-1 & Figure 5-2**, respectively for the 3 field visits.

The resistivity distribution profile generated by ERT surveys was analysed and interpreted by comparing the resistivity with the lithological logs of the bores (e.g. p2s and p2d) located in Alma Almond Orchards parallel to the transect **(Figure 5-3)** and also using stratigraphy information from the state observation bores (**Figure 5-4)** which is represented in **Figure 3-5 & Figure 4-1 in chapter-3 & 4.**

The topography in the study area is naturally undulating and forms a distinct pattern of dune swales and ridges, which is also observed in the resistivity profiles (**Figures 5-1& 5-2).** In the resistivity profiles, the red colours represent more conductive material whereas the blue colours indicate resistive material as indicated in the legend at the bottom of the resistivity profile. Likewise, the material with intermediate resistivity value is represented by ranges of colour between red and blue, which includes yellow and green.

High resistivity dune ridge and Less resistive dune swale:

There is a significant change in the resistivity along the ridge and swales of the dunes showing the variation in thickness of the Woorinen Formation (1- 2 m thick at an elevation ranging from 54.5 mAHD – 52.5 mAHD), its lithology, water saturation content, and water quality. The ridge of the dunes forms the highly resistive material, which is due to the presence of sandy aeolian soil

deposits. Sand and silt content of the soil are electrically neutral and acts as good insulators (McNeill 1980), therefore sand generally has higher resistivity. The resistivity of the dune ridges ranges from 100 ohm.m to greater than 500 ohm.m. In the swales of dunes, the resistivity is lower and ranges from 8 ohm.m to 65 ohm.m, which can be due presence of more clay material, higher water saturation content and higher water salinity. Overall this thin layer at the near surface is continuous along the transect. The closest swale towards the northern end of the 475m transect has the least resistive values (i.e. highest conductivity) as represented by the orange layer. Likewise, the swale towards the southern end of the transect has also comparatively less resistive values compared to the ridge but higher than that of the swale at the northern end of the transect.

The lithological logs of the bores within the Alma Almonds orchards, which are parallel with the survey line and the stratigraphic cross-section of state bores verify the presence of the brown fine sand (aeolian sand deposits) in this area at an elevation between 57 to 55 mAHD is the Woorinen Formation **(Figure 5-3** & **Figure 5-4).**

Conductive Sandy Clay Alluvium: Underlying the Woorinen Formation is a less resistive sandy clay layer that has a resistivity of about 3 ohm.m (indicated by a dark and light orange band in the 2D resistivity profile). It is around 13-15 m in thickness at an elevation ranging from 52.5 mAHD to 40.5 mAHD and appears to be laterally continuous.

The lithological log of the bores within the study area showed the presence of different clayey sand layers comprised of red brown fine clayey sand, brown fine sandy clay and brown sandy clay with limestone **(Table 5-1).** Similarly, the comparison with the stratigraphic logs of the state observation bores suggested this conductive sandy clay formation to be an Alluvial Formation of around 13 m thickness **(Figure 5-3).** This Alluvium Formation comprises alluvial sediments from the Murray River Trough known as the Coonambidgal Formation and the Monoman Formation (Hoban & Daamen 2007).

Electrical resistivity is also dependent on the clay content and mineralogy and the salinity of the pore water along with other factors as the water content, the temperature (Revil et al. 2012). The lower resistivity values in this clayey Alluvial Formation can be both due to the clay content and higher salinity level. The plot of the measured chloride and electrical conductivity (EC) of the groundwater samples from the piezometers screened in this clayey layer (P1d & P3d) also showed higher concentrations of Cl and EC **(Figure 5-5 & Figure 5-6).**

Electrically conductive Blanchetown Clay layer:

Beneath the conductive Alluvium there is a slightly less conductive layer of 10 m thickness and with resistivity values between 8.31 ohm.m to 23.3 ohm.m. Comparing with the lithological details of the bores located in the vicinity of the study area and the stratigraphy information from the state bores confirmed the occurrence of a 19 m thick clay formation comprised of Grey Brown Medium Heavy Clay, Brown Fine Sandy Clay, Brown Clayey Fine Sand and Grey Silty Clay at an elevation ranging from 54.8 mAHD to 35.57 mAHD **(Figure 5-1 and Figure 5-3).** This formation is known as the Blanchetown Clay which at the study site is around 10 m thick.

It is important to note the conductivity of the overlying alluvium has a higher conductivity value than the Blanchetown Clay. This can be due to higher EC and Cl contents in the alluvium, therefore, increasing its conductivity **(Figure 5-5 & Figure 5-6).**

Resistive Parilla Sands layer:

Beneath the Blanchetown Clay, there is another layer (dark green continuous layer) which has higher resistivity values around 65.5 ohm.m at an elevation of 30.5 mAHD to much greater depths of the resistivity profile. The lithological logs of the bores verified the presence of Brown Fine Sand similar to the sand formation on the top of the profile **(Table 5-1).** The stratigraphic logs of state bores parallel to the ERT transect showed the presence of Parilla Sands underlying the Blanchetown Clay layer.

However, the resistivity of the similar brown fine sand layer is different than the one deposited at the top which can be due to the salinity level of the pore water in the sand. Fresh irrigation water is resistive, and the saturated brown fine sand on the land's surface would also have a higher resistivity compared to clay. In contrast, the sand layer of the Parilla Sands aquifer beneath the Blanchetown Clay is filled with highly less resistive saline groundwater such that the resultant resistivity is less.

The plot of chloride (Cl) and electrical conductivity (EC) of the water samples from piezometers, state bores, drainage pits, and test wells showed that the EC and chloride concentration of the piezometers (P2d) and all state bores screening the Parilla sands has highest EC and Cl concentration (**Figure 5-5 & Figure 5-6).**

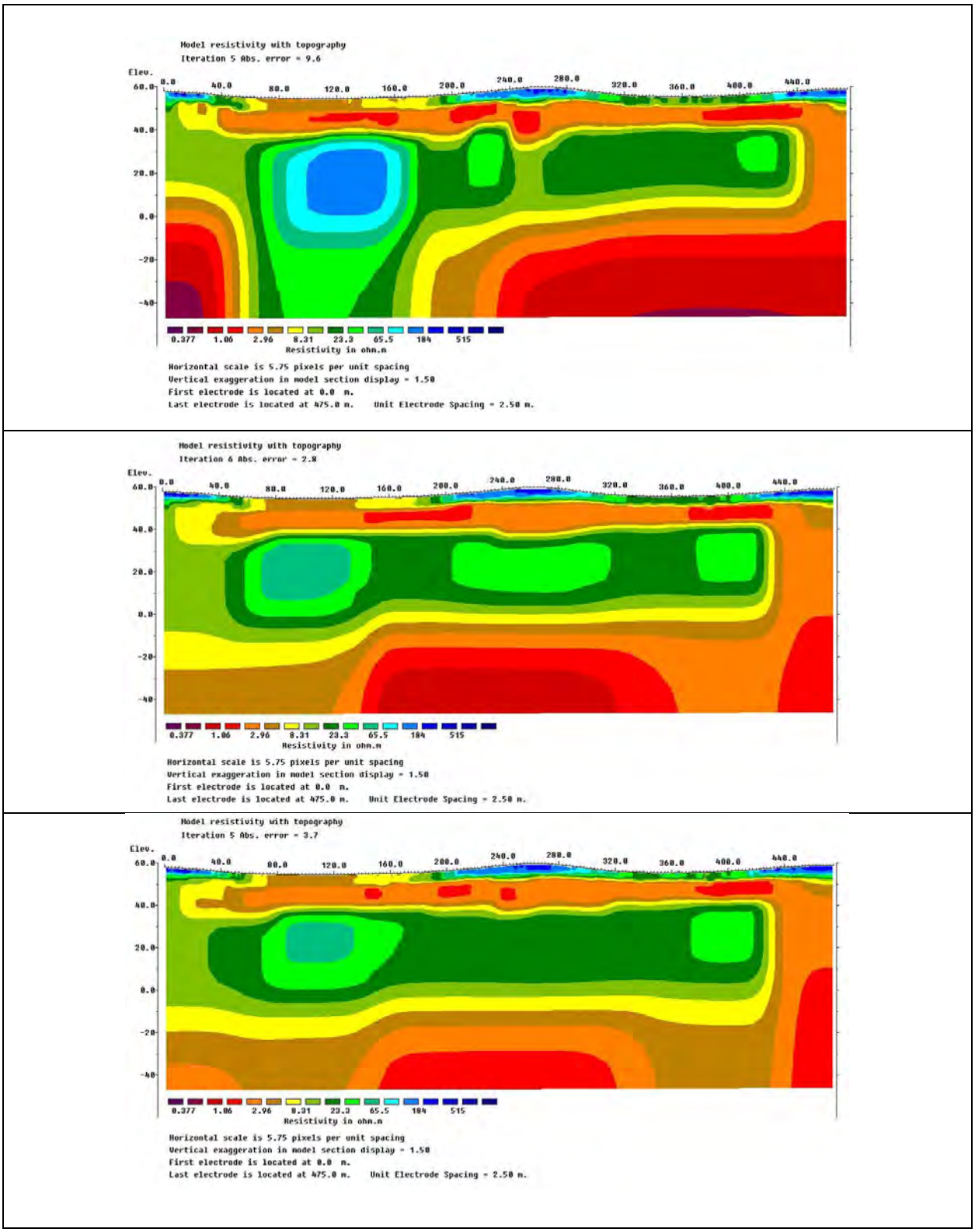

Figure 5-1: 2D resistivity cross sections for Wenner-Schlumberger array along the 475m north-south orientated transect (north at the left hand side and south end at the right hand side of the profile) for May 2019 (top), July 2019 (middle) and September 2019 (bottom).

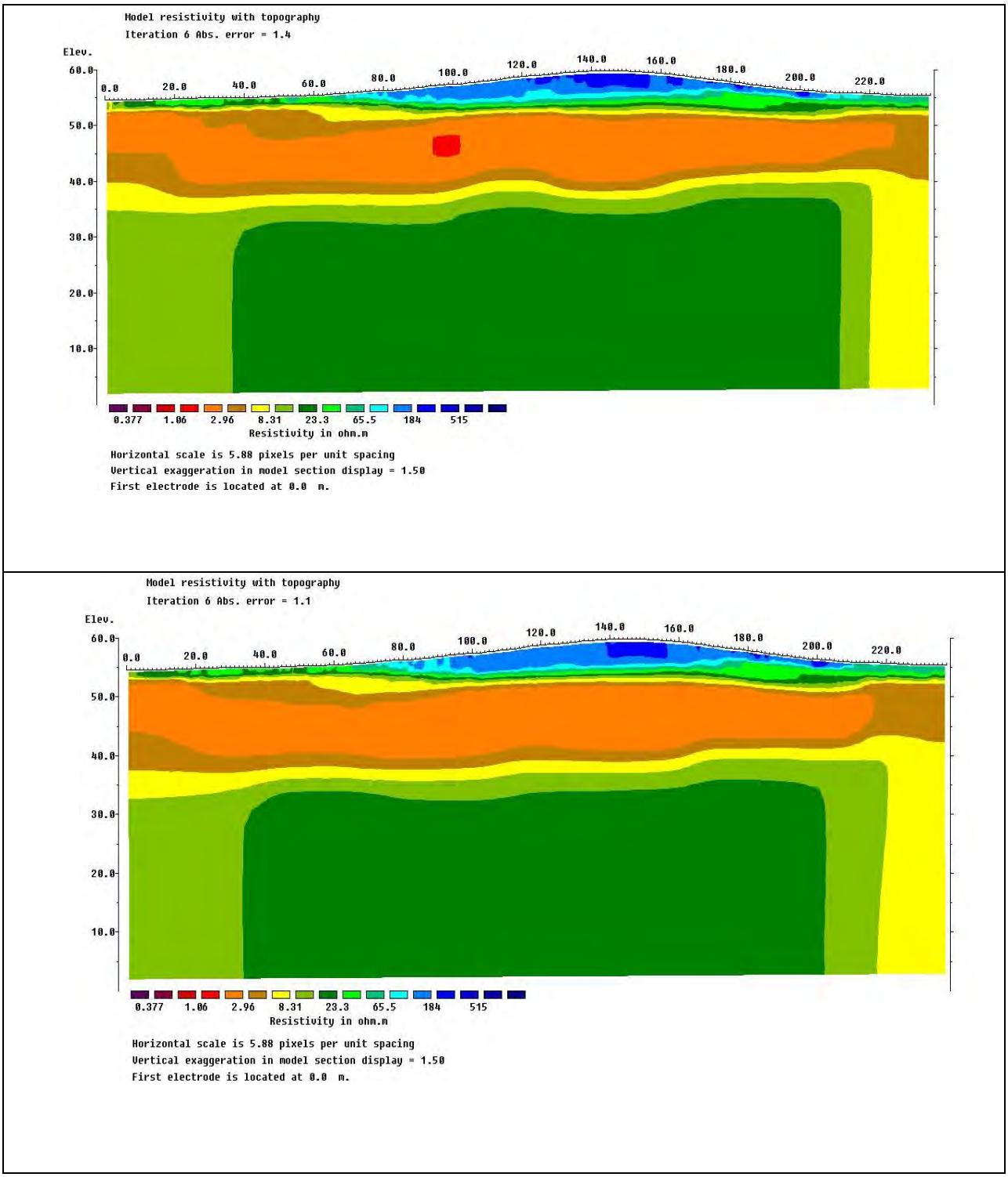

Figure 5-2: 2D resistivity cross sections for Wenner-Schlumberger array along the 237.5m north-south orientated transect (north at the left hand side and south end at the right hand side of the profile) for July 2019 (top) and September 2019 (bottom).

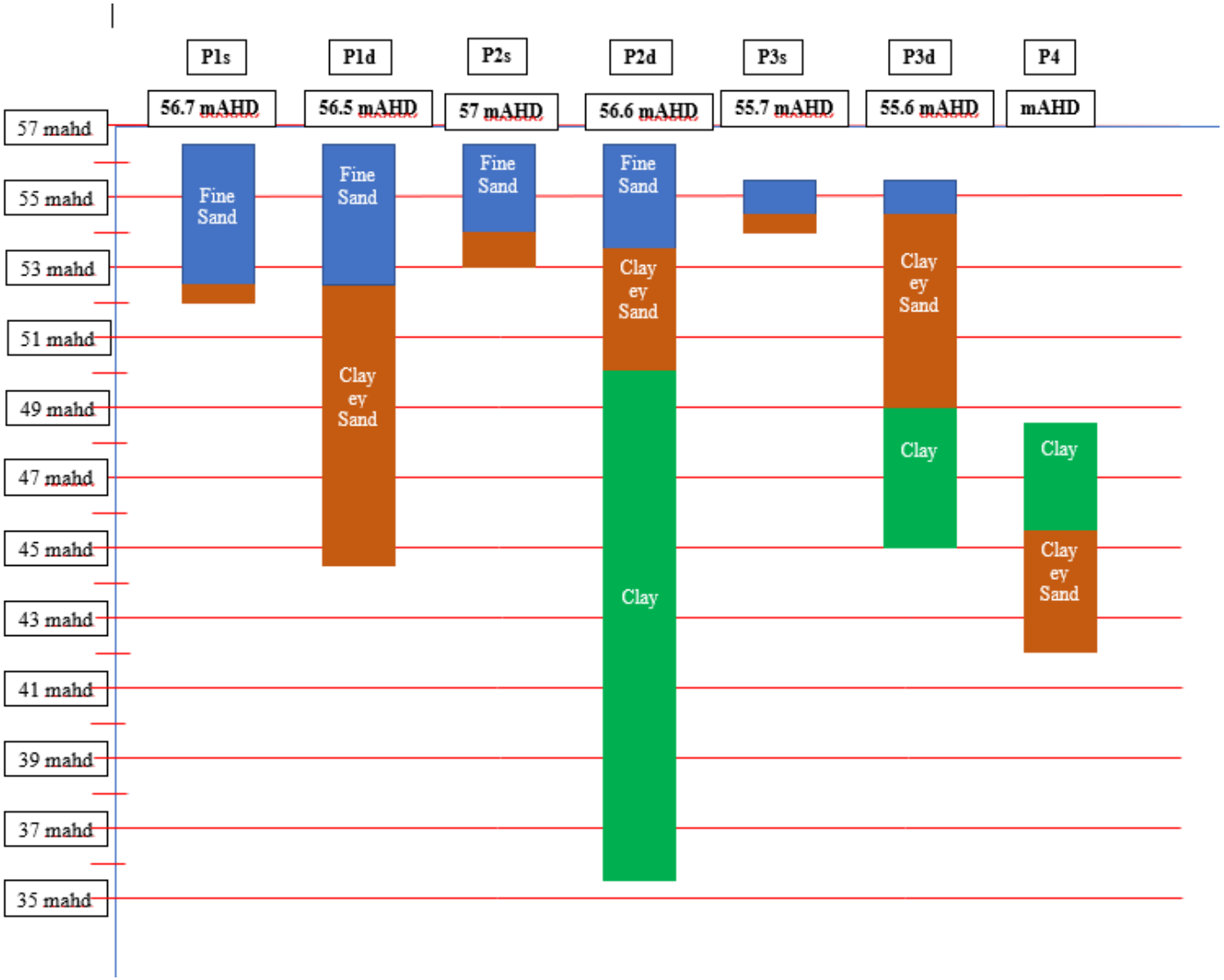

Figure 5-3:Lithological logs of the seven piezometers located in the study area parallel to the ERT transect

Table 5-1: Lithological logs of the seven piezometers located in the study area parallel to the ERT transect.

Bore	**p2d**	**p2s**	**p1d**	**p1s**	**p3s**	**p3d**	**p4**
Brown Fine Sand	56.57	56.95	56.52	56.65	55.78	55.63	
Red Brown Fine Clayey Sand	53.57	53.95	52.52	52.65	54.78	54.63	
Brown Fine Sandy Clay	52.07						
Brown Sandy Clay with Limestone			51.52	52.15			
Grey Brown Med Heavy clay	50.07	52.95			54.28	49.13	48.67
Brown Fine Sandy Clay	45.57		48.52				45.67
Brown Clayey Fine Sand	37.57		44.52				
Grey Silty Clay	35.57						
White Brown Silty Clay						47.13	
Brown Fine Sand						45.13	
Brown Med Fine Sand							42.17

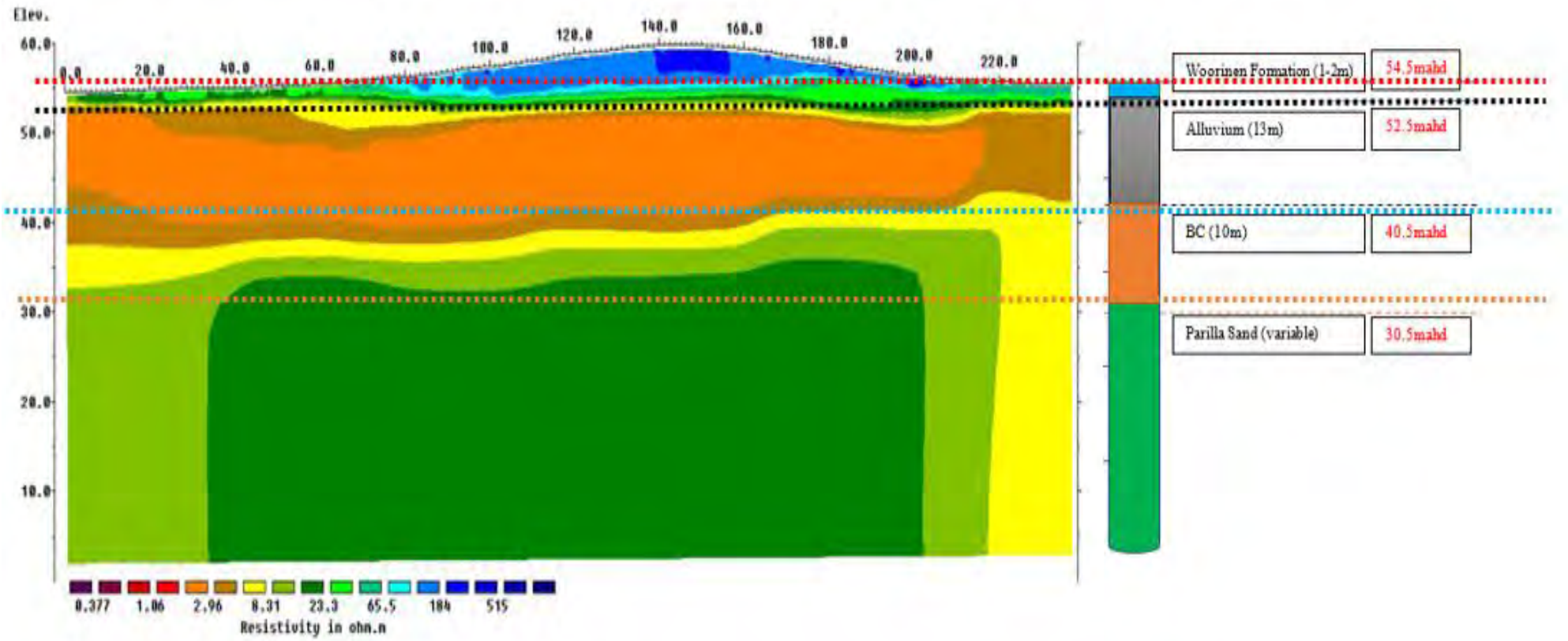

Figure 5-4: Comparison of the 2D resistivity profile along the 237.5m long transect with the stratigraphic logs of the state bores. Here the Blanchetown Clay layer is referred as BC.

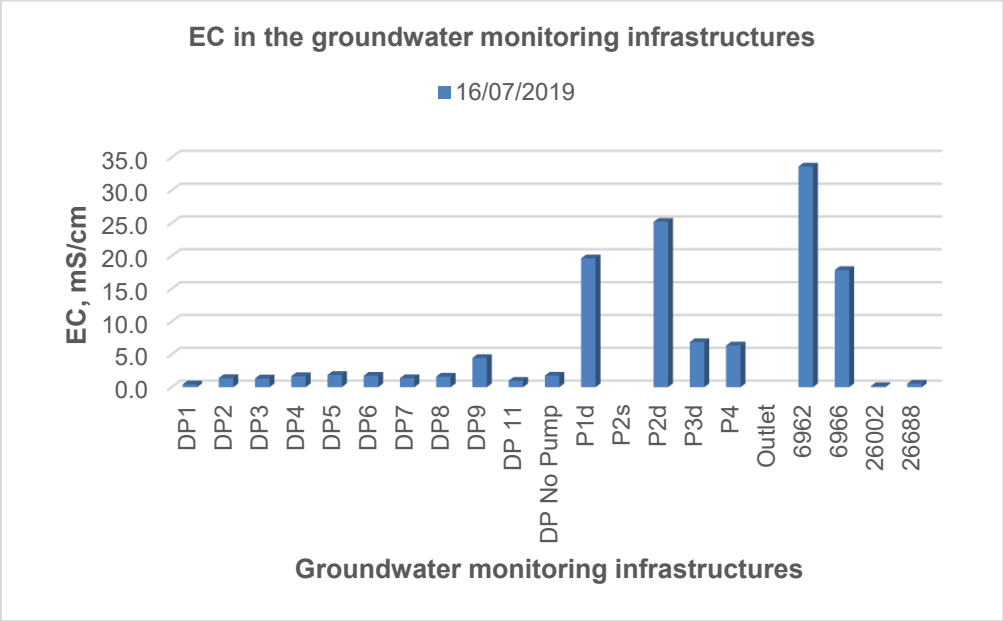

Figure 5-5: Electrical conductivity (mS/cm) in the different water monitoring infrastructure.

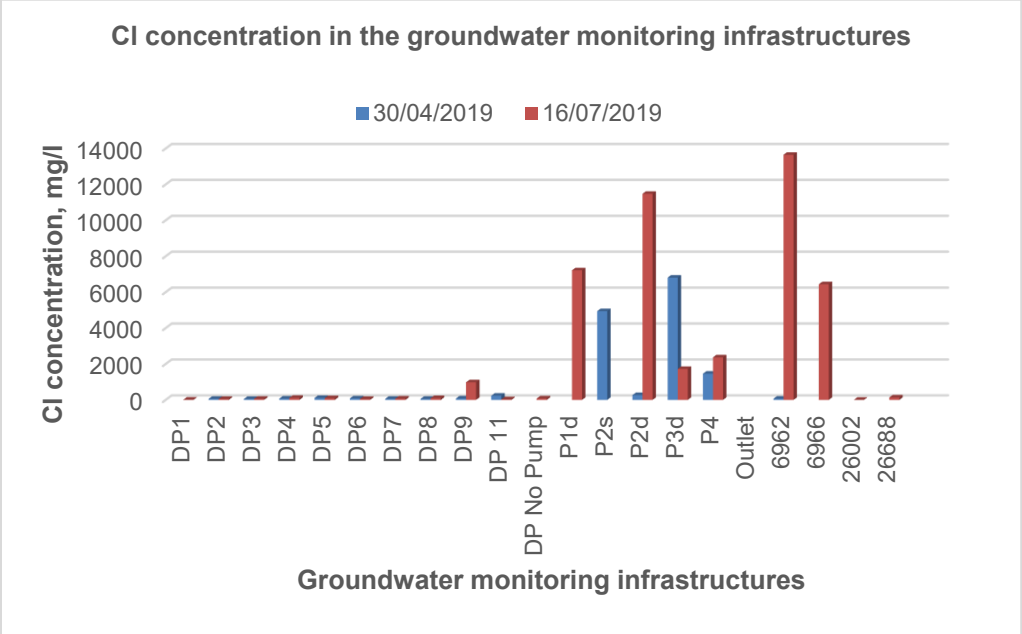

Figure 5-6: Chloride concentration (mg/L) in the different water monitoring infrastructure

Perched Water Table Conditions Above the Blanchetown Clay

Clay generally acts as a confining and semi-confining layer in the groundwater system and which significantly impedes vertical groundwater flow through it (Knight et al. 2018). The resistivity profile from the ERT surveys in the study area and the lithological logs of the bores confirmed the existence of the thick alluvial and Blanchetown Clay layer underneath the study area. Here the conductive alluvial and Blanchetown Clay in the study area acts as an imperfect aquitard where it likely forms perched water table/ aquifer conditions over the Blanchetown Clay. Therefore, repeated geophysical resistivity surveys were conducted with an aim to investigate the perched groundwater system, in three different months at the end of April/early May, mid-July and early September. The change in resistivity values indicates the change in water content in the subsurface (Schlosser 2017), which helps to investigate whether the water is perching or not over the Blanchetown Clay layer. Besides the change in water content, the change in resistivity is governed by the salinity of the water in the pore space.

However, it is not easy to visualise a distinct change in resistivity from the 2D resistivity profile from the ERT survey from different months. Therefore, time lapse resistivity (TLR) calculation from repeated ERT surveys at different times enables estimation of the temporally dynamic soil properties such as water content and pore water electrical conductivity. In the following section, the time lapse resistivity is calculated between May-July and between July-September.

Calculation of variation in resistivity between May-July

The percentage change in the resistivity values between early May and mid-July was calculated using time lapse resistivity based on the data that was collected using the Wenner-Schlumberger array for the 475 m long transect (**Figure 5-7).**

The large increase in the apparent resistivity can be observed near the ground surface where there is a 100% to 200% change at a depth of 10 m in the Alluvium. However, there is no change in resistivity under the dunes at 200m to 300m along the transect and there was no change in resistivity in the remaining area of the profile as the geology does not change and there is not much change in water and salt content. The overall increase in apparent resistivity in the near subsurface can be due to an increase in soil water content following rainfall in the month of July. On the other hand, the flushing of the salts from the topsoil downwards can result in a decrease in resistivity values because of the higher salinity content of the water.

Timelapse calculation of the variation in resistivity between mid-July to early September

Time lapse resistivity was used to calculate the percentage variation in the apparent resistivity measurements between mid-July to early September with the Wenner-Schlumberger array for the 475 m long transect (**Figure 5-8)** and for 237.5 m long transect (**Figure 5-9).**

Large resistivity variations were observed near the surface at less than 10m depth in Alluvium, although the change is not as large was observed between May to July. The increase in resistivity ranges are around 50% to 150%, which showed an overall decline in resistivity from July-September. The overall decline in apparent resistivity from July to September can be due to a decline in water content with less rainfall towards the end of the winter rains. In addition, the flushing of more salts by rainfall infiltration downwards by the end of the rainy season can cause an overall decline in resistivity. The time lapse resistivity between mid-July and early September for the higher resolution 237.5 m long transect situated along the ridge of the sand dune showed no significant change in resistivity during that time. However, the Alluvium layers beneath the dune has become less resistive by around 30% which can be due to flushing of salts downwards from winter rain.

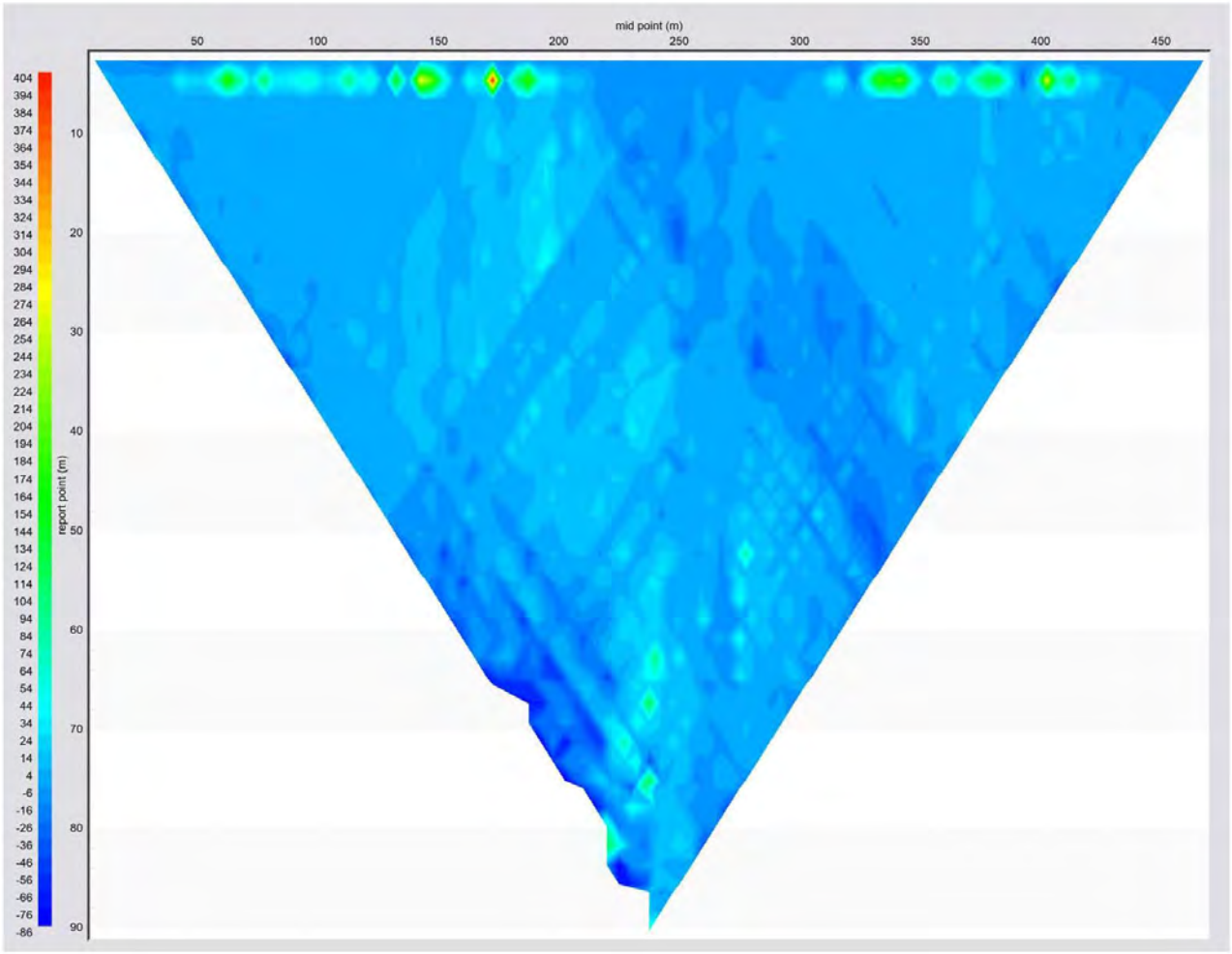

Figure 5-7: Percentage change in resistivity between early May and mid-July using time lapse resistivity for the Wenner-Schlumberger array along the 475 m long transect. The vertical axis shows the percentage change in resistivity between early May and mid-July.

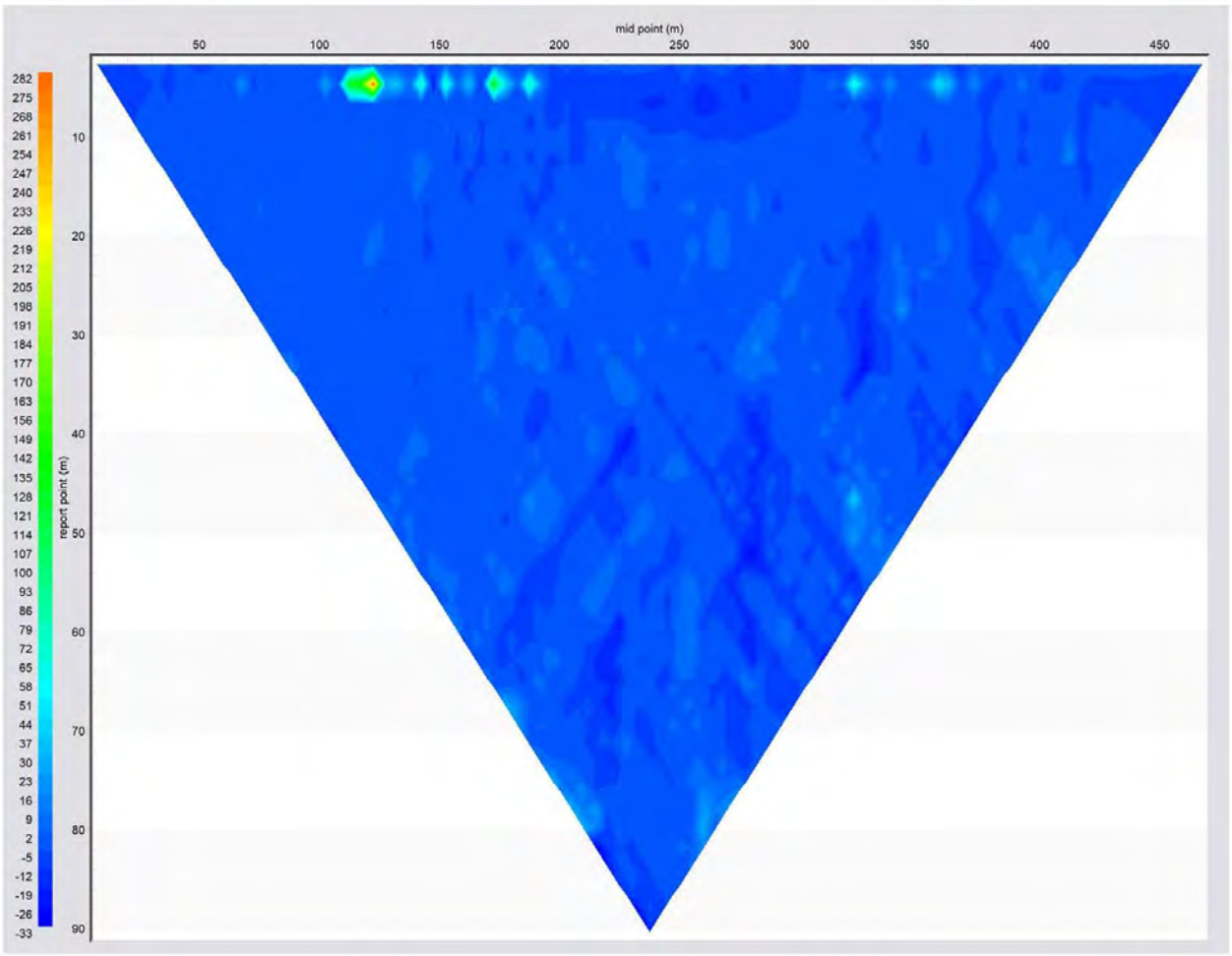

Figure 5-8: Percentage change in resistivity between mid-July and early September using time lapse resistivity for the Wenner-Schlumberger array along the 475 m long transect. The vertical axis shows the percentage change in resistivity between mid-July and early September. Note Scale change from the previous figure.

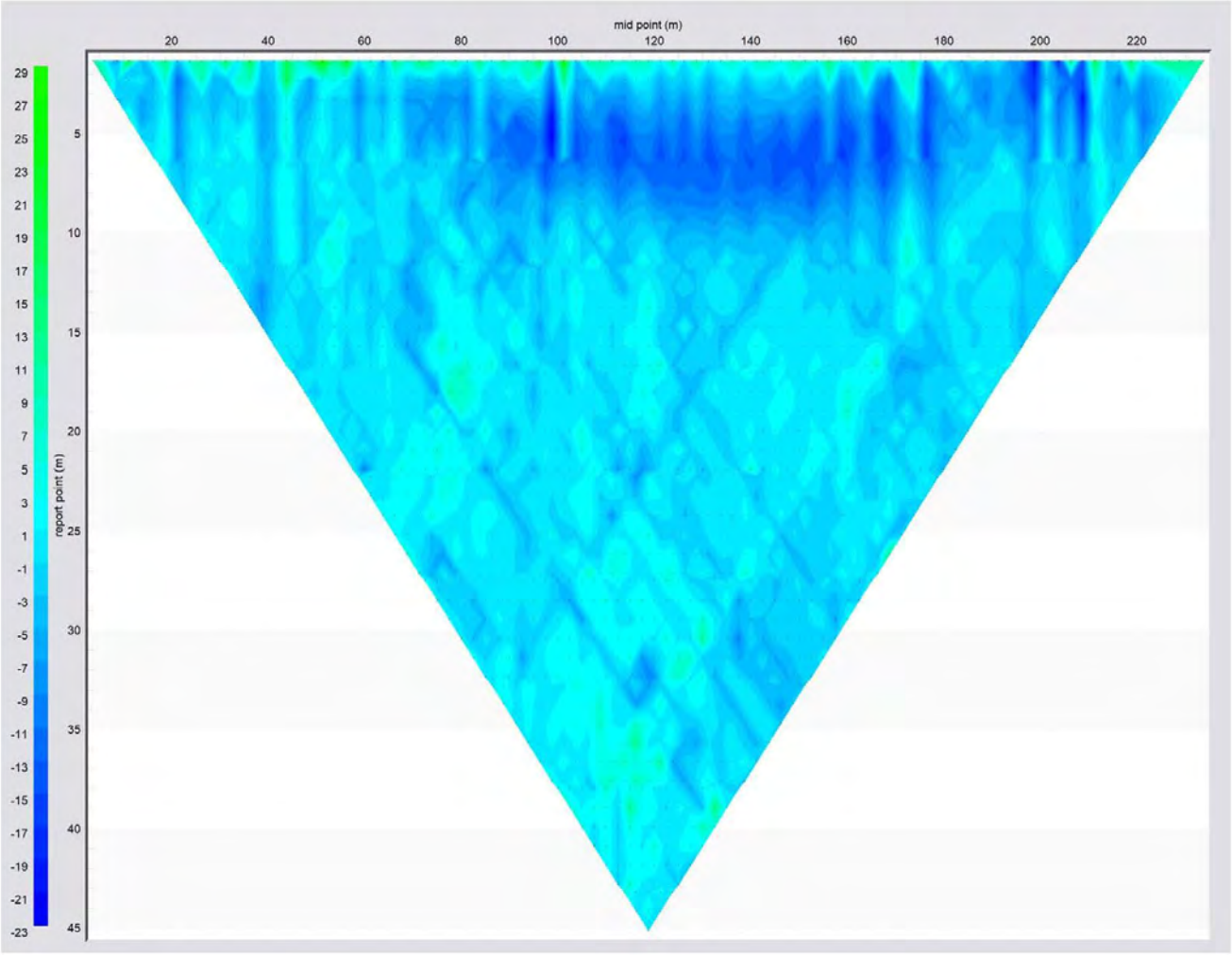

Figure 5-9: Percentage change in resistivity between mid-July and early September using time lapse ERT for resistivity measurement with the Wenner-Schlumberger array along the 237.5 m long transect. The vertical axis shows the percentage change in resistivity between mid-July and early September. Note scale change from the previous figure.

Summary of the electrical resistivity profiles

The resistance of particular subsurface geological formation or rock is influenced by various geological properties such as the clay content in lithology, saturation or water content, the porosity, and the concentration of dissolved salts (Barrett et al. 2002; Brindt, Rahav & Wallach 2019; Loke 2000). The resistivity values of the sedimentary rock and sediments is comparatively lower due to its porous nature and its higher water content in its pores, which conducts electricity (Knight et al. 2018; Loke 2000).

The analysis of the 2D resistivity confirmed the occurrence of the 13 m thick conductive Alluvial Formation- Alluvium, which is underlain by a 10 m thick Blanchetown Clay and that this clay rich alluvial layer is laterally extensive across the study area. The clay has significantly high surface conduction because it has a relatively high surface area (Knight et al. 2018).

The time lapse calculation of the resistivity in different months showed high resistivity variations, especially near subsurface within less than 10m depth. This can be due to variation in infiltration in the subsurface from the rainfall and irrigation, which is varied in different months/ season. In addition, the flushing of salts from topsoil to subsurface following the rainy season can also be accounted for by this high variation in resistivity in the near subsurface.

5.2 Frequency Domain Electromagnetic Induction Conductivity Survey

FDEM conductivity surveys were conducted along 13 transects across the study area as shown in **Figure 4-2 in Chapter 4**. Whilst the ERT surveys confirmed the occurrence of the Alluvium and the Blanchetown Clay Formation at one part of the study area, FDEM was used to investigate the continuity of the clay layers in the study area with it rapid acquisition time.

The terrain conductivity meter (CMD-Explorer) outputs three conductivity values which are sensitive to three depth ranges that are based on the coil transmitter and receiver coil separation distances of the instrument. Conductivity-1 corresponds to the bulk conductivity over 2.2m, conductivity-2 over 4.2 m and conductivity-3 over a depth of 6.7m

The variation of all conductivity values (Conductivity 1,2 & 3) along all 13 survey transects with respect to elevation is shown in **Figure 5-10.** As observed in **Figure 5-10**, conductivity is generally

low at the ridge of the dune and high in the dune swale in all the transects. The highest & the lowest conductivity value was with the shallowest depth range (2.2m); 310 and 4 mS/m, respectively. The findings from the FDEM survey were similar to the results of the ERT surveys, which also found that the conductivity is higher in the swale and lower at the ridge of the dunes. This somewhat confirms that the transects selected for the ERT surveys are representative of the study area

Similarly, the conductivity at 2.2m depth (conductivity-1) for all the 13 transects were plotted against elevation variation along the transects and showed two important outcomes (**Figure 5-11)**. Firstly, the conductivity decreases with an increase in ground elevation and vice versa, which aligned with the finding from the ERT survey Figure 5-10). This variation of conductivity with elevation across the study area can be accounted for the variation in the surfaces and stratigraphy of the geological formations. As discussed earlier in **Section 5.1.1,** the sandy resistive soil occurred on the elevated ridges of the dune, while conductive clays exist in the low-lying swale region of dune in the study area. Secondly, the conductivity value at a specific elevation for all the transects is similar, which infer the existence of the uniform and laterally continuous lithology throughout the study area.

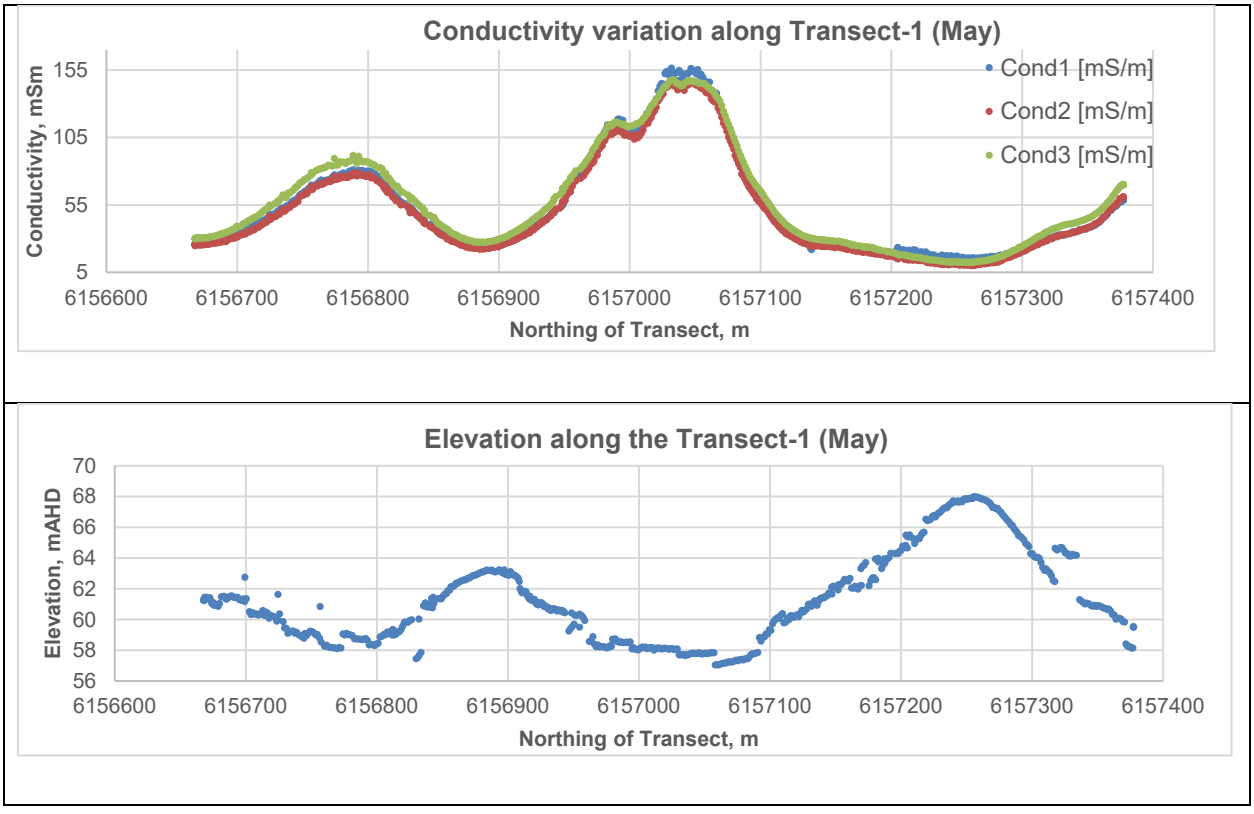

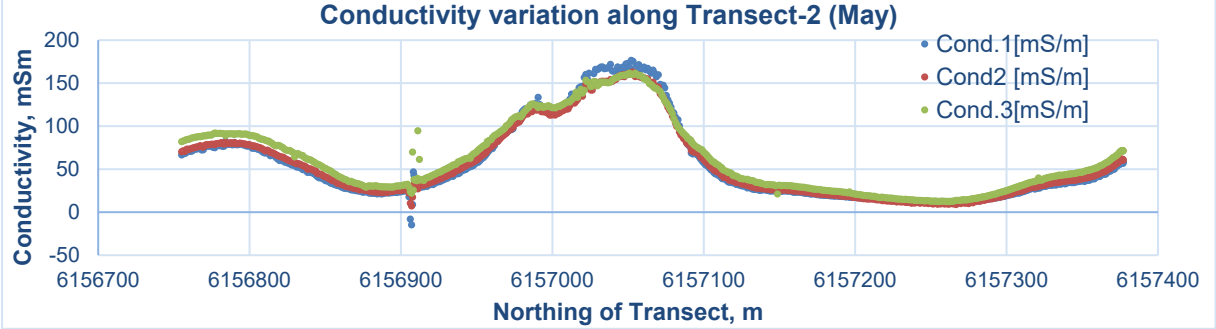
Conductivity variation along Transect-2 (May)
Conductivity, mSm
200
150
100
50
0
-50
6156700
6156800
6156900
6157000
6157100
6157200
6157300
6157400
Northing of Transect, m
Cond.1[mS/m]
Cond2 [mS/m]
Cond.3[mS/m]

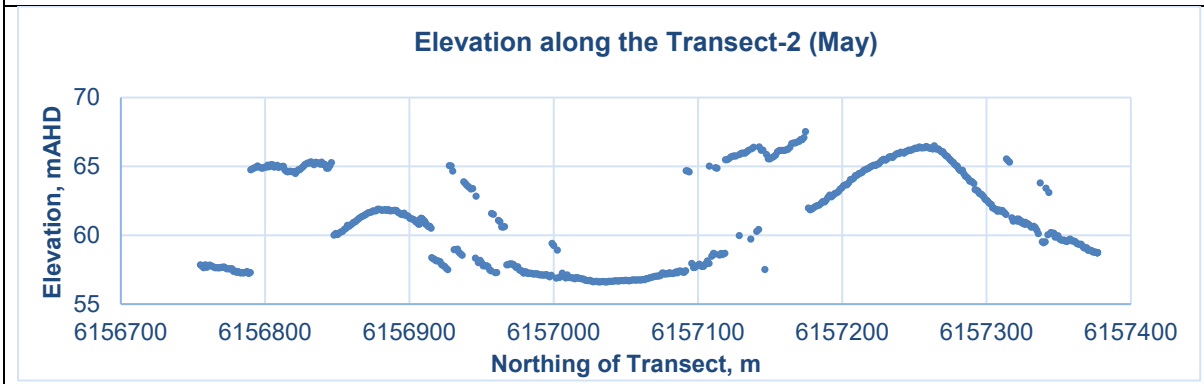
Elevation along the Transect-2 (May)
Elevation, mAHD
70
65
60
55
6156700
6156800
6156900
6157000
6157100
6157200
6157300
6157400
Northing of Transect, m

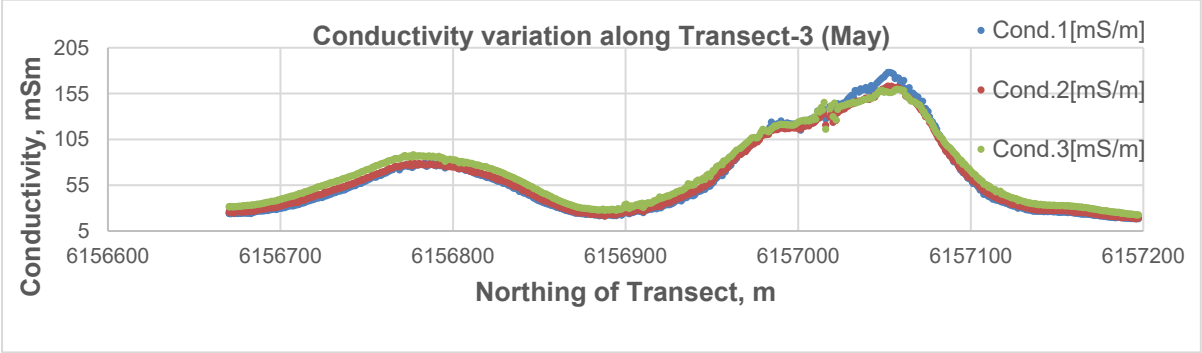
Conductivity variation along Transect-3 (May)
Conductivity, mSm
205
155
105
55
5
6156600
6156700
6156800
6156900
6157000
6157100
6157200
Northing of Transect, m
Cond.1[mS/m]
Cond.2[mS/m]
Cond.3[mS/m]

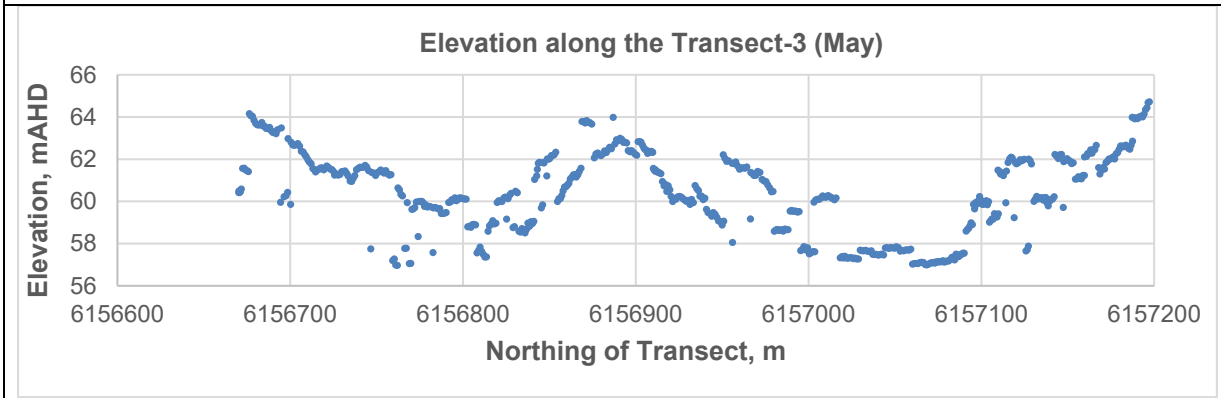
Elevation along the Transect-3 (May)
Elevation, mAHD
66
64
62
60
58
56
6156600
6156700
6156800
6156900
6157000
6157100
6157200
Northing of Transect, m

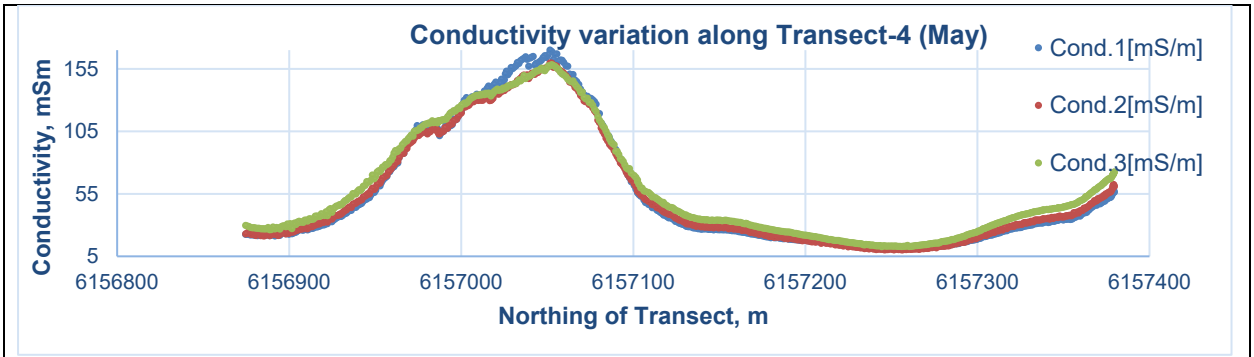
Conductivity variation along Transect-4 (May)
Conductivity, mSm
155
105
55
5
6156800
6156900
6157000
6157100
6157200
6157300
6157400
Northing of Transect, m
Cond.1[mS/m]
Cond.2[mS/m]
Cond.3[mS/m]

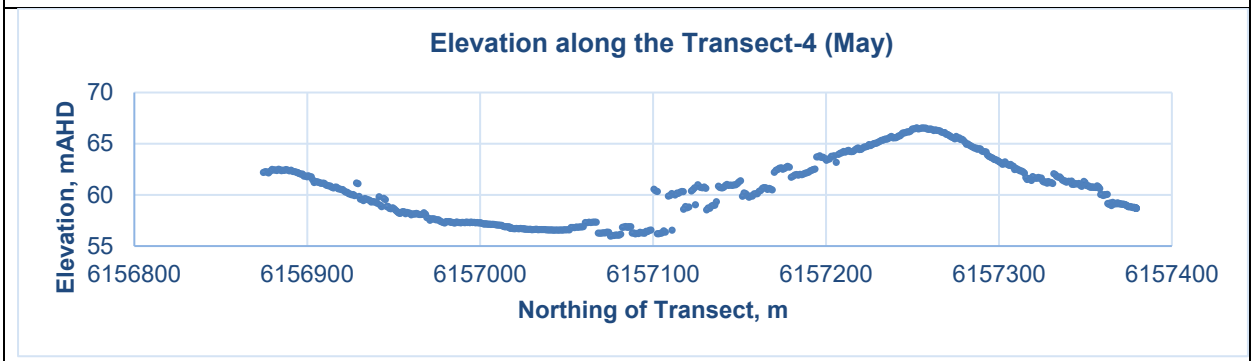
Elevation along the Transect-4 (May)
Elevation, mAHD
70
65
60
55
6156800
6156900
6157000
6157100
6157200
6157300
6157400
Northing of Transect, m

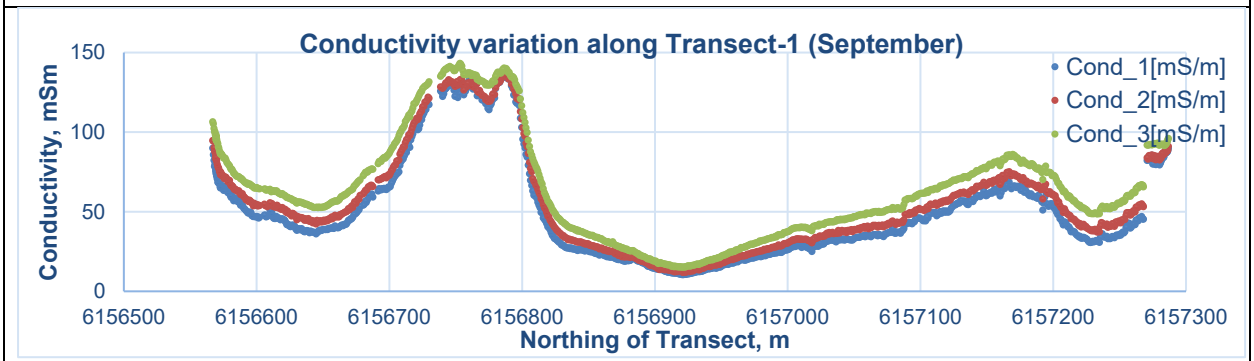
Conductivity variation along Transect-1 (September)
Conductivity, mSm
150
100
50
0
6156500
6156600
6156700
6156800
6156900
6157000
6157100
6157200
6157300
Northing of Transect, m
Cond_1[mS/m]
Cond_2[mS/m]
Cond_3[mS/m]

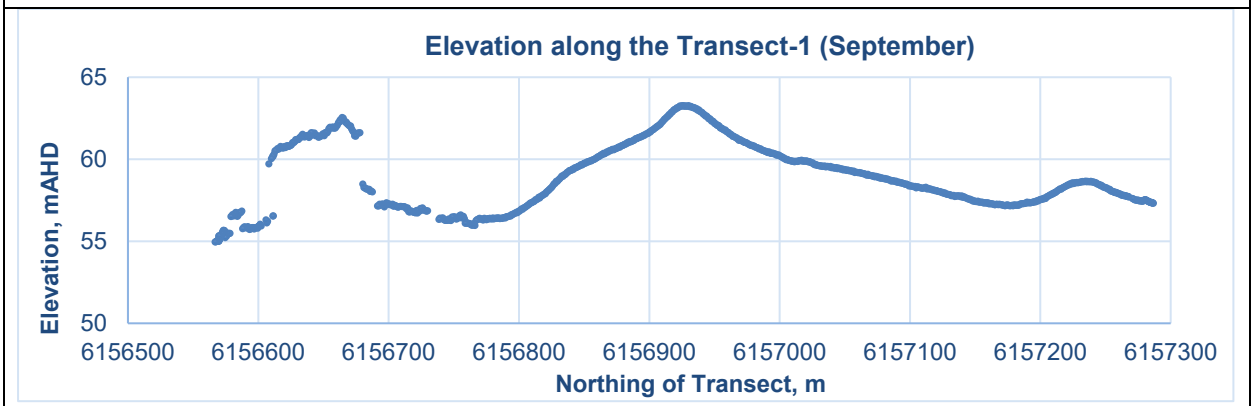
Elevation along the Transect-1 (September)
Elevation, mAHD
65
60
55
50
6156500
6156600
6156700
6156800
6156900
6157000
6157100
6157200
6157300
Northing of Transect, m

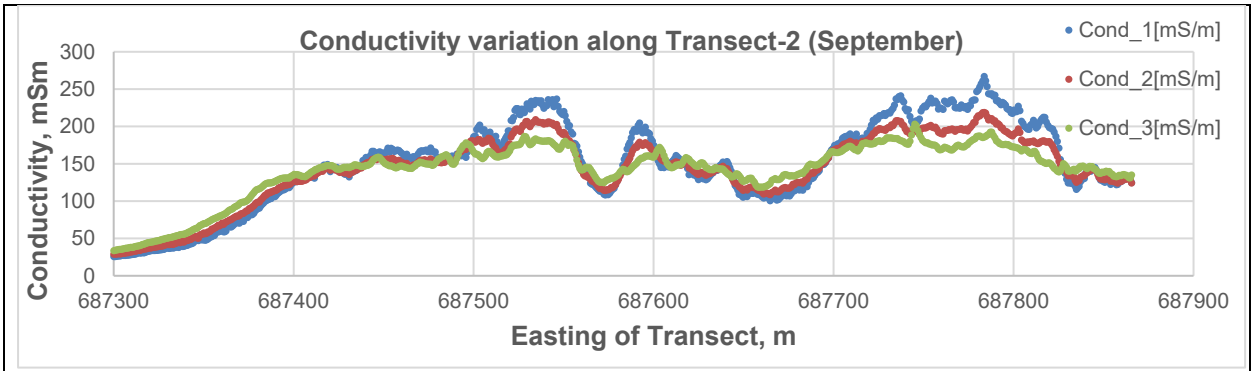
Conductivity variation along Transect-2 (September)
Cond_1[mS/m]
Cond_2[mS/m]
Cond_3[mS/m]
Conductivity, mSm
300
250
200
150
100
50
0
687300
687400
687500
687600
687700
687800
687900
Easting of Transect, m

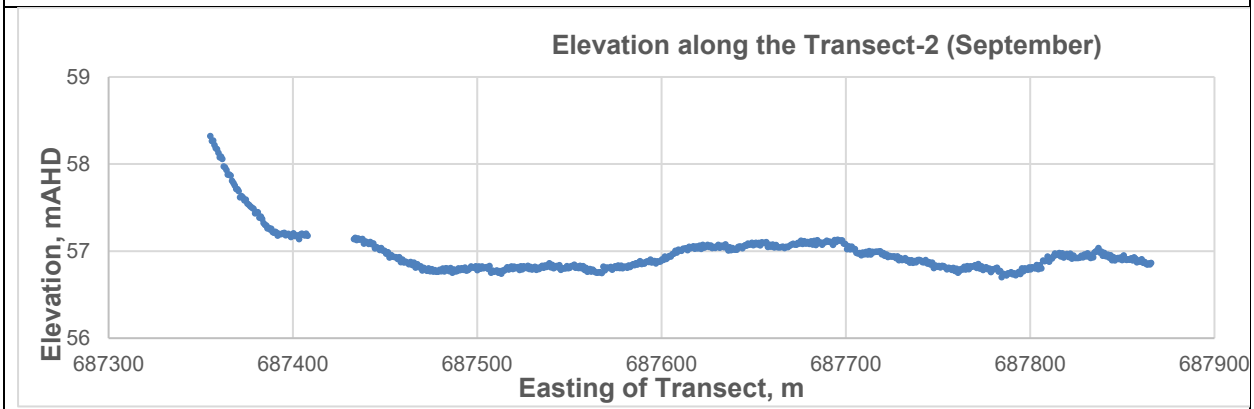
Elevation along the Transect-2 (September)
Elevation, mAHD
59
58
57
56
687300
687400
687500
687600
687700
687800
687900
Easting of Transect, m

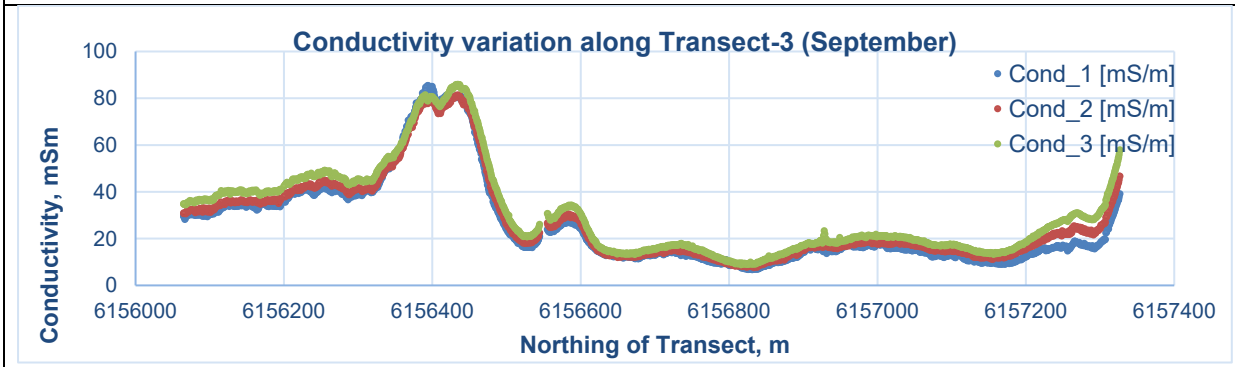
Conductivity variation along Transect-3 (September)
Cond_1 [mS/m]
Cond_2 [mS/m]
Cond_3 [mS/m]
Conductivity, mSm
100
80
60
40
20
0
6156000
6156200
6156400
6156600
6156800
6157000
6157200
6157400
Northing of Transect, m

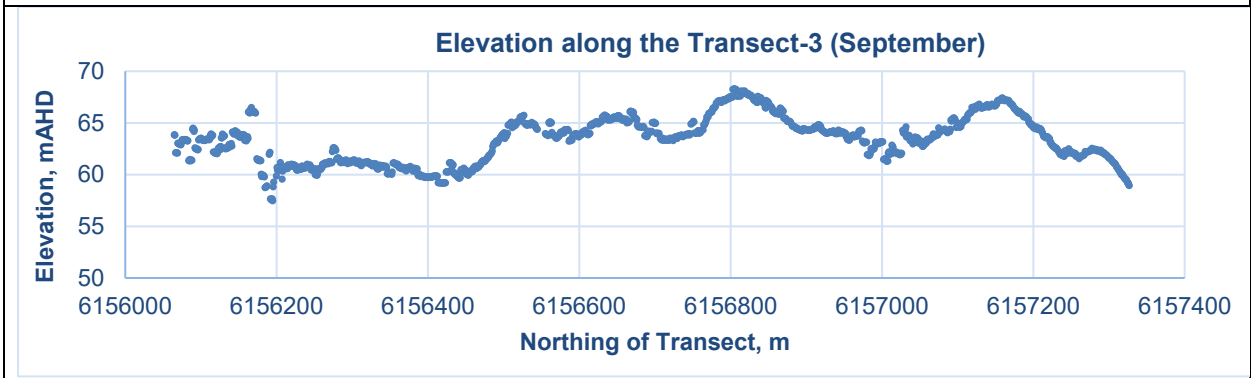
Elevation along the Transect-3 (September)
Elevation, mAHD
70
65
60
55
50
6156000
6156200
6156400
6156600
6156800
6157000
6157200
6157400
Northing of Transect, m

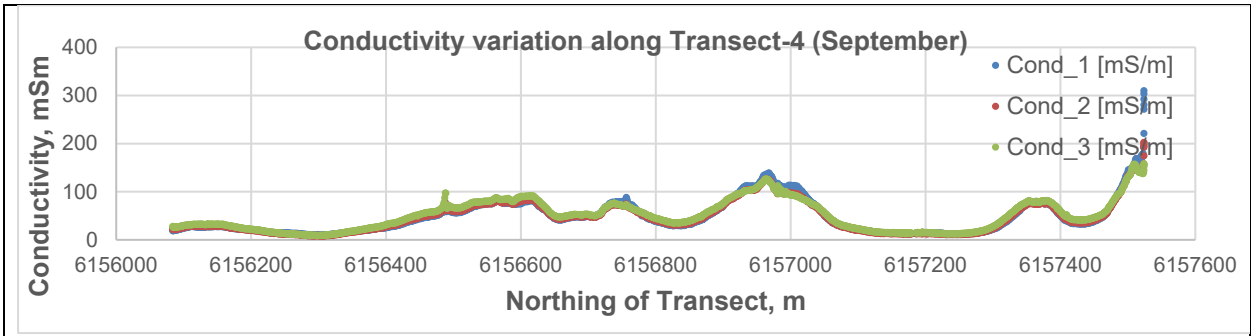
Conductivity variation along Transect-4 (September)
Conductivity, mSm
400
300
200
100
0
6156000
6156200
6156400
6156600
6156800
6157000
6157200
6157400
6157600
Northing of Transect, m
Cond_1 [mS/m]
Cond_2 [mS/m]
Cond_3 [mS/m]

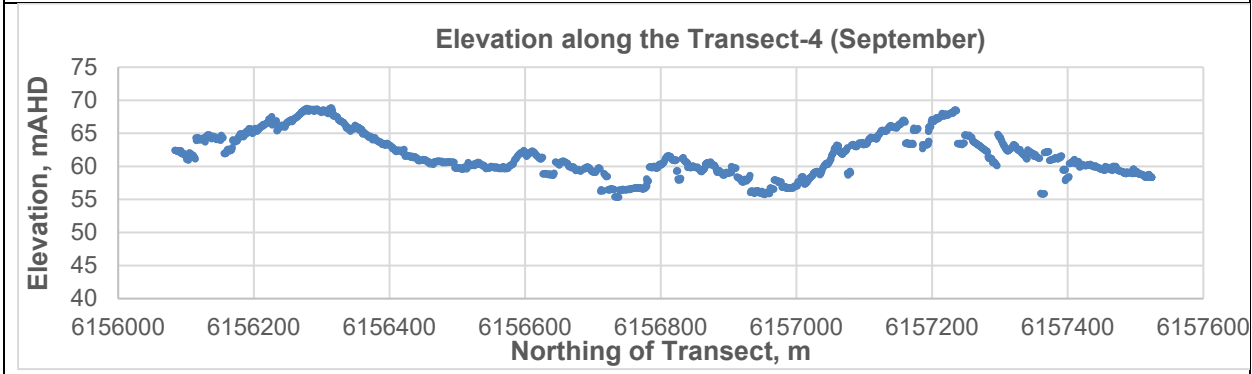
Elevation along the Transect-4 (September)
Elevation, mAHD
75
70
65
60
55
50
45
40
6156000
6156200
6156400
6156600
6156800
6157000
6157200
6157400
6157600
Northing of Transect, m

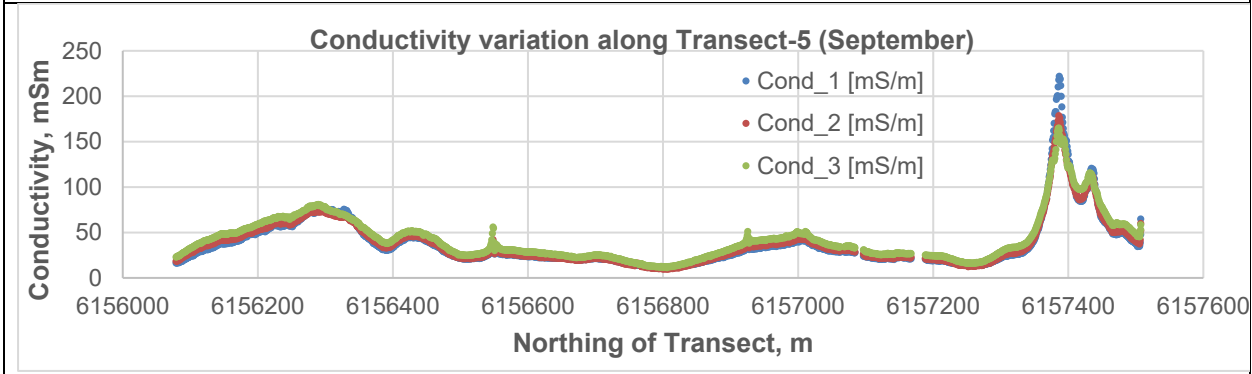
Conductivity variation along Transect-5 (September)
Conductivity, mSm
250
200
150
100
50
0
6156000
6156200
6156400
6156600
6156800
6157000
6157200
6157400
6157600
Northing of Transect, m
Cond_1 [mS/m]
Cond_2 [mS/m]
Cond_3 [mS/m]

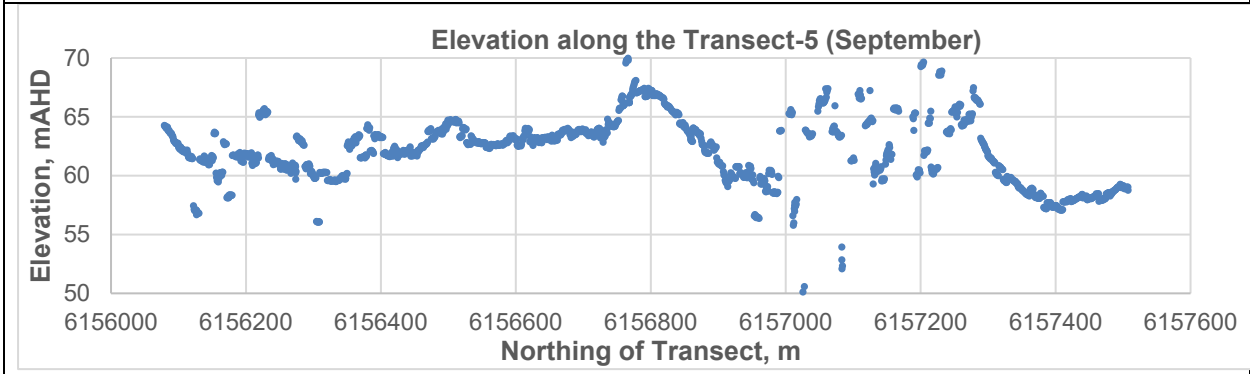
Elevation along the Transect-5 (September)
Elevation, mAHD
70
65
60
55
50
6156000
6156200
6156400
6156600
6156800
6157000
6157200
6157400
6157600
Northing of Transect, m

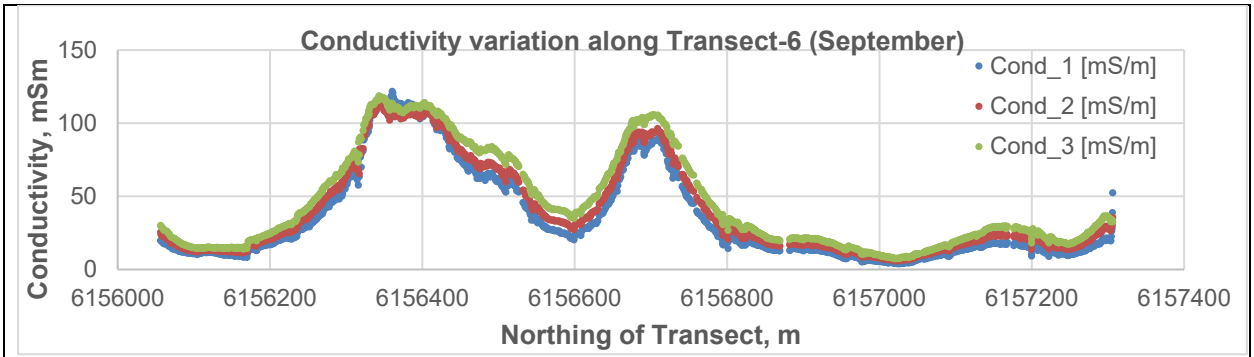
Conductivity variation along Transect-6 (September)
Conductivity, mSm
150
100
50
0
6156000
6156200
6156400
6156600
6156800
6157000
6157200
6157400
Northing of Transect, m
Cond_1 [mS/m]
Cond_2 [mS/m]
Cond_3 [mS/m]

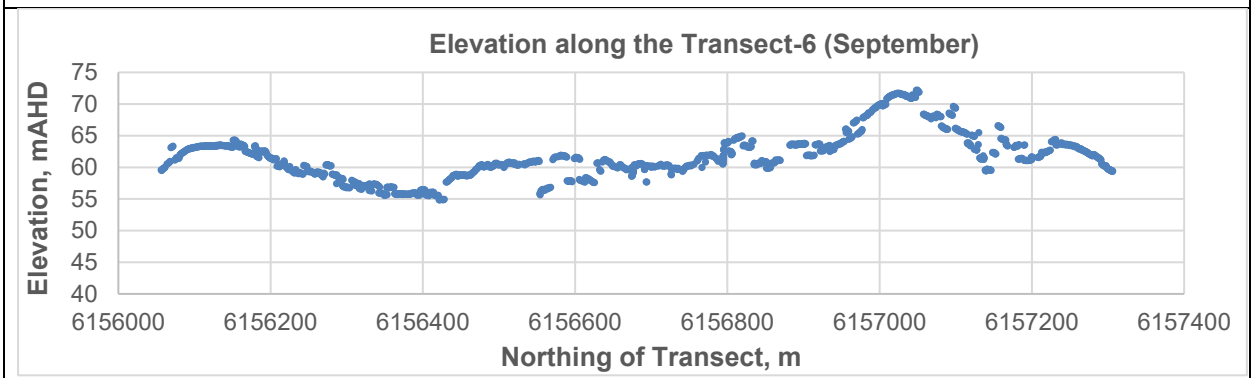
Elevation along the Transect-6 (September)
Elevation, mAHD
75
70
65
60
55
50
45
40
6156000
6156200
6156400
6156600
6156800
6157000
6157200
6157400
Northing of Transect, m

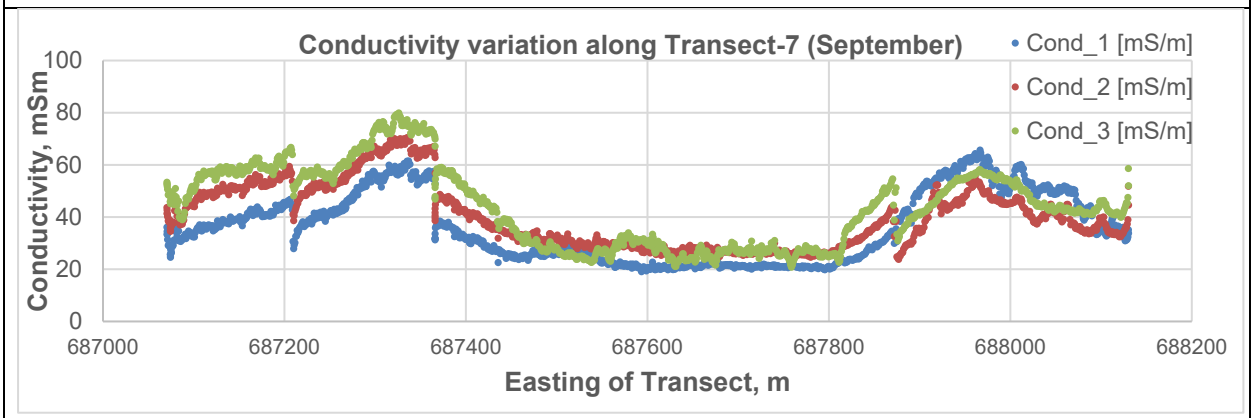
Conductivity variation along Transect-7 (September)
Conductivity, mSm
100
80
60
40
20
0
687000
687200
687400
687600
687800
688000
688200
Easting of Transect, m
Cond_1 [mS/m]
Cond_2 [mS/m]
Cond_3 [mS/m]

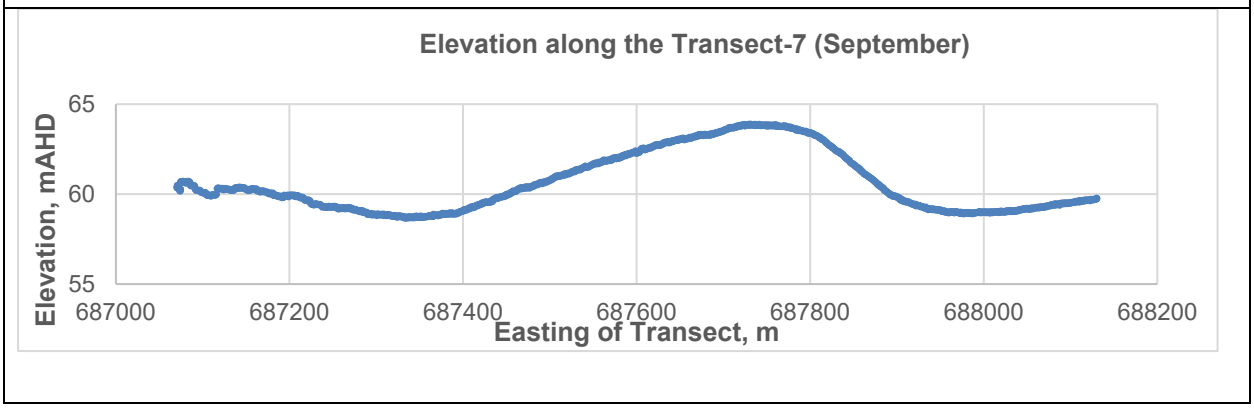
Elevation along the Transect-7 (September)
Elevation, mAHD
65
60
55
687000
687200
687400
687600
687800
688000
688200
Easting of Transect, m

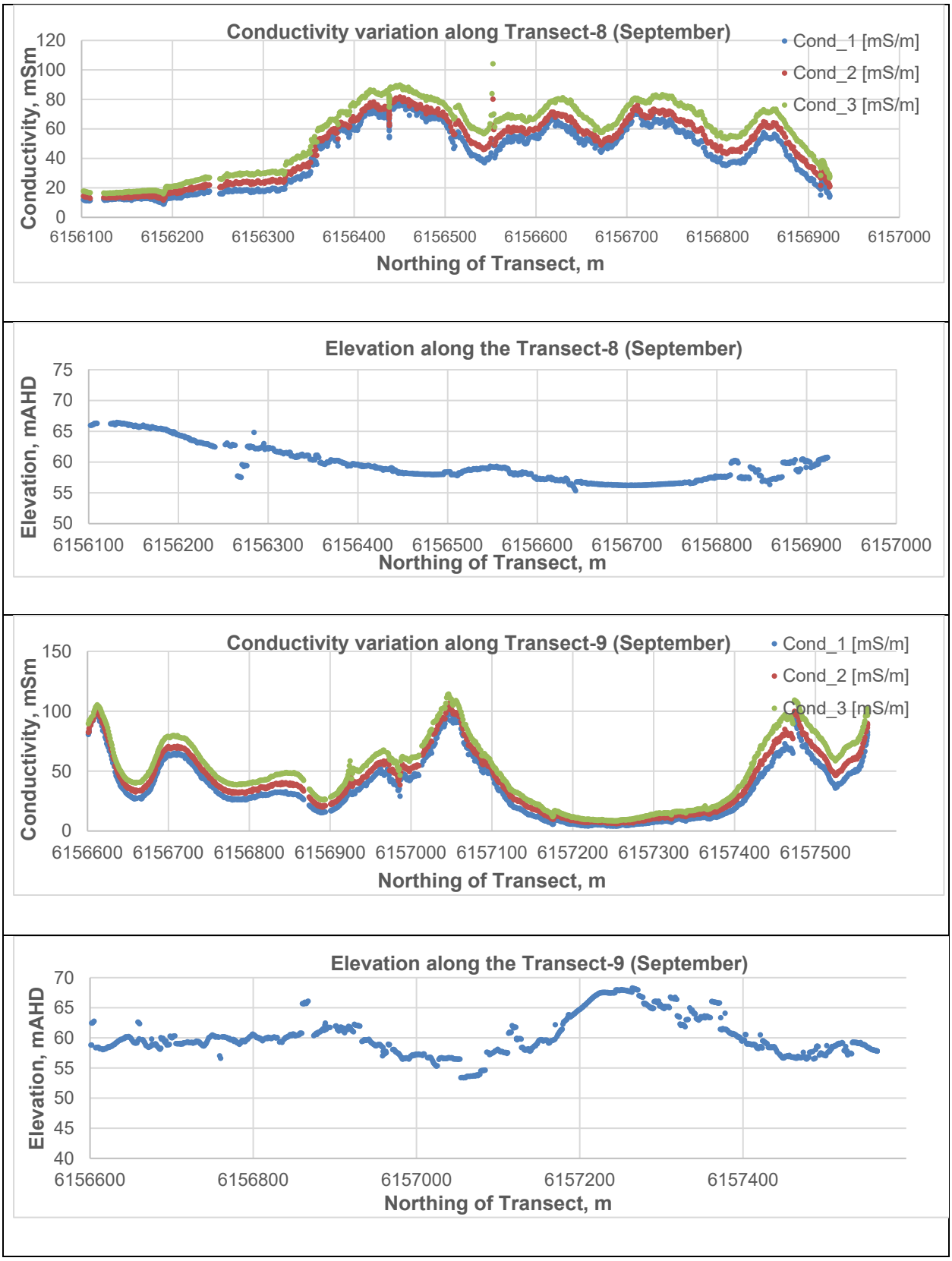

Figure 5-10: Measured bulk conductivity using the terrain conductivity meter along the transects across the survey area (Figure 4-2) from May 2019 and September 2019.

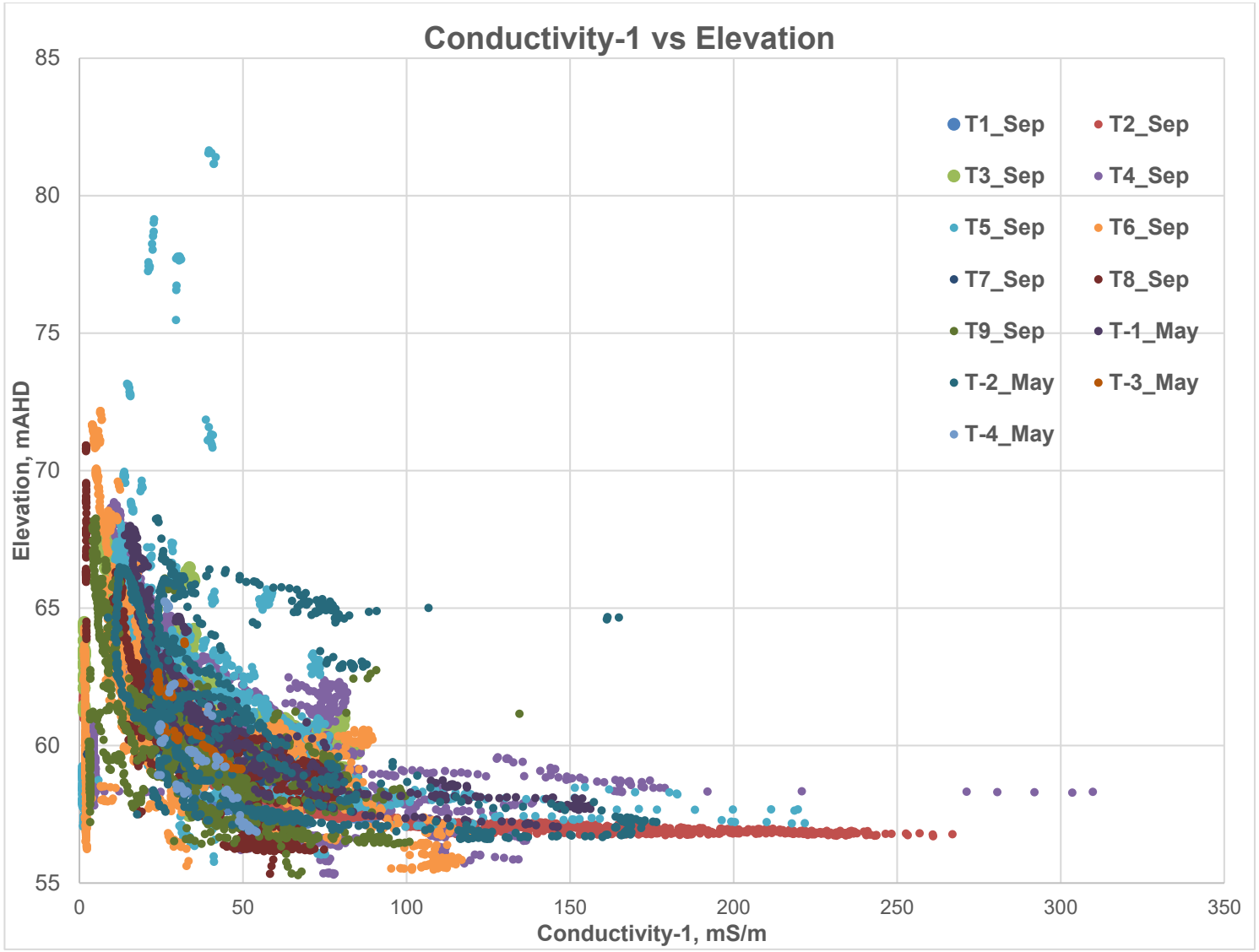

Figure 5-11: Relationship of conductivity-1 with elevation for all FDEM surveys conducted across the study area.

5.3 Monitoring groundwater level

The water level in both the local groundwater system and the regional groundwater systems were monitored by installing pressure transducers in test wells, drainage pits, and piezometers in the study area and state bores in the vicinity. The main objective of monitoring these groundwater structures was to investigate whether the perching of the aquifer occurred underneath the irrigated almond farm.

In the following sections, the water level monitoring data of the regional aquifer and perched aquifer are analysed and described which is followed by the section which seeks to examine the correlation of water levels data with irrigation and rainfall.

5.3.1 Monitoring water level in regional Parilla Sands Aquifer

The regional groundwater was monitored through four-state bores namely, 26002, 26688, 6962 and 6966 and a deep bore P2d, which are screened in the regional Parilla Sands aquifer.

The reduced standing water level (RSWL) time series data in the state bores (from 17 July 2019 to 3 September 2019) and P2d bore (April to September) shows that there was only a slight change in the overall water level during the monitored time period. The water level progressively rises by less than 10 cm from mid-July and peaked in early August and then declines gradually in all bores (**Figure 5-12)**. A longer period of monitoring, years to several of years would be necessary to evaluate the seasonal responses in the water levels and changes to the hydraulic gradients in the aquifer. The average RSWL from the bores screened in the regional Parilla Sands aquifer ranges from 48.5 mAHD to 50.7 mAHD.

The water level in these monitored bores is plotted along with the total depth of the groundwater monitoring infrastructure, screen depth, and screened geological formation (**Figure 5-13).** The four monitored state observation bores are in a transect in north-south direction **(Figure 3-2)** and the hydraulic gradient of the regional Parilla Sands aquifers is from the south towards the Murray River in the north **(Figure 5-13).** The water level in the southmost bore, 6962 is 50.7 mAHD, and that of the northernmost bore is 48.52mAHD while the two bores (6966 & 26688) located in between bores, 6962 in south and 26002 in north, is 49.45 mAHD, and the water table is located within the alluvium formation as observed in **Figure 5-13.**

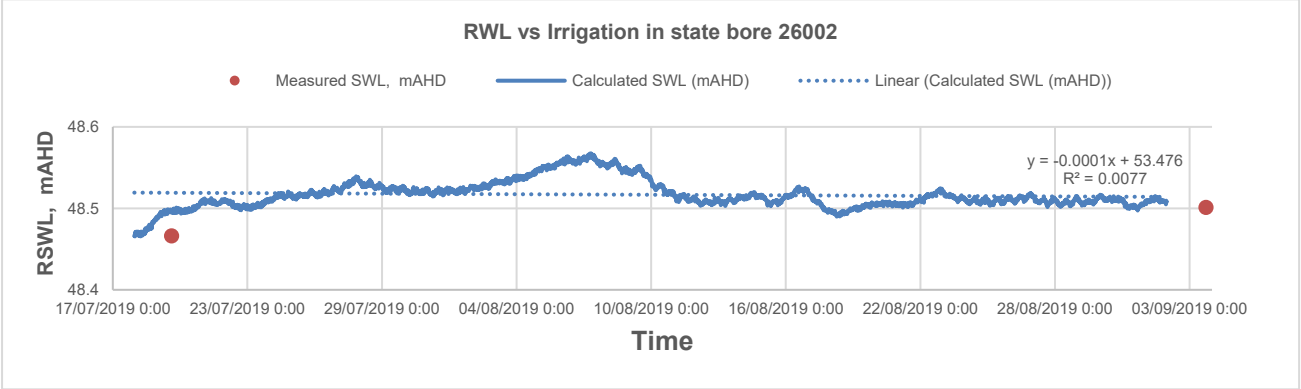
RWL vs Irrigation in state bore 26002
Measured SWL, mAHD
Calculated SWL (mAHD)
Linear (Calculated SWL (mAHD))
RSWL, mAHD
48.6
48.5
48.4
y = -0.0001x + 53.476
R² = 0.0077
17/07/2019 0:00
23/07/2019 0:00
29/07/2019 0:00
04/08/2019 0:00
10/08/2019 0:00
16/08/2019 0:00
22/08/2019 0:00
28/08/2019 0:00
03/09/2019 0:00
Time

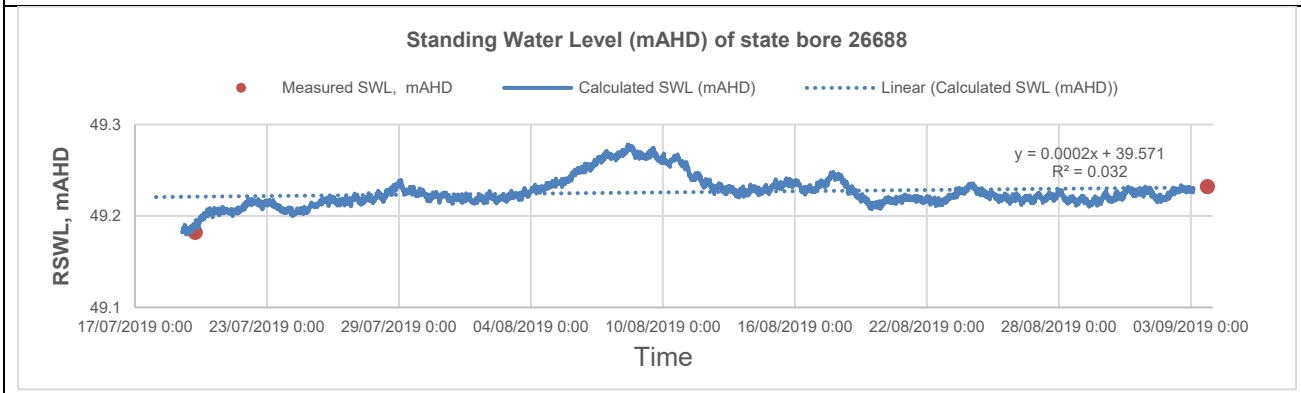
Standing Water Level (mAHD) of state bore 26688
Measured SWL, mAHD
Calculated SWL (mAHD)
Linear (Calculated SWL (mAHD))
RSWL, mAHD
49.3
49.2
49.1
y = 0.0002x + 39.571
R² = 0.032
17/07/2019 0:00
23/07/2019 0:00
29/07/2019 0:00
04/08/2019 0:00
10/08/2019 0:00
16/08/2019 0:00
22/08/2019 0:00
28/08/2019 0:00
03/09/2019 0:00
Time

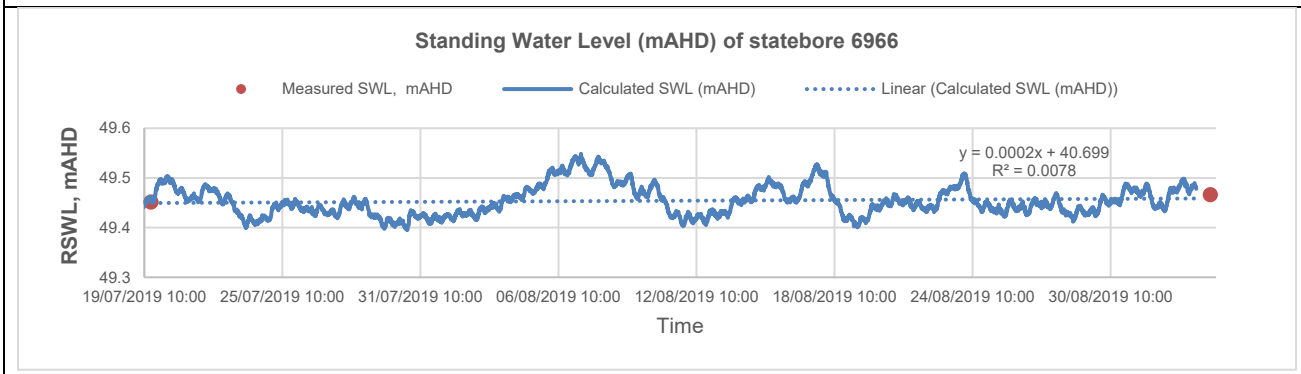
Standing Water Level (mAHD) of statebore 6966
Measured SWL, mAHD
Calculated SWL (mAHD)
Linear (Calculated SWL (mAHD))
RSWL, mAHD
49.6
49.5
49.4
49.3
y = 0.0002x + 40.699
R² = 0.0078
19/07/2019 10:00
25/07/2019 10:00
31/07/2019 10:00
06/08/2019 10:00
12/08/2019 10:00
18/08/2019 10:00
24/08/2019 10:00
30/08/2019 10:00
Time

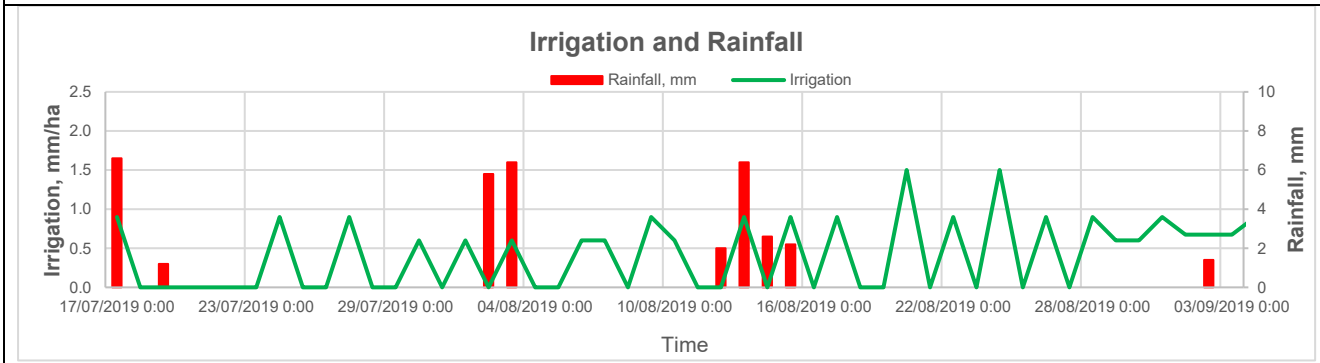
Irrigation and Rainfall
Rainfall, mm
Irrigation
Irrigation, mm/ha
2.5
2.0
1.5
1.0
0.5
0.0
Rainfall, mm
10
8
6
4
2
0
17/07/2019 0:00
23/07/2019 0:00
29/07/2019 0:00
04/08/2019 0:00
10/08/2019 0:00
16/08/2019 0:00
22/08/2019 0:00
28/08/2019 0:00
03/09/2019 0:00
Time

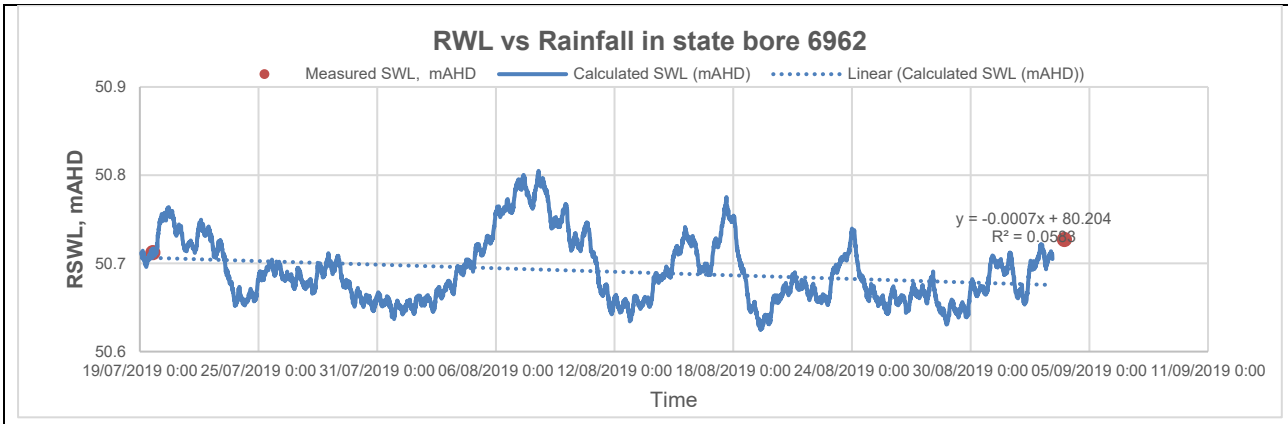
RWL vs Rainfall in state bore 6962
Measured SWL, mAHD
Calculated SWL (mAHD)
Linear (Calculated SWL (mAHD))
RSWL, mAHD
50.9
50.8
50.7
50.6
y = -0.0007x + 80.204
R² = 0.0588
19/07/2019 0:00
25/07/2019 0:00
31/07/2019 0:00
06/08/2019 0:00
12/08/2019 0:00
18/08/2019 0:00
24/08/2019 0:00
30/08/2019 0:00
05/09/2019 0:00
11/09/2019 0:00
Time

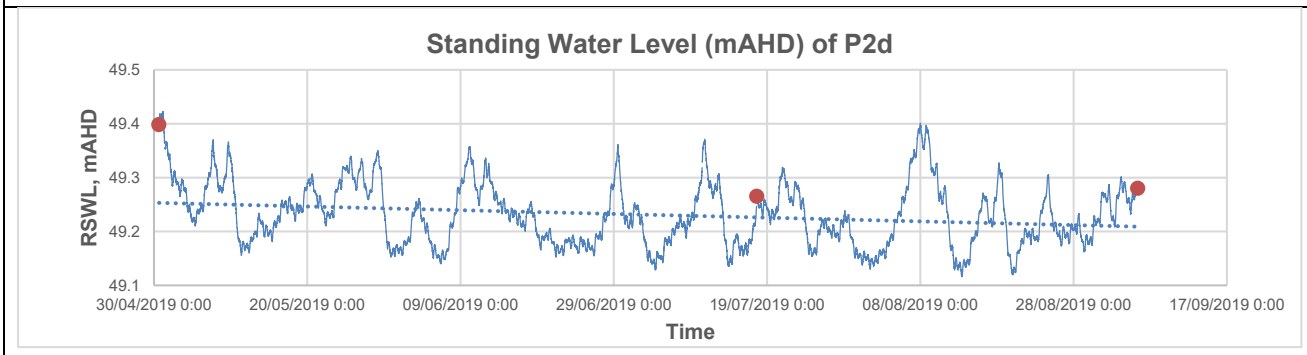
Standing Water Level (mAHD) of P2d
RSWL, mAHD
49.5
49.4
49.3
49.2
49.1
30/04/2019 0:00
20/05/2019 0:00
09/06/2019 0:00
29/06/2019 0:00
19/07/2019 0:00
08/08/2019 0:00
28/08/2019 0:00
17/09/2019 0:00
Time

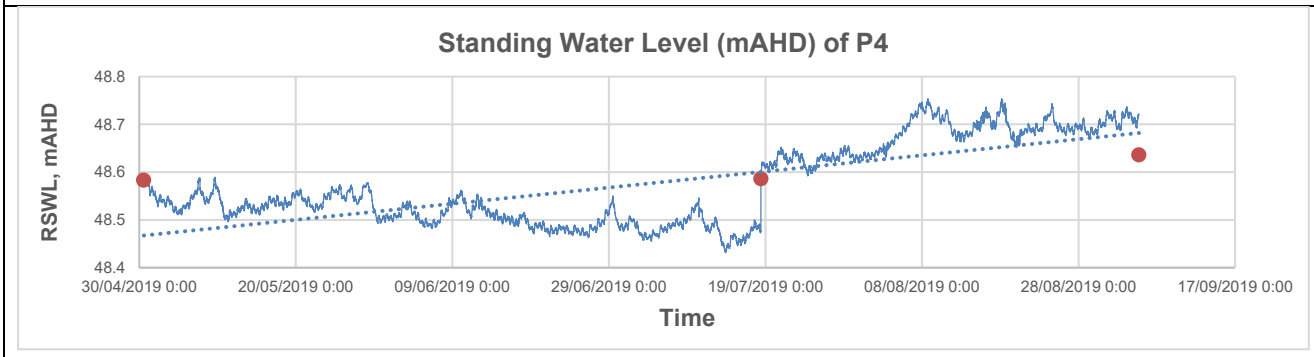
Standing Water Level (mAHD) of P4
RSWL, mAHD
48.8
48.7
48.6
48.5
48.4
30/04/2019 0:00
20/05/2019 0:00
09/06/2019 0:00
29/06/2019 0:00
19/07/2019 0:00
08/08/2019 0:00
28/08/2019 0:00
17/09/2019 0:00
Time

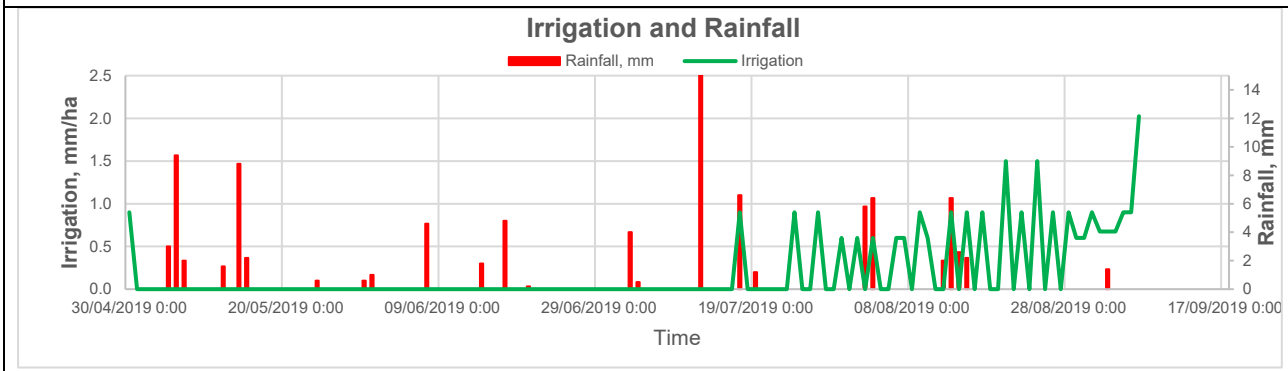
Irrigation and Rainfall
Rainfall, mm
Irrigation
Irrigation, mm/ha
2.5
2.0
1.5
1.0
0.5
0.0
Rainfall, mm
14
12
10
8
6
4
2
0
30/04/2019 0:00
20/05/2019 0:00
09/06/2019 0:00
29/06/2019 0:00
19/07/2019 0:00
08/08/2019 0:00
28/08/2019 0:00
17/09/2019 0:00
Time

Figure 5-12: Reduced Standing Water Level in the bores screened in the Parilla Sands aquifer between May and September 2019. The irrigation and rainfall over the same period is also shown. RSWL stands for a reduced standing water level.

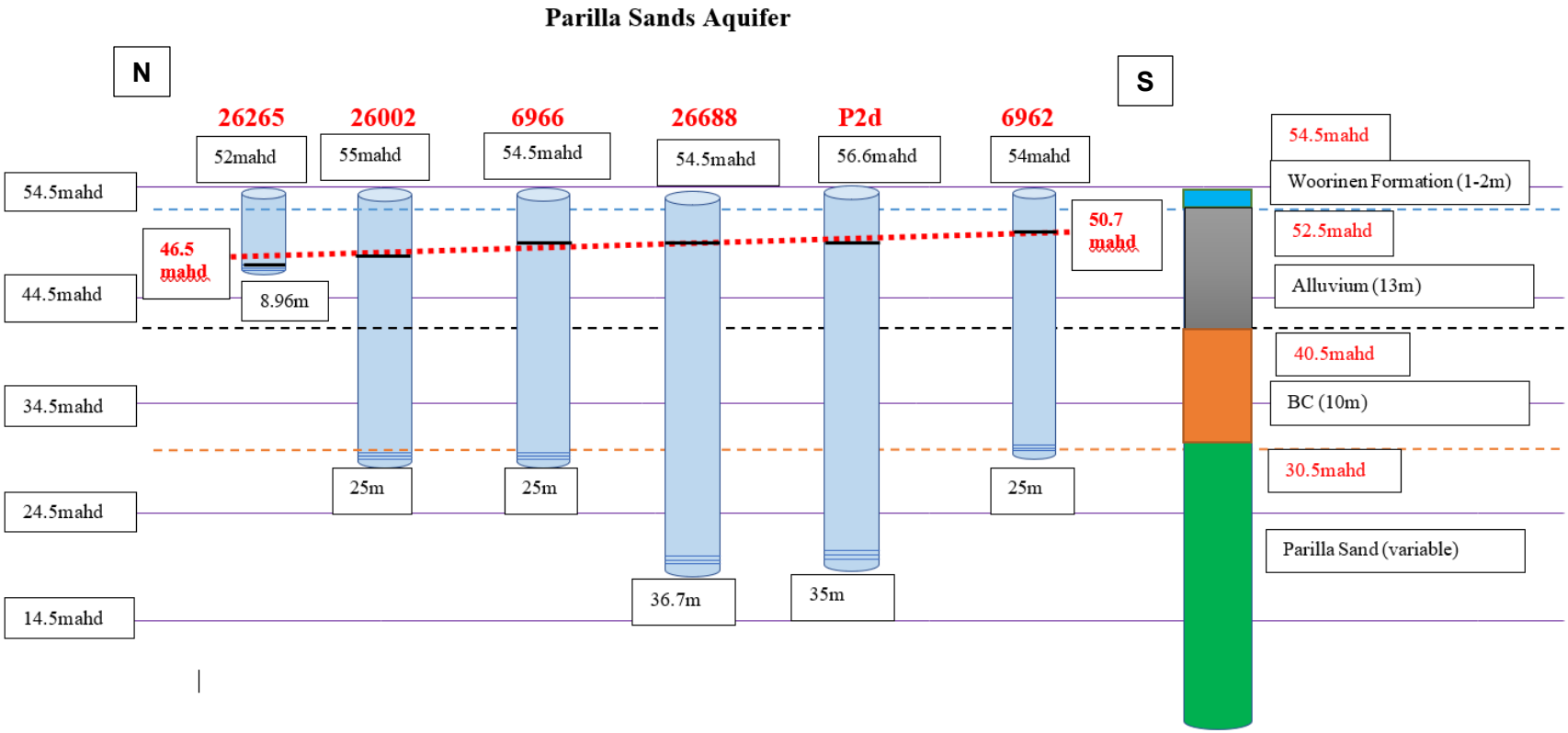

Figure 5-13: Hydrogeology of the Parrilla Sands aquifer

5.3.2 Monitoring water level in the Alluvium & Blanchetown Clay

The study monitored several different types of groundwater monitoring infrastructures which screened the Woorinen Formation, Alluvium and Blanchetown Clay layer, namely- 9 drainage pits, 8 test wells, 5 piezometers distributed across the study area for four complete months from the end of April (29 April 2019) to early September (3 September 2019).

The following section describes the water level in each of these groundwater monitoring structures.

Drainage pits: Based on water level data recorded in four months from May to early September, the water level in these pits ranged between 50.5 mAHD to 53.2 mAHD, which is just above the regional water table (46.5 mAHD to 50.7 mAHD) and very near to the land surface **(Figure 5-14, 5-15 & 5-16).** The water level fluctuation in each drainage pit is plotted in **Figure 5-15** and indicated that drainage water is collected up to a certain level in the drainage pits and later pumped out to the shallow drainage outlet until the water dropped to a certain level in a daily basis**.** The time series data showed that there were no clear trends in the water levels in these pits despite the variation in irrigation and rainfall **(Figure 5-14 & Figure 5-16).**

Test wells: As discussed earlier, the topmost soil layer constitutes the aeolian sand deposits on the ridge of the dunes and clayey layers in the swales. The depth of these test wells is around 1.8 m whereas the water level in all test wells is around 1.7 m below TOC which suggests nearly 0.1m of stagnant water with no water level fluctuation and as a result, all 8 test wells were dry **(Figure 5-19).**

Piezometers: The shallow piezometers screened between the Woorinen Formation and the Alluvium are installed to monitor the occurrence of a perched water table that may result from root zone drainage of irrigation water **(Figure 5-18).** The depth of the piezometers (P1s, P2s, P3s, P1d & P2d) usually range from 2m to 13 m and their screens are located across the Alluvium (*refer Appendix-1)* **(Figure 5-18).** P2d bore is screened in the regional Parilla Sands aquifer. *(Refer Appendix-1). Two of the* three shallow piezometers (P1s & P3s) were dry (**see Figure 5-18 &Table 5-3).** which may be accounted for by the daily draining of water from the subsurface via a tile drainage network installed in the study area. While the average water level in the P2s piezometer is around 54 mAHD*,* the water level in piezometers P1d, P3d and P4d, along a transect from the south towards the Murray River in the north was 50.4 mAHD, 49.2 mAHD, and 48.6 mAHD, respectively. Based on these levels, the hydraulic gradient of the perched water table

is towards the Murray River, much like the regional water table gradient of the Parilla Sands aquifer **(Figure 5-17, 5-18 & 5-19).**

The time series water level data has shown that there is a regional and local aquifer system in the study area. The vertical head difference between the two different aquifers is small in a downwards direction such that (the water table of the regional Parilla Sands aquifer ranges from 46.5 mAHD to 50.7 mAHD, while that of the local perched water table within the Alluvium ranges from 50.5 mAHD to 54 mAHD. It is important to note that both the aquifer systems have a hydraulic gradient towards the Murray River to the north of the study area.

The change in water level in the test wells, drainage pits, and piezometers screened within the Alluvium confirms shallow perched water table conditions where water resides above this Blanchetown Clay Formation. The perched water is intercepted and is drained regularly via the shallow tile drainage network towards the designated drainage pits in the study area. The total volume of the perched water intercepted is calculated in the following section.

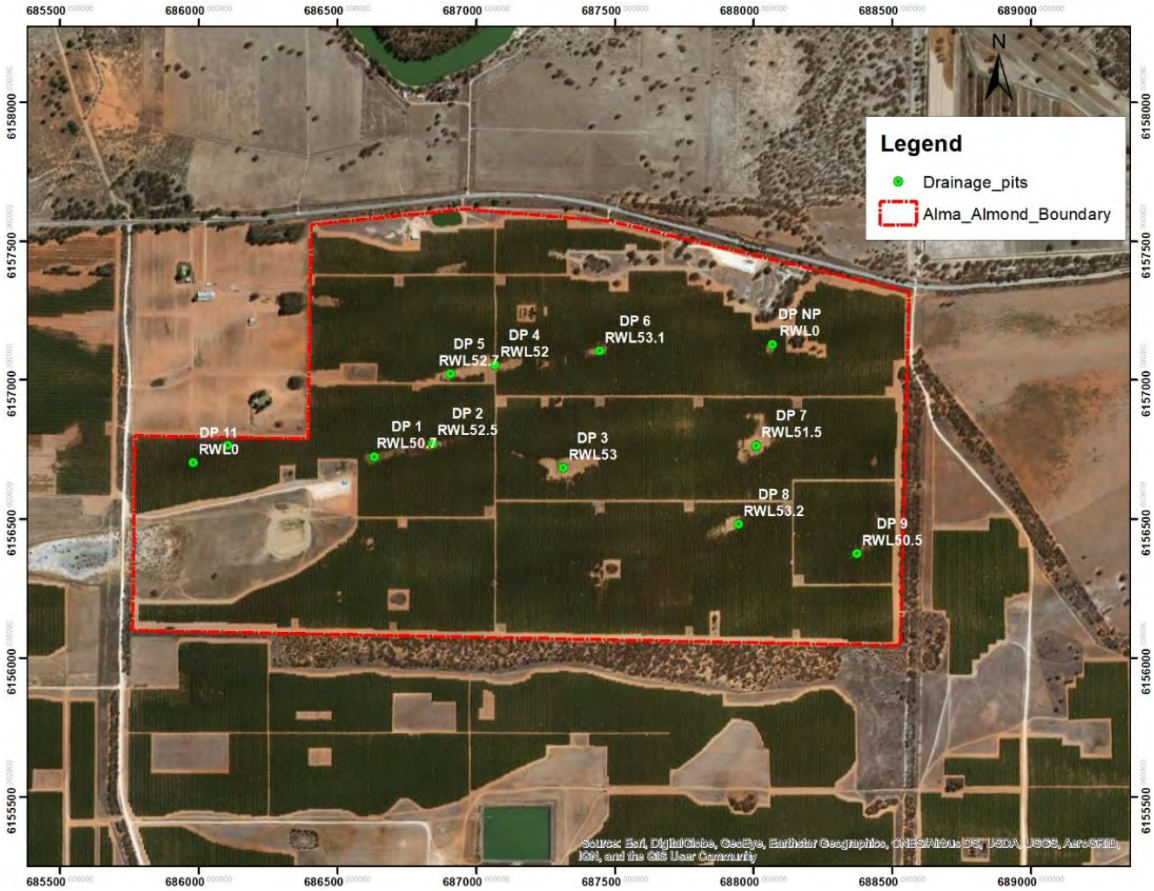

Figure 5-14: Average RSWL in the shallow drainage pits across the study area.

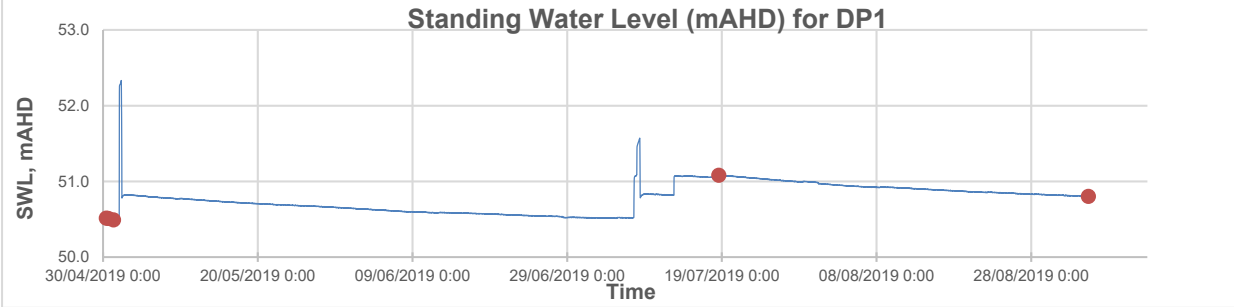
Standing Water Level (mAHD) for DP1
SWL, mAHD
53.0
52.0
51.0
50.0
30/04/2019 0:00
20/05/2019 0:00
09/06/2019 0:00
29/06/2019 0:00
19/07/2019 0:00
08/08/2019 0:00
28/08/2019 0:00
Time

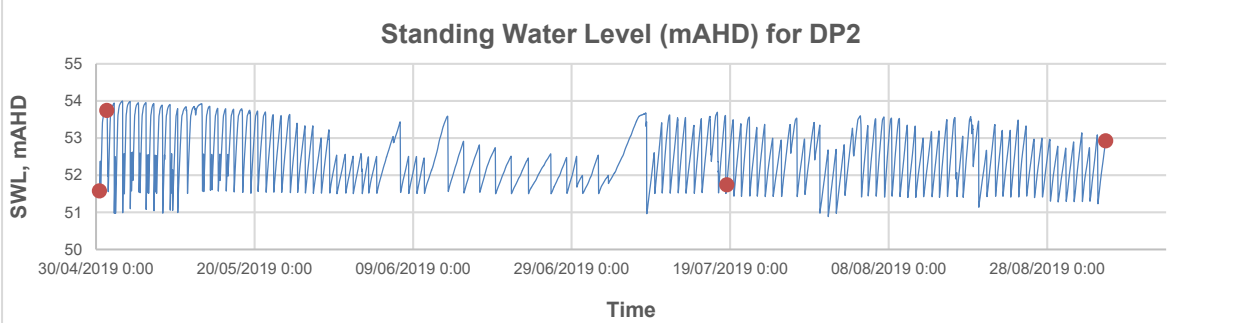
Standing Water Level (mAHD) for DP2
SWL, mAHD
55
54
53
52
51
50
30/04/2019 0:00
20/05/2019 0:00
09/06/2019 0:00
29/06/2019 0:00
19/07/2019 0:00
08/08/2019 0:00
28/08/2019 0:00
Time

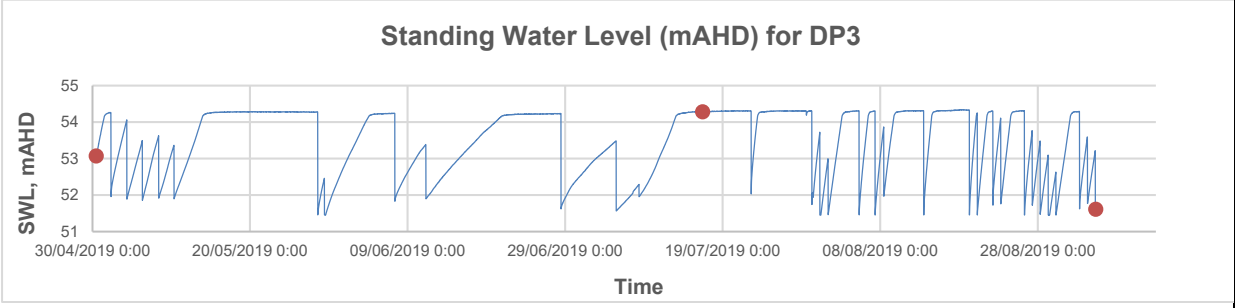
Standing Water Level (mAHD) for DP3
SWL, mAHD
55
54
53
52
51
30/04/2019 0:00
20/05/2019 0:00
09/06/2019 0:00
29/06/2019 0:00
19/07/2019 0:00
08/08/2019 0:00
28/08/2019 0:00
Time

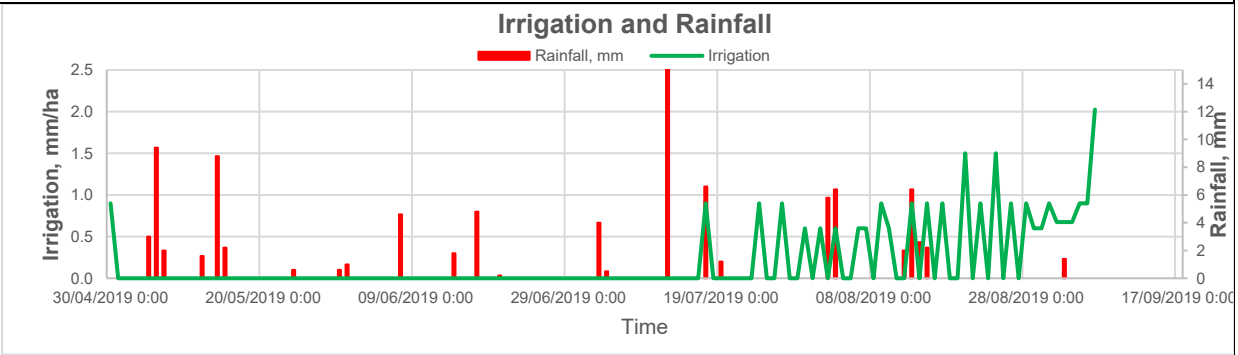
Irrigation and Rainfall
Rainfall, mm
Irrigation
Irrigation, mm/ha
2.5
2.0
1.5
1.0
0.5
0.0
Rainfall, mm
14
12
10
8
6
4
2
0
30/04/2019 0:00
20/05/2019 0:00
09/06/2019 0:00
29/06/2019 0:00
19/07/2019 0:00
08/08/2019 0:00
28/08/2019 0:00
17/09/2019 0:00
Time

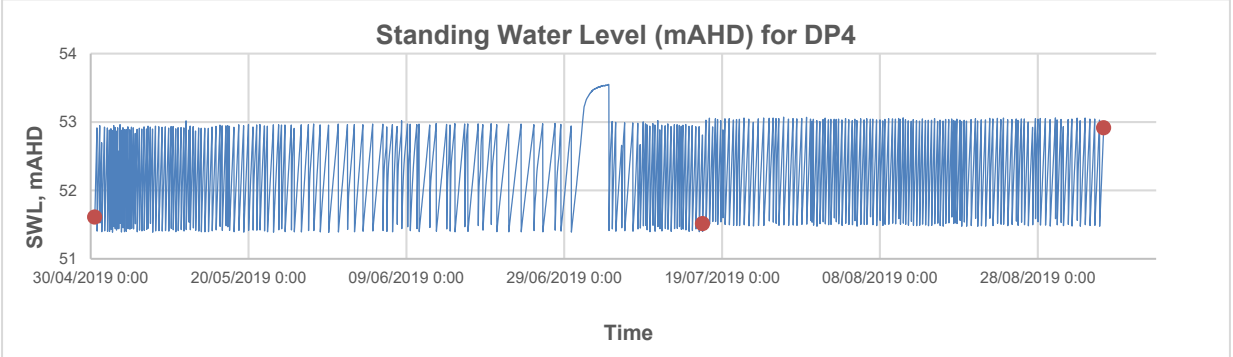
Standing Water Level (mAHD) for DP4
SWL, mAHD
54
53
52
51
30/04/2019 0:00
20/05/2019 0:00
09/06/2019 0:00
29/06/2019 0:00
19/07/2019 0:00
08/08/2019 0:00
28/08/2019 0:00
Time

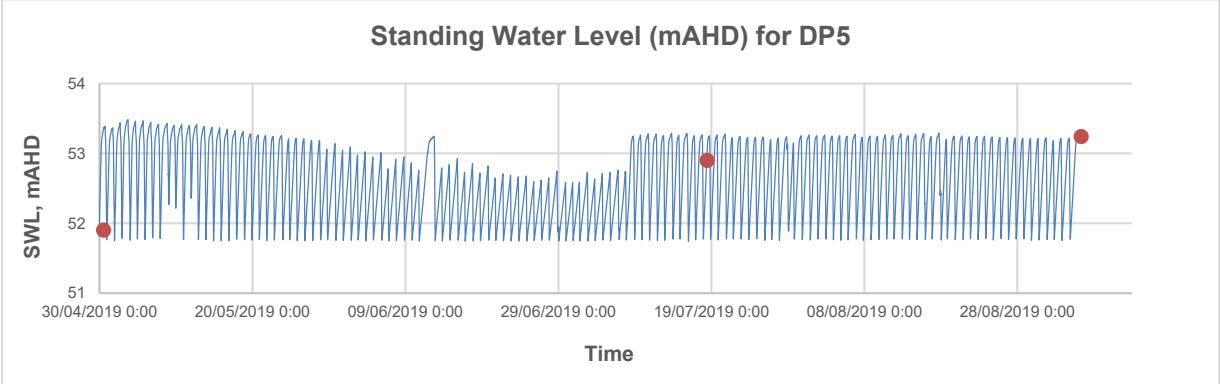
Standing Water Level (mAHD) for DP5
SWL, mAHD
54
53
52
51
30/04/2019 0:00
20/05/2019 0:00
09/06/2019 0:00
29/06/2019 0:00
19/07/2019 0:00
08/08/2019 0:00
28/08/2019 0:00
Time

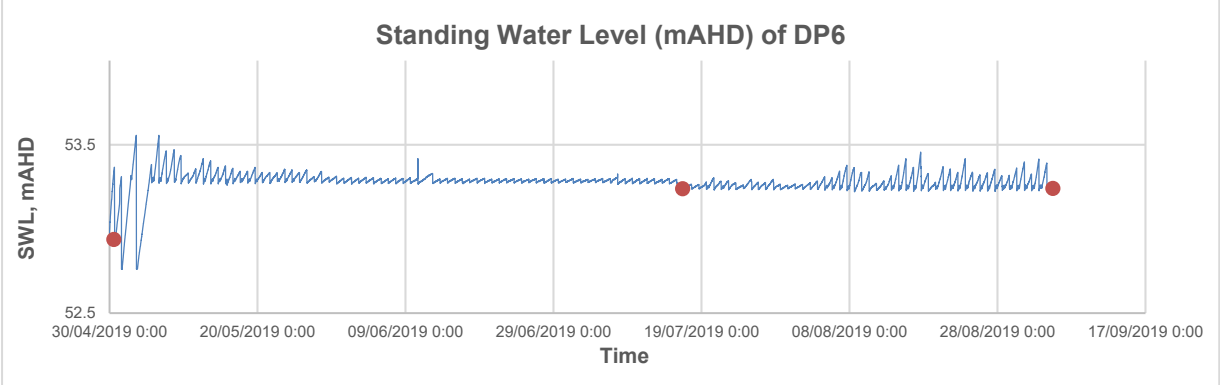
Standing Water Level (mAHD) of DP6
SWL, mAHD
53.5
52.5
30/04/2019 0:00
20/05/2019 0:00
09/06/2019 0:00
29/06/2019 0:00
19/07/2019 0:00
08/08/2019 0:00
28/08/2019 0:00
17/09/2019 0:00
Time

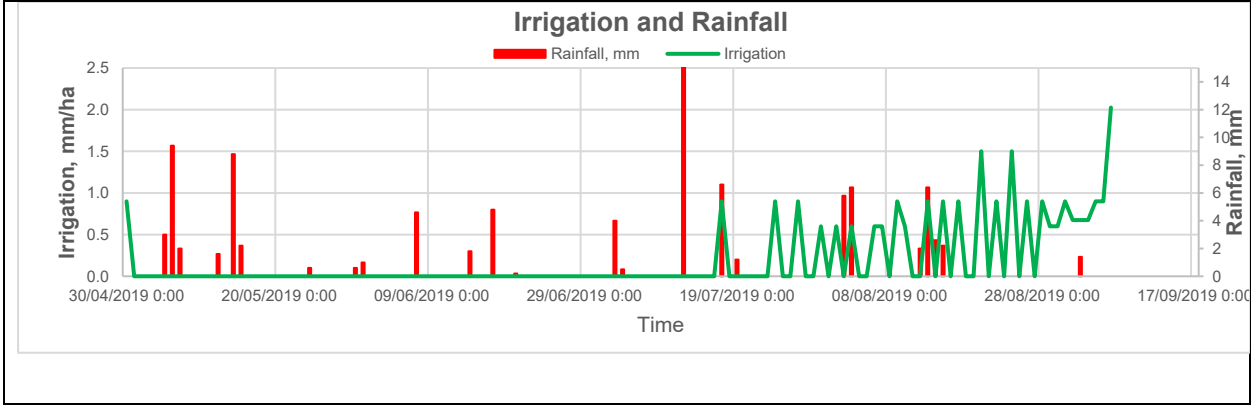
Irrigation and Rainfall
Rainfall, mm
Irrigation
Irrigation, mm/ha
2.5
2.0
1.5
1.0
0.5
0.0
Rainfall, mm
14
12
10
8
6
4
2
0
30/04/2019 0:00
20/05/2019 0:00
09/06/2019 0:00
29/06/2019 0:00
19/07/2019 0:00
08/08/2019 0:00
28/08/2019 0:00
17/09/2019 0:00
Time

Figure 5-15: Time series of water level measurements (mAHD) in the shallow drainage pits. The irrigation rate and rainfall over the same period is also shown.

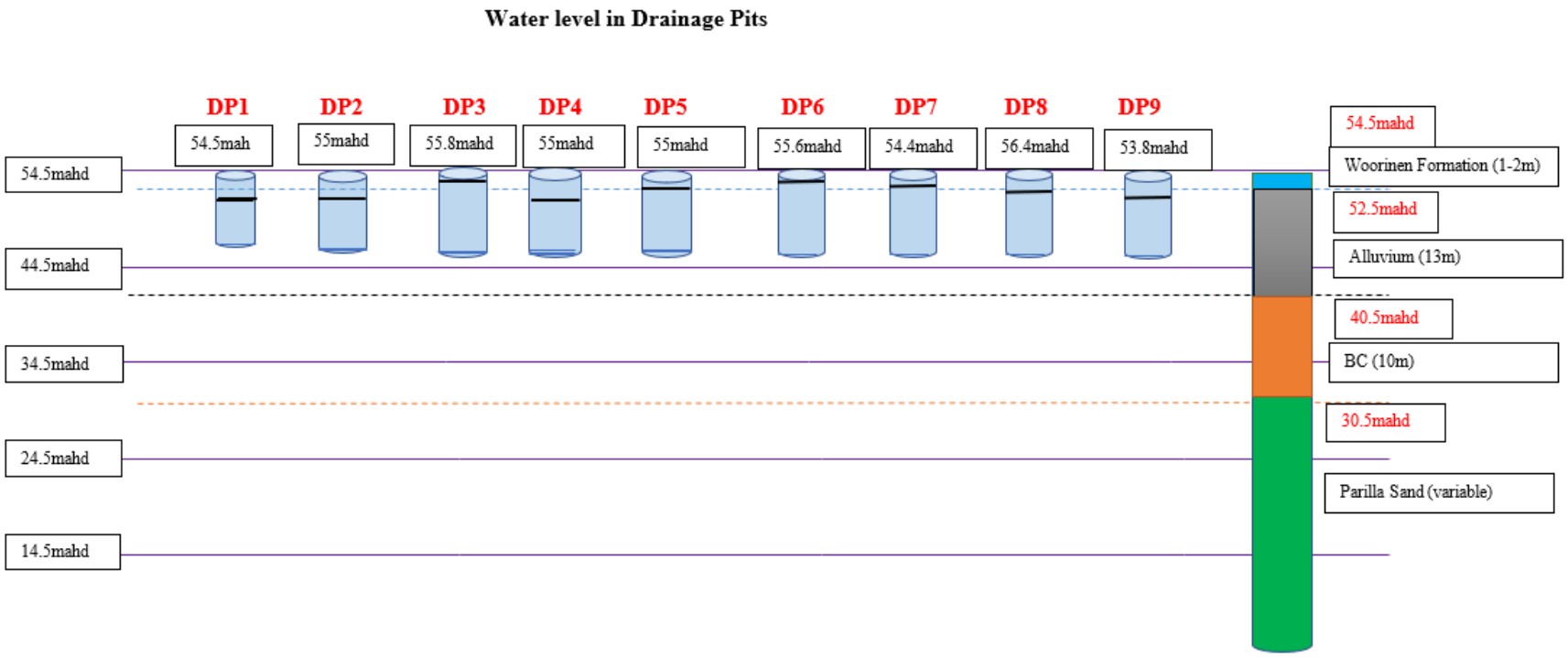

Figure 5-16: Measured average water level (mAHD) in the shallow drainage pits installed across the study area

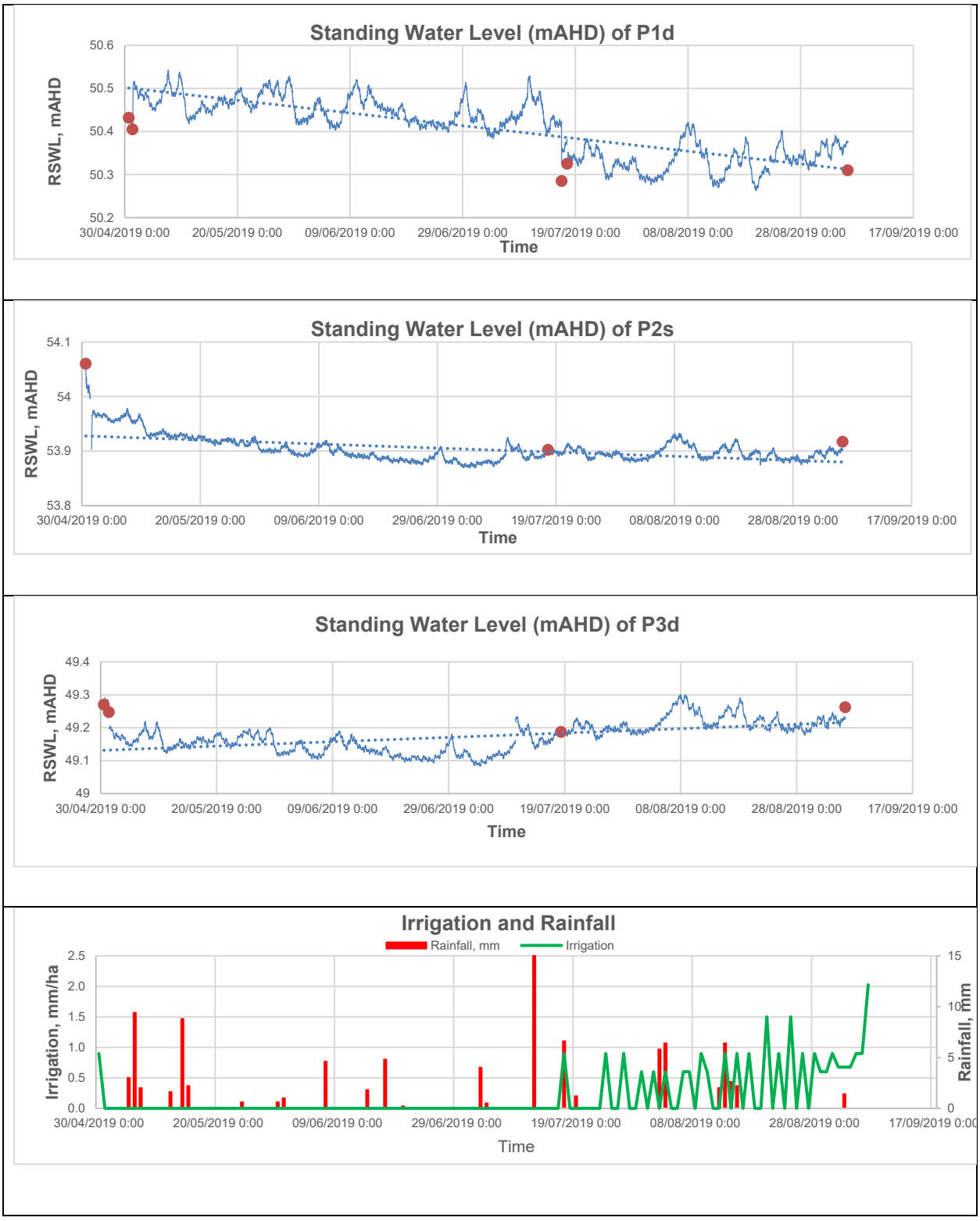

Figure 5-17: Reduced standing water level (RSWL) (mAHD) in piezometers from 30 April to 3 September 2019.

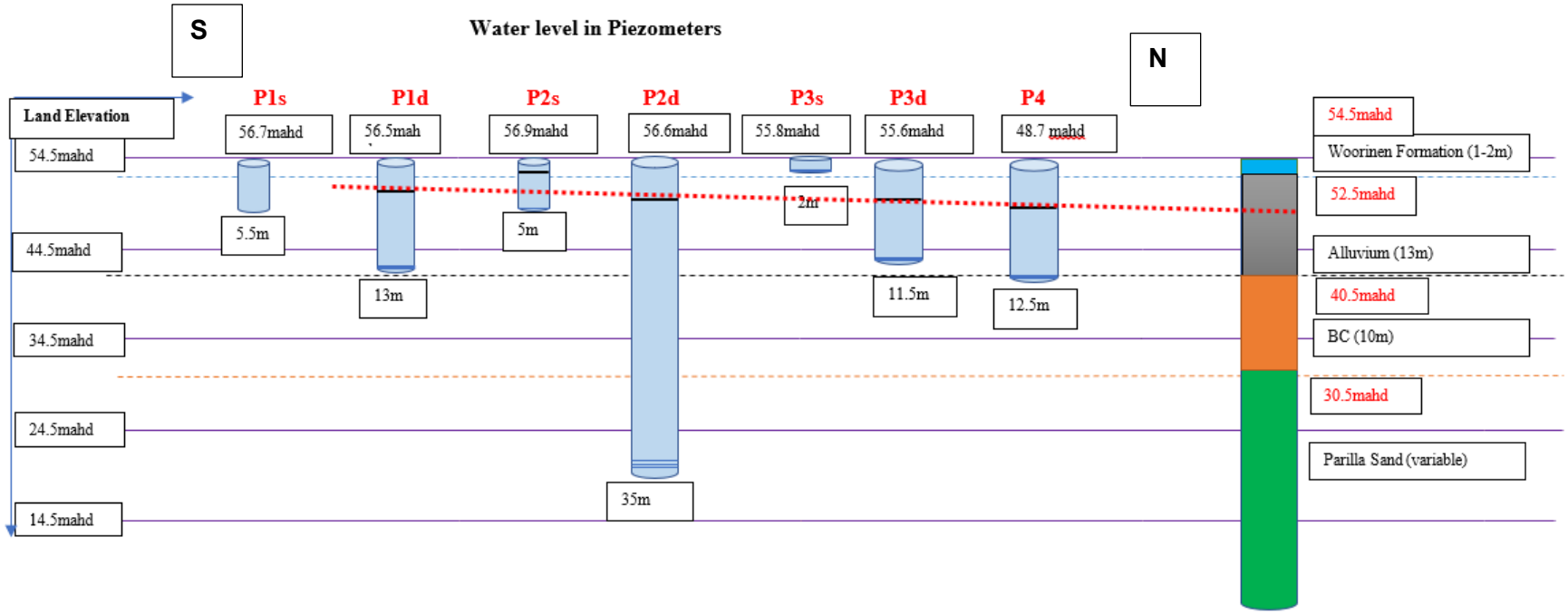

Figure 5-18: Average measured water levels in piezometers that are installed across the study area. The piezometers are plotted in south (left) to north (right) orientation.

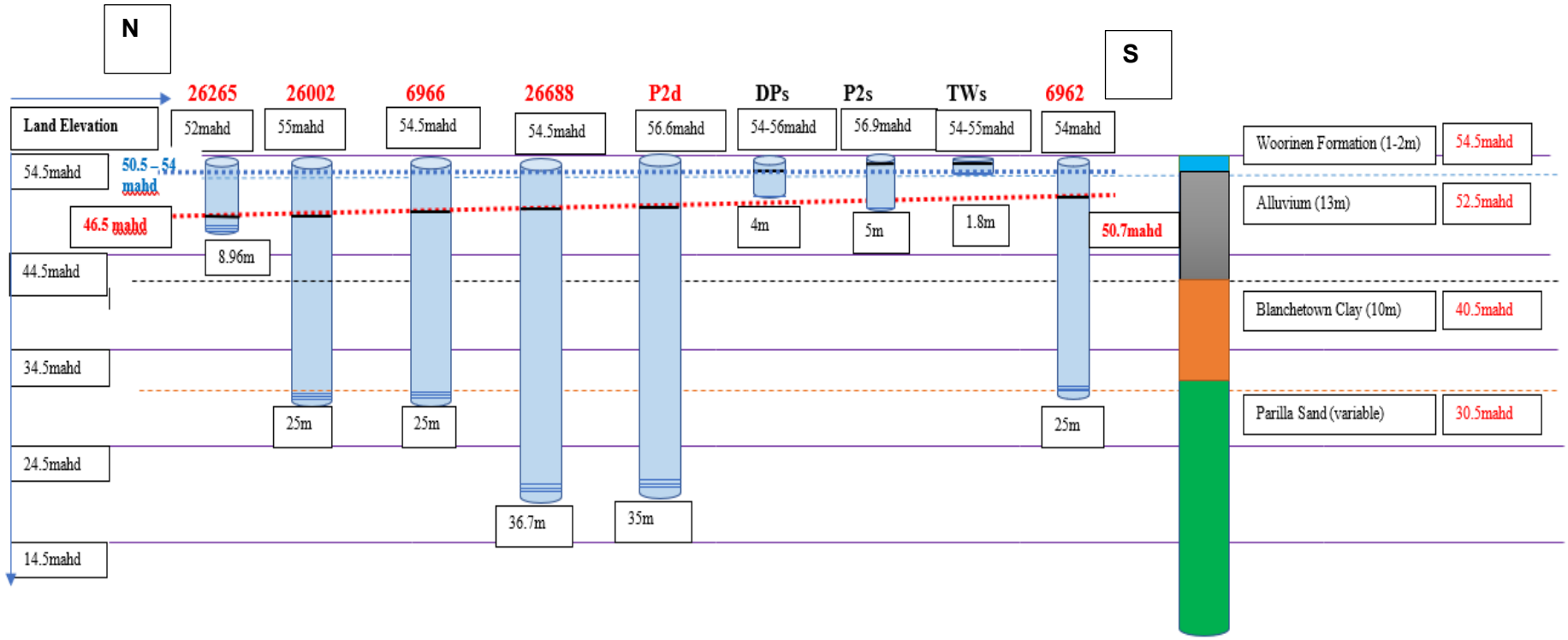

Figure 5-19: Watertable elevations (mAHD) in the shallow perched Alluvium aquifer system (Blue dotted line). Also shown is the regional water table elevation in the Parilla Sands aquifer (Red dotted line). The other blue line represents the boundary between the Woorinen Formation and Alluvium. The groundwater monitoring structures are plotted in north (left) to south (right) orientation.

Table 5-2: Maximum and Minimum water level in bores.

Bore	Max RWL, mAHD	Min RWL, mAHD	Average, mAHD	TOC, mAHD	Remarks
P1d	50.54	50.26	50.41	57.515	Piezometer
P2d	49.42	49.12	49.23	57.57	Piezometer
P3d	49.30	49.30	49.30	56.632	Piezometer
P4	48.75	48.43	48.57	54.671	Piezometer
P1s	0	0	0	57.52	DRY
P2s	0	0	0	57.952	DRY (No Water)
P3s	0	0	0	56.783	DRY (No Water)
6966	49.55	49.40	49.45	54.42	State bore
6962	50.80	50.62	50.69	53.70	State bore
26002	48.57	48.47	48.52	54.83	State bore
26688	49.28	49.18	49.23	54.43	State bore

5.3.3 Relationship of regional groundwater table with local rainfall and irrigation

The relationship of the regional groundwater table to the rainfall and irrigation was examined by plotting rainfall and irrigation data against time and compared with the water level time series data in state observation bores and deep piezometers screened in the regional Parilla Sands aquifer as shown in **Figure 5-13**.

There is no significant correlation of change in water level in bores screened in the Parilla Sands aquifer with irrigation and rainfall. **(Figure 5-13**). The water level slowly declined from mid-August and remained almost constant with minor intermittent rise and fall in water level.

5.3.4 Relationship of the perched water table with local rainfall and irrigation

The water level data in the shallow piezometers, drainage pits, and test wells were compared with rainfall data to examine the relationship between change in water level with irrigation and rainfall in the study area (**Figure 5-15 & Figure 5-17**). However, it was difficult to see the distinct correlation of changes in water levels in test wells, drainage pits and shallow bores with rainfall and irrigation.

5.4 Estimation of the Total Volume and Rate of Root Zone Drainage

In this section, the total volume of the RZD intercepted by the alluvial clay formation during the study period of four months is calculated and later compared with the total water discharged through the v-notch weir installed at the outlet of all the drainage pits.

The cumulative volume of the RZD progressively increases in each pit over the sample period **(Figure 5-20).** The total cumulative volume of inflow in drainage pits is equal to 885 m^3 over 4 months from the end of April 2019 to early September 2019**.** The total cumulative volume of inflow in drainage pits provided the approximate estimate of the volume of perched RZD within the Alluvium in the study area.

The total inflow into the drainage pits is used to estimate the total rate of RZD. Each drainage pit is designed to drain excess water in the subsurface from the specified area through a shallow tile drainage system. The rate of RZD is estimated by dividing the total volume of inflow drainage from the nine drainage pits by the total study area, which is estimated to be around 0.27 mm over the four months of monitoring. If we assume that the inflow drainage is similar for the other months of the year, the average annual RZD is equivalent to 0.80 mm/yr**.** The rate of RZD is very small in comparison to the rate of irrigation in the study area, which is on average around 1000 mm/yr, based on the field irrigation record. The RZD is calculated based on four months of data in which the total irrigation is minimal which could result in lower value of the estimated RZD rate. Therefore, the RZD estimated based on data collected for a year is required which will be collected by the ongoing research. In addition, such a low rate of RZD indicates that either the consumptive use of the irrigated water by the almond trees is highly efficient or there is rapid transport and bypass flow of the RZD downward through areas of the subsurface where the alluvial clay material is more permeable and recharges the regional aquifer. These findings highlight the necessity of further research to quantify the recharge rate through the alluvial clay formation.

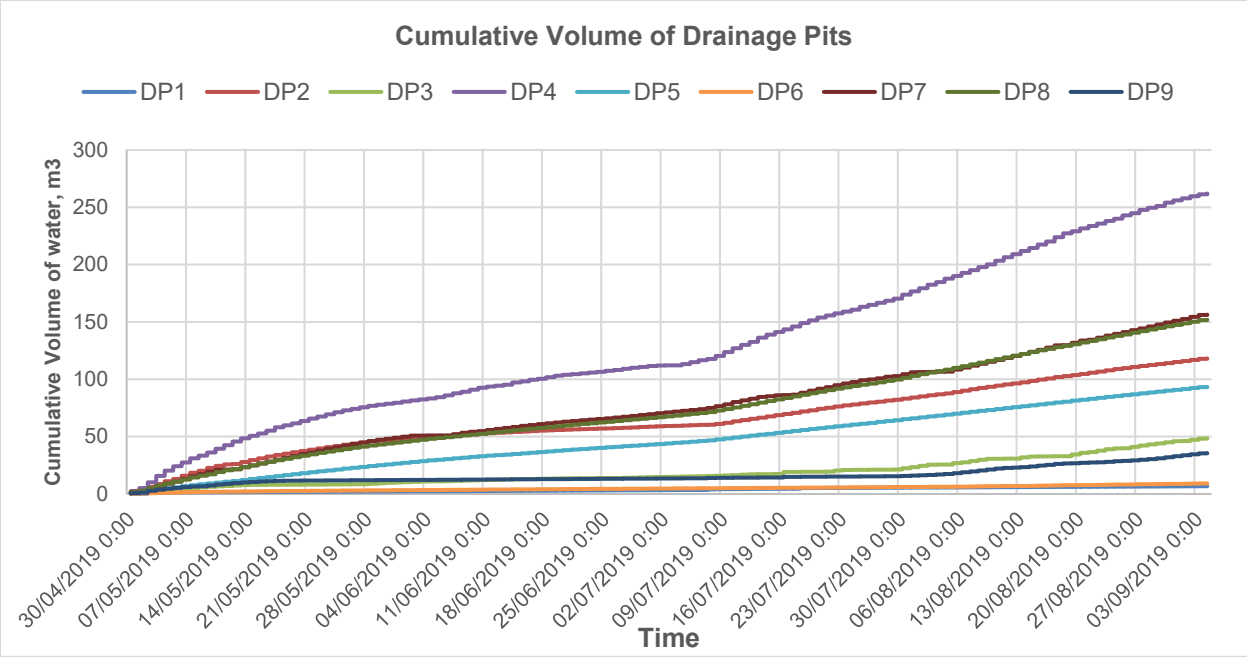

Figure 5-20: Cumulative volume of drainage inflow into the drainage pits between 30 April and 3 September 2019.

5.4.1 The water level in Weir and volume of water collected in weir

The data was downloaded from the pressure transducers loggers installed in a weir. The change in water level over time from mid-July to early September 2019 is plotted in **Figure 5-22**. The water level in the weir change between 0.2m to 0.3 m with some exception of water level change higher than 0.3m in both weirs. The trend of change in the water level in both weirs is similar.

The preliminary calibration of weirs was conducted with manual discharge measurements in weirs and the water pressure recorded at the same time which gives the calibration curves of each weir (**Figure 5-21)**. Further, the equation from the weir calibration was used to calculate the discharge rate corresponding to the barometric pressure corrected water pressure recorded by the pressure transducers installed in the weirs **(Figure 5-23)**. The data showed that the average flow rate in the north weir was 3.46 m3/d but also had a number of measurements that were high (0.018 m3/s and 0.025 m3/s) (**Figure 5-23)**. Likewise, the plot of flowrate in the south weir showed the average flowrate was 0.00006m3/s **(Figure 5-23)**. The high variability in the flow may be due to pumping out water from drainage pits at the same time so the flow rate peak rapidly.

The sum of the inflow volume of water from mid-July (19/07/2019 10:15) to early September (3/09/2019 9:45) gives the total volume of water collected and discharged by the weir in that time

period (**Figure 5-24**). The total volume of water drained was calculated to be 107 m^3 and 102 m^3 for the Weir-north and Weir-south, respectively **(Table 5-4)**. The total volume of water discharge from both weirs, 209 m^3, is less than the calculated total inflow volume from all of the drainage pits, 375 m^3 for the same time span.

This difference in the total volume of drainage in the drainage pits and weirs is 166 m^3. All the drainage pits are not designed to drain to the two outlets in the study area. Some drainage pits are not connected to the drainage network in the study area and discharge directly to the natural land/ dam site in the northern boundary of the study area which could account for the difference. In addition, there is continuous minimal leakage from one of the outlet pipes just near Salt Lake. This can also be accounted to the weir's calibration. The calibration of weirs is only preliminary due to a limited number of discharge measurements over the full range of manual flow measurements from the weir. The detailed calibration of both weirs will be conducted later in this ongoing project.

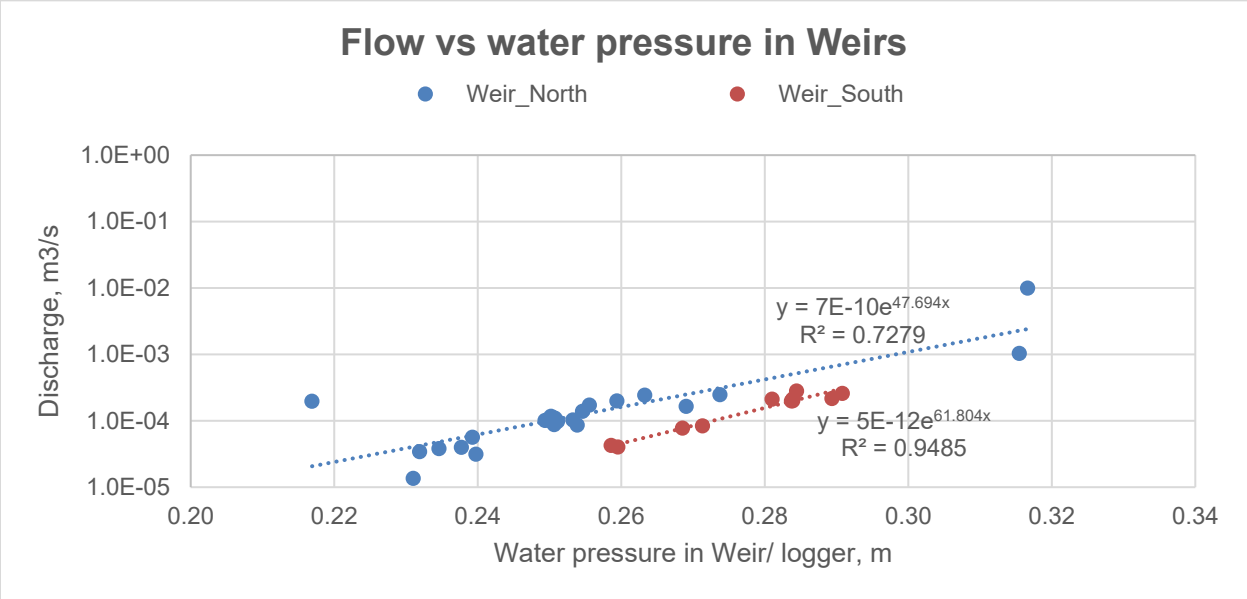

Figure 5-21: Calibration results of the two weirs located at the drainage discharge outlet.

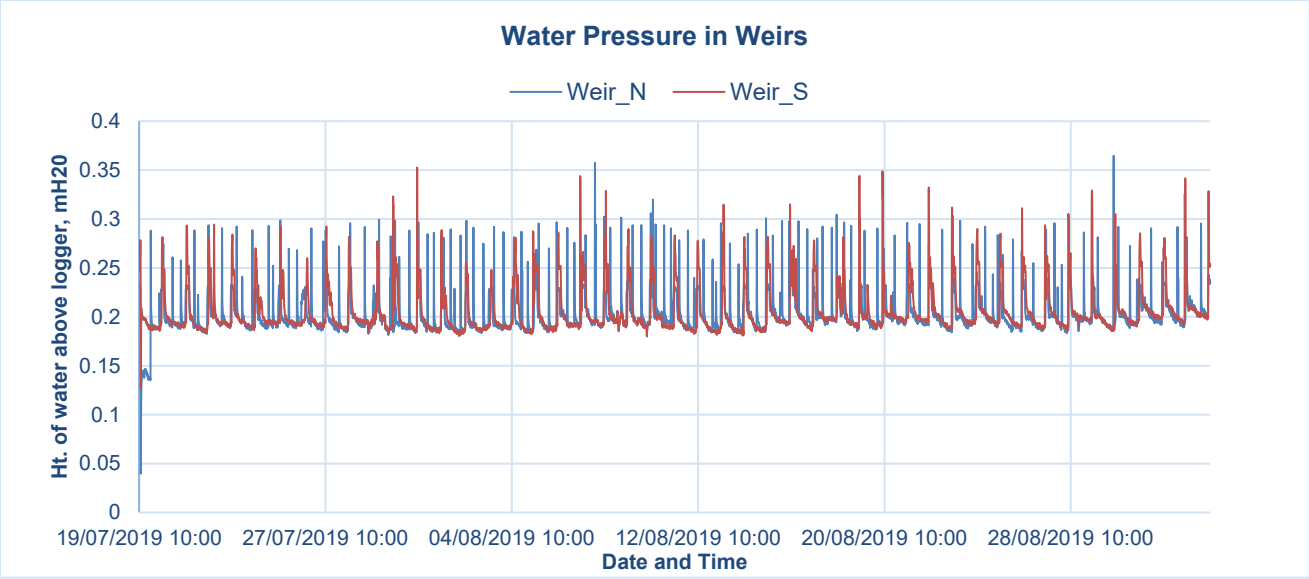

Figure 5-22: Continuous water levels in the two weirs measured by the dataloggers installed at the discharge outlet in every 15 minutes interval, between 19 July to 3 September 2019.

Table 5-3: Volume of water discharge from the shallow drainage pits.

	Weir N	**Weir S**
Date & Time	19/07/2019 10:15	3/09/2019 9:45
Data logger	1a	2a
Volume, m^3	107	102
TOTAL Volume	209 m^3	

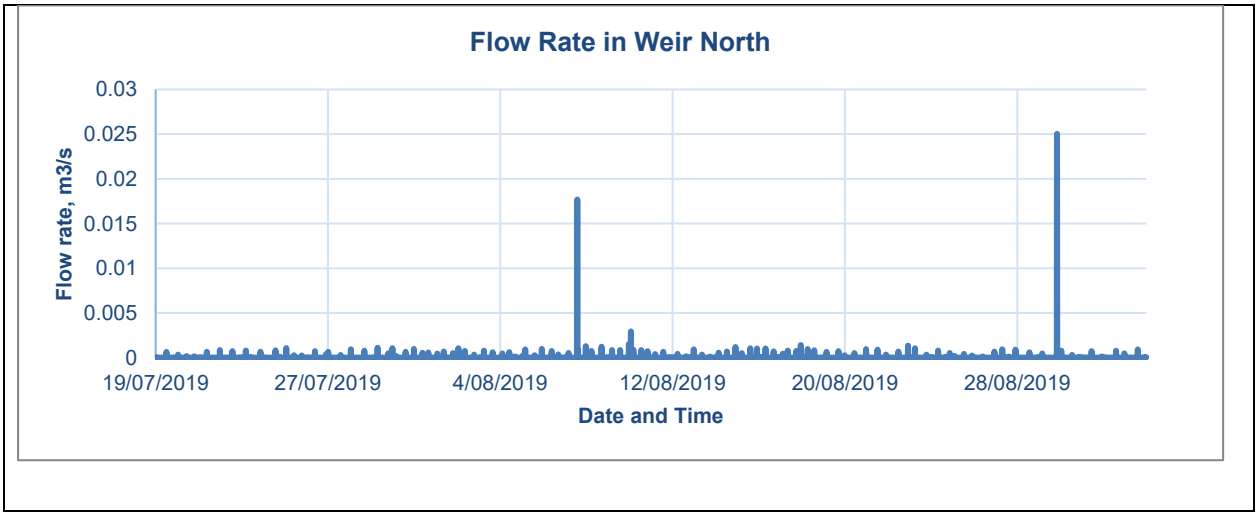

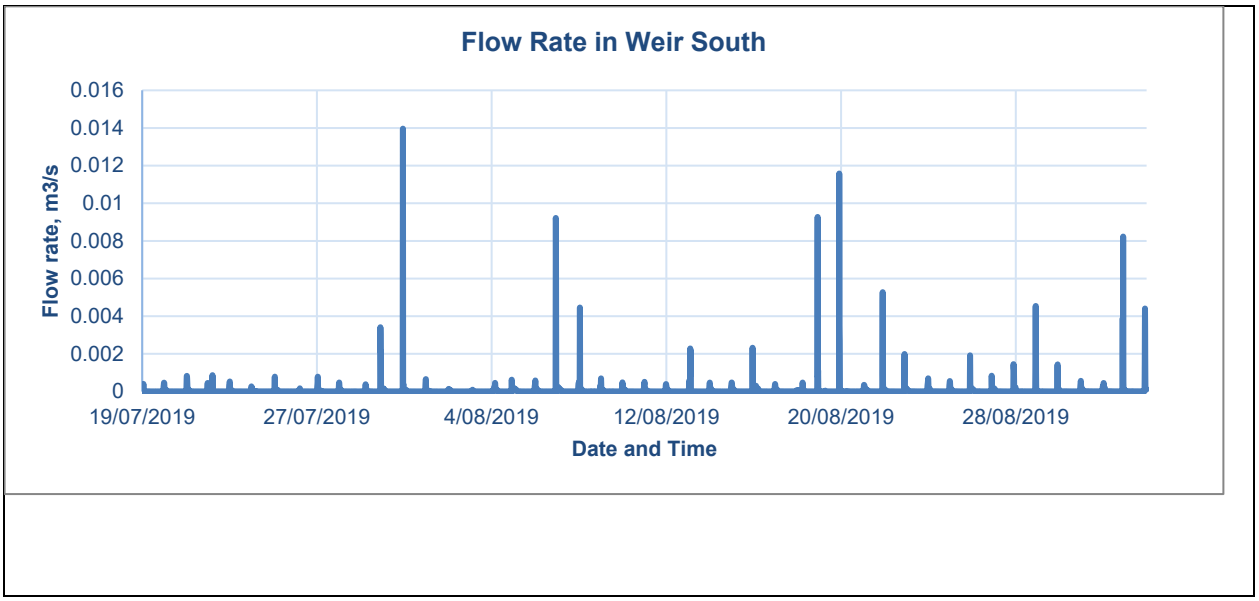

Figure 5-23: Flow rate (m3/s) at the two weirs of the captured water from the drainage pits 19 July to 3 September 2019.

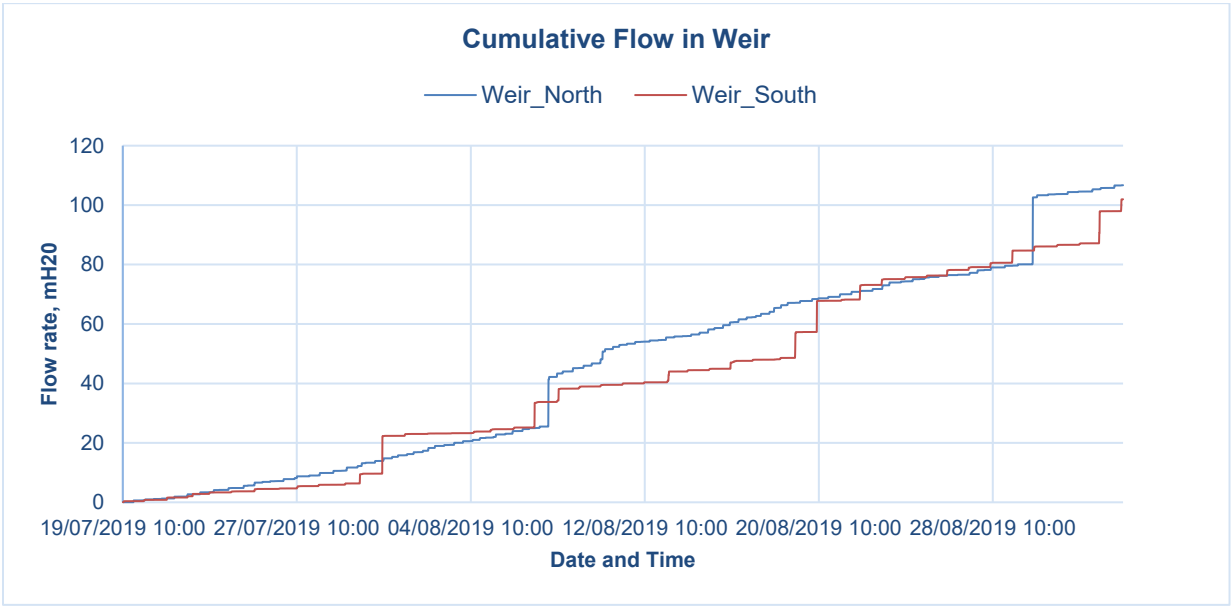

Figure 5-24: Cumulative volume (m3) of captured water from the drainage pits, 19 July to 3 September 2019

5.5 Discussion

This study was carried out to understand the processes in the unsaturated zone which determine the transport of RZD under irrigated almonds orchards, and ultimately influence the overall groundwater recharge and salinity of the Murray River. The research findings concluded the existence of the thick Alluvial Formation and Blanchetown Clay Formation underneath the study area where the shallow unconfined aquifers are perching within the Alluvial Formation over Blanchetwon Clay layer. Also, the total volume of RZD perching during the study period and RZD rate was estimated to be 885 m^3 and 0.80 mm/yr respectively.

The comparison of 2D ERT profiles with the stratigraphy of state observation bores and lithological logs of the piezometers in the vicinity of the study area showed the occurrence of 13 m thick Alluvium and 10 m thick Blanchetown Clay. In addition, the resistivity profile showed that the elevated ridge of the dunes is sandier and more resistive, while the low-lying dune swales have a higher clay content and are more conductive. This was also confirmed with the FDEM conductivity survey. The FDEM conductivity surveys across the study area confirmed two facts. Firstly, the ERT transect is representative of the study area which means that throughout the study area the conductivity decreases with an increase in elevation and vice versa, which is aligned with the ERT findings. Secondly, the range of conductivity values at the same topographic elevations along the different transects was similar, which inferred that the Alluvium is fairly uniform across the study area.

The thick Alluvium and Blanchetown Clay layers act as an aquitard layer, which favours the formation of shallow perched water tables, however, it is difficult to visualise the distinct change in resistivity in the resistivity profile between the different months. Time lapse resistivity measurements at different time periods were conducted to examine changes to the shallow water table. The change in resistivity values between surveys showed the greatest change in the near surface, less than 10 m depth and within the dune swales. The significant resistivity variation can be accounted for the change in temporally variable soil properties such as water content and salt content. On top of that, the comparison of the two time lapse resistivity measurements showed that the resistivity variation is higher between May to July than between July to September, which was likely due to higher rainfall in the first period and flushing of salts downwards through the soil profile following the rain.

The water level monitoring of the piezometers, test wells, drainage pits, and state observation bores, screened at the different depths confirmed the existence of the perched water table just a few metres below the land surface. The water table of the regional Parilla Sands aquifers ranges from 46.5 mAHD to 50.7 mAHD, while that of the local Alluvium ranges from 50.5 mAHD to 54 mAHD. All the four state observation bores and piezometers (P2d) are used to monitor the regional Parilla Sands aquifer while 8 test wells monitored the topmost 1-2m Woorinen Formation, while 9 drainage pits and remaining 6 piezometers in the study area monitored Alluvium and Blanchetown Clay Formation. Both the perched and regional water table is located within the Alluvial Formation and has its hydraulic gradient from the south towards the Murray River in the north. In addition, the study showed a poor correlation of change in water levels in groundwater with rainfall and irrigation.

The drainage system monitoring method of the RZD estimation was used and monitored the 9 drainage pits distributed across the study area which roughly estimated RZD rate of 0.80 mm/yr and total volume of RZD equal to 885 m^3 in around 4 months from the end of April 2018 to early September 2019. RZD is usually considered to be around 5-10% of irrigation as estimated by different regional based measurements of RZD (Newman et al. 2009), however, the calculated RZD 0.80 mm/yr is less than 100 mm/yr which is 10 percent of irrigation (1000 mm/yr) in the study area. This lower value of RZD can be accounted to a few major reasons; firstly, the lesser RZD can be accounted to the consumptive use of irrigation water by the almond's trees. However, this study has not considered the evapotranspiration loss which is likely to reduce the net RZD in the study area. It is because the evaporation is higher across the Murray Basin such that average evaporation is many times higher than the average rainfall (Brown & Stephenson 1991). Further research is essential with focus on evapotranspiration loss in the almond orchards. Secondly, the RZD is extrapolated based on the RZD rate of four months, such that the first three months (May to July) is almost without any irrigation followed by intermittent irrigation in August. Therefore, this ongoing research study needs to monitor the water levels for remaining eight months to get the real estimate of the RZD of the study area. Lastly, the leakage of RZD through clay layer is unknown which subsequently recharge the regional aquifer, therefore, the RZD leakage through the clay layer needs to be assessed.

The drainage network system in the study area is designed such that all the 9 drainage pits are designed to discharge at Salt Lake through the tile drainage system via two outlet pipes. The monitoring of the flow rate at the V-notch weirs at the two outlets pipes from mid-July (19/07/2019 10:15) to early September (3/09/2019 9:45) showed that the total volume of discharge from the

shallow drainage network was 209 m^3, which is less than the total inflow volume into the drainage pits, 375 m^3. This difference in volume can be accounted to the preliminary calibration of the weirs, and that some drainage pits are not connected to the drainage network and discharge directly to the natural land/ dam site in the northern boundary of the study area. In addition, there is some minimal leakage from one of the outlet pipes just near Salt Lake. Further, the flow rate at weirs needs to be fully calibrated with a different range of flow rates to get the accurate total volume of discharge which will be conducted in this ongoing project.

6 CONCLUSION

This research sought to investigate whether water is perching in the unsaturated zone beneath an almond grove orchard and the hydrological processes that govern the transport of root zone drainage and ultimately determines the total recharge to the regional groundwater aquifer system and salt load to the Murray River. Based on the analysis of temporal water level data of the perched and regional groundwater aquifers and the near surface geophysical surveys, it can be concluded that RZD establishes shallow perched watertable conditions over the thick alluvial and Blanchetown Clay Formation in the study area near Boundary Bend, Victoria.

The electrical resistivity surveys in combination with frequency domain electromagnetic induction measurements effectively illustrated the subsurface geology in the study area. The 2D resistivity survey cross sections, when compared with the stratigraphy of the state observation bores and lithological logs of the piezometers in the study area, confirmed the presence and lateral extent of the thick semi-confining alluvial and clay layer just a few meters below the land's surface thereby favouring the perched watertable conditions. The terrain conductivity meter showed that the spatial distribution of this clay layer extended across the study area.

The volume of water from the RZD that was intercepted via the network of shallow drainage pits over the study area was 885 m^3 between late April and early September 2019. Extrapolating this over a year equates to a volume of 2652 m^3. The calculated rate of RZD is equal to 0.80 mm/yr, which is small in comparison to the rate of annual irrigation of 1000 mm/yr. This difference in the water balance can be attributed to a few major reasons, firstly, the consumptive use of the irrigation water by the almond trees or transport of RZD through the clay layer downward to the regional aquifer. Estimates of evapotranspiration rates over the study area would be required to determine the proportion of the RZD that is recharging the regional aquifer system and at what rate. Secondly, the flow RZD through the clay layer is unknown which ultimately recharge the regional aquifer. The rate of flow of RZD through the underlying clay layer will be assessed by the ongoing research in the study area. Lastly, the estimated RZD rate (0.80 mm/yr) is extrapolated based on four months data from late April to early September where the irrigation is least which is directly likely to result in the lower RZD.

Based on the study findings, there are three key recommendations for the ongoing research project. Firstly, the water levels need to be monitored throughout a year to calculate the actual estimate of RZD. Secondly, the rate of transport of RZD through the clay layer needs to be

assessed. Lastly, it is essential to consider the evapotranspiration loss from the study area. All of these contribute to calculating the water balance of the study area.

From a broader perspective, this research study contributes to estimating the salinity impact from irrigated agriculture in the Murray Basin, which is not known exactly in the present context. Moreover, the quantification of irrigation drainage at the root zone can contribute to water management plans for farmers to help them improve irrigation and drainage efficiency.

7 REFERENCES

Allison, GB, Cook, PG, Barnett, SR, Walker, GR, Jolly, ID & Hughes, MW 1990, 'Land clearance and river salinisation in the western Murray Basin, Australia', *Journal of Hydrology*, vol. 119, no. 1-4, pp. 1-20.

Allison, GB, Gee, G & Tyler, S 1994, 'Vadose-zone techniques for estimating groundwater recharge in arid and semiarid regions', *Soil Science Society of America Journal*, vol. 58, no. 1, pp. 6-14.

Allison, GB & Hughes, MW 1983, 'The use of natural tracers as indicators of soil-water movement in a temperate semi-arid region', *Journal of Hydrology*, vol. 60, no. 1, pp. 157-73.

Athavale, R & Rangarajan, R 1988, 'Natural recharge measurements in the hard rock regions of semi-arid India using tritium injection—A review', in *Estimation of Natural Groundwater Recharge*, Springer, pp. 175-94.

Barnett, S 1990, 'Effect of land clearance in the mallee region on river Murray salinity and land salinisation', *BMR Journal of Australian Geology & Geophysics BJAGDT*, vol. 11, no. 2, pp. 205-8.

Barrett, B, Heinson, G, Hatch, M & Telfer, A 2002, 'Geophysical methods in saline groundwater studies: locating perched water tables and fresh-water lenses', *Exploration Geophysics*, vol. 33, no. 2, pp. 115-21.

Beff, L, Günther, T, Vandoorne, B, Couvreur, V & Javaux, M 2012, 'Three-dimensional monitoring of soil water content in a maize field using electrical resistivity tomography', *Hydrology and Earth System Sciences Discussions*, vol. 9, no. 7, pp. 8535-78.

Bowler, J 1980, 'Quaternary chronology and palaeohydrology in the evolution of Mallee landscapes', *Aeolian Landscapes in the Semi-arid Zone of southeastern Australia*, pp. 35-45.

Brindt, N, Rahav, M & Wallach, R 2019, *ERT and salinity – A method to determine whether ERT-detected preferential pathways in brackish water-irrigated soils are water-induced or an artifact of salinity (Book review)*, 00221694.

Brown, CM & Stephenson, AE 1991, *Geology of the Murray Basin, southeastern Australia*, vol. 235, Australian Govt. Pub. Service.

Cartwright, I, CendóN, D, Currell, M & Meredith, K 2017, 'A review of radioactive isotopes and other residence time tracers in understanding groundwater recharge: Possibilities, challenges, and limitations', *Journal of Hydrology*, vol. 555, pp. 797-811.

Cook, P, Jolly, I, Walker, G & Robinson, N 2003, 'From drainage to recharge to discharge: some timelags in subsurface hydrology', in AS Abdulrahman & W W.W. (eds), *Developments in Water Science*, Elsevier, vol. 50, pp. 319-26.

Cook, P, Kennett-Smith, A, Walker, G, Budd, G, Williams, R & Anderson, R 1996, 'Impact of dryland agriculture on land and river salinisation in the western lands, New South Wales'.

Crabb, P & Milligan, A 1997, *Murray-Darling basin resources*, Murray-Darling Basin Commission.

Crosbie, R, Jolly, I, Leaney, F & Petheram, C 2010, 'Can the dataset of field based recharge estimates in Australia be used to predict recharge in data-poor areas?', *Hydrology and Earth System Sciences*, vol. 14, no. 10, p. 2023.

Crosbie, RS, Peeters, LJM, Herron, N, McVicar, TR & Herr, A 2018, 'Estimating groundwater recharge and its associated uncertainty: Use of regression kriging and the chloride mass balance method', *Journal of Hydrology*, vol. 561, pp. 1063-80.

De Vries, J, Selaolo, E & Beekman, H 2000, 'Groundwater recharge in the Kalahari, with reference to paleo-hydrologic conditions', *Journal of Hydrology*, vol. 238, no. 1-2, pp. 110-23.

Dick, J, Tetzlaff, D, Bradford, J & Soulsby, C 2018, 'Using repeat electrical resistivity surveys to assess heterogeneity in soil moisture dynamics under contrasting vegetation types', *Journal of Hydrology*, vol. 559, pp. 684-97.

Environment Protection Authority 2000, *Groundwater Sampling Guidelines*, State Government of Victoria.

Evans, W & Kellett, J 1989, 'The hydrogeology of the Murray Basin, southeastern Australia', *BMR Journal of Australian Geology and Geophysics*, vol. 11, pp. 147-66.

FAO 1990, *Water and sustainable agricultural development: an international action plan. A strategy for the implementation of the Mar del Plata Action Plan for the 1990s.* , Food and Agricultural Organization of the United Nations, Rome.

Firman, J 1965, 'Late Cainozoic lacustrine deposits in the Murray Basin, South Australia', *Quarterly Geological Notes of the Geological Survey of South Australia*, vol. 16, pp. 1-2.

—— 1973, *Regional stratigraphy of surficial deposits in the Murray Basin and Gambier Embayment*, AB James, Government Printer.

Ghassemi, F 1995, 'Salinisation of land and water resources: human causes, extent, management and case studies', *Salinisation of land and water resources*.

Han, D, Currell, MJ, Cao, G & Hall, B 2017, 'Alterations to groundwater recharge due to anthropogenic landscape change', *Journal of Hydrology*, vol. 554, pp. 545-57.

Healy, RW 2010, *Estimating Groundwater Recharge*, Cambridge University Press.

Healy, RW & Cook, PG 2002, 'Using groundwater levels to estimate recharge', *Hydrogeology Journal*, vol. 10, no. 1, pp. 91-109.

Heaney, A, Beare, S & Bell, R 2001, 'Evaluating improvements in irrigation efficiency as a salinity mitigation option in the South Australian Riverland', *Australian Journal of Agricultural and Resource Economics*, vol. 45, no. 3, pp. 477-93.

Hillman, RM 1981, 'Land and stream salinity in Western Australia', *Agricultural Water Management*, vol. 4, no. 1, pp. 11-8.

Hoban, M & Daamen, C 2007, *Boundary Bend East Almond Development- Hydrogeological Investigation of proposed Irrigation Developemnt*, Sinclair Knight Merz Pty Ltd., Victoria, Australia.

Jacobsen, T & Adams, RM 1958, 'Salt and silt in ancient Mesopotamian agriculture', *Science*, vol. 128, no. 3334, pp. 1251-8.

Jazaei, F, Simpson, MJ & Clement, TP 2014, 'An analytical framework for quantifying aquifer response time scales associated with transient boundary conditions', *Journal of Hydrology*, vol. 519, no. PB, pp. 1642-8.

Jenkin, JJ 1981, 'Terrain, groundwater and secondary salinity in Victoria, Australia', *Agricultural Water Management*, vol. 4, no. 1, pp. 143-71.

Jolly, ID, Cook, PG, Allison, GB & Hughes, MW 1989, 'Simultaneous water and solute movement through an unsaturated soil following an increase in recharge', *Journal of Hydrology*, vol. 111, no. 1, pp. 391-6.

Knight, R, Smith, R, Asch, T, Abraham, J, Cannia, J, Viezzoli, A & Fogg, G 2018, 'Mapping Aquifer Systems with Airborne Electromagnetics in the Central Valley of California', *Groundwater*, vol. 56, no. 6, pp. 893-908.

Lapham, WW 1989, *Use of temperature profiles beneath streams to determine rates of vertical ground-water flow and vertical hydraulic conductivity*, Dept. of the Interior, US Geological Survey; USGPO; Books and Open-File ….

Lawrence, CR 1975, *Geology, hydrodynamics and hydrochemistry of the southern Murray Basin*, Geol. Surv. Vict. Mem., 30, 359 pp.

Loke, M 2000, 'Electrical imaging surveys for environmental and engineering studies: A practical guide to 2-D and 3-D surveys', *Electronic version available from http://www. terra plus. com*.

McNeill, J 1980, *Electrical conductivity of soils and rocks*, Geonics Limited, Ontario, Canada.

MDBMC 1999, *The salinity audit of the Murray–Darling Basin: A 100 year perspective,1999*, Muaary-Darling Basin Commission, Canberra, ACT.

Morton, R & Cunningham, RB 1985, 'Longitudinal profile of trends in salinity in the river murray', *Australian Journal of Soil Research*, vol. 23, no. 1, pp. 1-13.

Nativ, R, Adar, E, Dahan, O & Geyh, M 1995, 'Water recharge and solute transport through the vadose zone of fractured chalk under desert conditions', *Water Resources Research*, vol. 31, no. 2, pp. 253-61.

Newman, B, Curry, D, Evans, R & Adams, T 2009, *Irrigated agriculture in the mallee: estimating root zone drainage*, Murray Darling Basin Authority, Canberra.

Newman, B & Goss, K 2000, 'The Murray-Darling Basin Salinity Management Strategy-Implications for the Irrigation Sector', in *Annual ANCID Conference, Toowoomba, Australia*.

Peck, AJ, Thomas, JF & Williamson, D 1983, 'Salinity issues: effects of man on salinity in Australia'.

Post, VEA & Von Asmuth, JR 2013, 'Review: Hydraulic head measurements - New technologies, classic pitfalls', *Hydrogeology Journal*, vol. 21, no. 4, pp. 737-50.

Reeve, RC & Fireman, M 1967, 'Salt problems in relation to irrigation', *Irrigation of agricultural lands*, no. irrigationofagr, pp. 988-1008.

Revil, A, Karaoulis, M, Johnson, T & Kemna, A 2012, 'Some low-frequency electrical methods for subsurface characterization and monitoring in hydrogeology', *Hydrogeology Journal*, vol. 20, no. 4, pp. 617-58.

Saintilan, N & Overton, I 2010, *Ecosystem response modelling in the Murray-Darling Basin*, Csiro Publishing.

Scanlon, B, Healy, R & Cook, P 2002, 'Choosing appropriate techniques for quantifying groundwater recharge', *Hydrogeology Journal*, vol. 10, no. 2, pp. 347-.

Scanlon, B, Keese, K, Flint, A, Flint, L, Gaye, C, Edmunds, WM & Simmers, I 2006, 'Global synthesis of groundwater recharge in semiarid and arid regions', *Hydrological Processes*, vol. 20, no. 15, pp. 3335-70.

Schlosser, K 2017, *Monitoring Infiltration From Natural Storms Using Time-Lapse Electrical Resistivity Tomography*, ProQuest Dissertations Publishing.

Sluggett, T, Waechter, S, Tandy, M & Burgemeister, K 2007, *Soil Survey- Irrigation and Drainage Management Plan*, AgriExchange Pty Ltd, Chowilla Street, Renmark , South Australia.

Stephenson, A 1986, 'Lake Bungunnia -- a Plio-Pleistocene megalake in southern Australia', *Palaeogeography, Palaeoclimatology, Palaeoecology*, vol. 57, no. 2-4, pp. 137-56.

Thorne, R 1990, 'Nyah to the South Australian border hydrogeological project'.

Vereecken, H, Huisman, J, Pachepsky, Y, Montzka, C, Van Der Kruk, J, Bogena, H, Weihermüller, L, Herbst, M, Martinez, G & Vanderborght, J 2014, 'On the spatio-temporal dynamics of soil moisture at the field scale', *Journal of Hydrology*, vol. 516, pp. 76-96.

Watkins, N & Waclawik, V 1996, 'River Murray water resource management assessment of salt load impacts and drainage hazard for new irrigation development along the River Murray in South Australia', *RD*, vol. 96, p. 17.

Williams, WD 2001, 'Anthropogenic salinisation of inland waters', in JM Melack, R Jellison & DB Herbst (eds), *Saline Lakes: Publications from the 7th International Conference on Salt Lakes, held in Death Valley National Park, California, U.S.A., September 1999*, Springer Netherlands, Dordrecht, pp. 329-37.

8 APPENDICES

Appendix 1: Lithological logs of the Piezometers in the Alma Almonds' Property

Bore_location	Bore	FROM (m)	TO (m)	Thickness	Elevation, mAHD	Strata Description		Screening Depth		DTW from ground, m	Easting	Northing	Elev
								From (m)	To (m)				
East Deep	**P4**	0	6	6	48.671	Grey Brown Medium Heavy Clay	48.671			5.45	687870.973	6157370.745	54.671
		6	9	3	45.671	Brown Fine Sandy Clay	45.671						
		9	12.5	3.5	42.171	Brown Med Fine Sand	42.171	9.5	12.5				
North Shallow	**P3s**	0	1	1	55.783	Brown Fine Sand	55.783						
		1	2	1	54.783	Red Brown Fine Sandy Clay	54.783	1.5	2.5	DRY	687082.768	6157478.404	56.783
		2	2.5	0.5	54.283	Grey Brown Med Heavy Clay	54.283						
North Deep	P3d	0	1	1	55.632	Brown Fine Sand	55.632						
		1	2	1	54.632	Red Brown Fine Sandy Clay	54.632						
		2	7.5	5.5	49.132	Grey Brown Med Heavy Clay	49.132						
		7.5	9.5	2	47.132	White Brown Silty Clay	47.132	8.5	11.5	7	687082.360	6157480.056	56.632
		9.5	11.5	2	45.132	Brown Fine Sand	45.132						
Shallow Middle	P2s	0	1	1	56.952	Brown Fine Sand	56.952						
		1	4	3	53.952	Red Brown Fine Clayey Sand	53.952						
		4	5	1	52.952	Grey Brown Med Heavy Clay	52.952	4	5	4.6	687067.791	6156846.379	57.952
Deep Middle	P2d	0	1	1	56.570	Brown Fine Sand	56.570						
		1	4	3	53.570	Red Brown Fine Clayey Sand	53.570						
		4	5.5	1.5	52.070	Brown Fine Sandy Clay	52.070						
		5.5	7.5	2	50.070	Grey + Brown Med Heavy clay	50.070						
		7.5	12	4.5	45.570	Brown Fine Sandy Clay	45.570			9			

		12	20	8	37.570	Brown Clayey Fine Sand	37.570						
		20	22	2	35.570	Grey Silty Clay	35.570	20	22		687067.480	6156847.608	57.570
Deep South	P1d	0	1	1	56.515	Brown Fine sand	56.515						
		1	5	4	52.515	Red Brown Fine Clayey Sand	52.515						
		5	6	1	51.515	Brown Sandy Clay with Limestone	51.515						
		6	9	3	48.515	Brown Fine Sandy Clay	48.515						
		9	13	4	44.515	Brown Fine Clayey Sand	44.515	10	13	10.6	687067.703	6156257.396	57.515
Shallow South	P1s	0	1	1	56.651	Brown Fine Sand	56.651						
		1	5	4	52.651	Red Brown Fine Clayey Sand	52.651	3.5	5.5	DRY	687067.674	6156255.717	57.651
		5	5.5	0.5	52.151	Brown Sandy Clay with Limestone	52.151						

Appendix 2: GPS position as measured by RTX Survey

Bore ID	Easting	Northing	Elevation(mAHD)	Latitude	Longitude	Feature Code
P1d	687067.703	6156257.396	57.515	-34.7187	143.0429	Piezometer
P1s	687067.674	6156255.717	57.651	-34.7187	143.0429	Piezometer
P2d	687067.480	6156847.608	57.570	-34.7133	143.0428	Piezometer
P2s	687067.791	6156846.379	57.952	-34.7133	143.0428	Piezometer
P3d	687082.360	6157480.056	56.632	-34.7076	143.0428	Piezometer
P3s	687082.768	6157478.404	56.783	-34.7076	143.0428	Piezometer
P4	687870.973	6157370.745	54.671	-34.7085	143.0514	Piezometer
6962	685715.892	6155884.216	53.697	-34.7223	143.0282	State Bore
6966	685777.450	6157255.700	54.421	-34.7099	143.0286	State Bore
26002	685811.307	6158969.332	54.831	-34.6944	143.0286	State Bore
26688	685777.710	6157254.751	54.432	-34.7099	143.0286	State Bore
DP 1	686633.149	6156722.333	54.539	-34.7145	143.0381	Drainage Pit
DP 2	686843.142	6156769.372	55.122	-34.7141	143.0403	Drainage Pit
DP 3	687314.779	6156681.745	55.824	-34.7148	143.0455	Drainage Pit
DP 4	687068.214	6157052.526	54.929	-34.7115	143.0427	Drainage Pit
DP 5	686908.204	6157020.455	54.974	-34.7118	143.041	Drainage Pit
DP 6	687445.247	6157103.525	55.665	-34.711	143.0468	Drainage Pit
DP 7	688009.674	6156762.291	54.360	-34.7139	143.0531	Drainage Pit
DP 8	687945.537	6156478.757	56.425	-34.7165	143.0524	Drainage Pit
DP 9	688372.528	6156373.302	53.790	-34.7174	143.0571	Drainage Pit
DP 10	686104.158	6156763.206	54.466	-34.7143	143.0323	Drainage Pit
DP 11	685980.771	6156701.223	53.994	-34.7148	143.0309	Drainage Pit
DP NP	688068.736	6157126.690	55.069	-34.7106	143.0536	Drainage Pit
Outlet	686383.572	6156490.120	52.919	-34.7167	143.0354	Outlet

TW 1	686024.225	6156708.347	54.010	-34.7148	143.0314	Test Well
TW 2	686168.931	6156159.335	55.326	-34.7197	143.0331	Test Well
TW 3	688416.457	6156688.886	54.768	-34.7145	143.0575	Test Well
TW 4	686995.311	6156786.984	55.747	-34.7139	143.042	Test Well
TW 5	686850.258	6156158.970	59.323	-34.7196	143.0406	Test Well
TW 6	687299.800	6156307.580	56.141	-34.7182	143.0454	Test Well
TW 7	687408.530	6157084.029	55.591	-34.7111	143.0464	Test Well
TW 8	686473.198	6157284.427	55.955	-34.7095	143.0362	Test Well
1	687020.792	6157028.924	54.601	-34.7117	143.0422	ERT
2	687020.760	6157026.368	54.603	-34.7117	143.0422	ERT
3	687020.746	6157023.945	54.620	-34.7117	143.0422	ERT
4	687020.732	6157021.522	54.637	-34.7118	143.0422	ERT
5	687020.748	6157019.058	54.687	-34.7118	143.0422	ERT
6	687020.763	6157016.594	54.736	-34.7118	143.0422	ERT
7	687020.707	6157014.073	54.783	-34.7118	143.0422	ERT
8	687020.650	6157011.552	54.829	-34.7119	143.0422	ERT
9	687020.644	6157008.984	54.883	-34.7119	143.0422	ERT
10	687020.637	6157006.416	54.936	-34.7119	143.0422	ERT
11	687020.623	6157003.892	54.979	-34.7119	143.0422	ERT
12	687020.608	6157001.368	55.022	-34.712	143.0422	ERT
13	687020.602	6156998.906	55.074	-34.712	143.0422	ERT
14	687020.595	6156996.443	55.125	-34.712	143.0422	ERT
15	687020.514	6156994.139	55.135	-34.712	143.0422	ERT
16	687020.433	6156991.834	55.144	-34.712	143.0422	ERT
17	687020.380	6156989.265	55.143	-34.7121	143.0422	ERT
18	687020.326	6156986.695	55.142	-34.7121	143.0422	ERT
19	687020.421	6156984.379	55.164	-34.7121	143.0422	ERT
20	687020.515	6156982.062	55.186	-34.7121	143.0422	ERT

21	687020.528	6156979.451	55.306	-34.7121	143.0422	ERT
22	687020.540	6156976.839	55.425	-34.7122	143.0422	ERT
23	687020.534	6156974.374	55.434	-34.7122	143.0422	ERT
24	687020.527	6156971.909	55.442	-34.7122	143.0422	ERT
25	687020.582	6156969.405	55.508	-34.7122	143.0422	ERT
26	687020.637	6156966.901	55.573	-34.7123	143.0422	ERT
27	687020.711	6156964.306	55.683	-34.7123	143.0422	ERT
28	687020.784	6156961.711	55.792	-34.7123	143.0422	ERT
29	687020.782	6156959.289	55.924	-34.7123	143.0422	ERT
30	687020.779	6156956.867	56.055	-34.7124	143.0422	ERT
31	687020.857	6156954.355	56.211	-34.7124	143.0422	ERT
32	687020.934	6156951.842	56.366	-34.7124	143.0422	ERT
33	687020.900	6156949.284	56.399	-34.7124	143.0422	ERT
34	687020.865	6156946.726	56.432	-34.7124	143.0422	ERT
35	687020.878	6156944.193	56.560	-34.7125	143.0422	ERT
36	687020.890	6156941.659	56.687	-34.7125	143.0422	ERT
37	687020.890	6156939.181	56.889	-34.7125	143.0422	ERT
38	687020.890	6156936.703	57.090	-34.7125	143.0422	ERT
39	687020.906	6156934.222	57.245	-34.7126	143.0422	ERT
40	687020.922	6156931.740	57.399	-34.7126	143.0422	ERT
41	687020.880	6156929.359	57.460	-34.7126	143.0422	ERT
42	687020.838	6156926.978	57.521	-34.7126	143.0422	ERT
43	687020.810	6156924.408	57.721	-34.7126	143.0422	ERT
44	687020.782	6156921.838	57.921	-34.7127	143.0422	ERT
45	687020.799	6156919.317	58.090	-34.7127	143.0422	ERT
46	687020.816	6156916.795	58.258	-34.7127	143.0422	ERT

47	687020.830	6156914.296	58.521	-34.7127	143.0422	ERT
48	687020.843	6156911.797	58.783	-34.7128	143.0422	ERT
49	687020.819	6156909.443	58.894	-34.7128	143.0422	ERT
50	687020.795	6156907.088	59.005	-34.7128	143.0422	ERT
51	687020.770	6156904.539	59.117	-34.7128	143.0422	ERT
52	687020.744	6156901.989	59.229	-34.7129	143.0422	ERT
53	687020.719	6156899.576	59.402	-34.7129	143.0422	ERT
54	687020.694	6156897.163	59.574	-34.7129	143.0422	ERT
55	687020.722	6156894.492	59.684	-34.7129	143.0422	ERT
56	687020.749	6156891.821	59.794	-34.7129	143.0422	ERT
57	687020.741	6156889.478	59.853	-34.713	143.0422	ERT
58	687020.733	6156887.135	59.912	-34.713	143.0423	ERT
59	687020.746	6156884.610	59.895	-34.713	143.0423	ERT
60	687020.758	6156882.084	59.877	-34.713	143.0423	ERT
61	687020.757	6156879.632	59.844	-34.713	143.0423	ERT
62	687020.755	6156877.180	59.810	-34.7131	143.0423	ERT
63	687020.791	6156874.706	59.691	-34.7131	143.0423	ERT
64	687020.827	6156872.232	59.572	-34.7131	143.0423	ERT
65	687020.843	6156869.719	59.447	-34.7131	143.0423	ERT
66	687020.858	6156867.206	59.321	-34.7132	143.0423	ERT
67	687020.862	6156864.761	59.114	-34.7132	143.0423	ERT
68	687020.866	6156862.315	58.906	-34.7132	143.0423	ERT
69	687020.833	6156859.825	58.681	-34.7132	143.0423	ERT
70	687020.799	6156857.334	58.455	-34.7133	143.0423	ERT
71	687020.738	6156854.805	58.303	-34.7133	143.0423	ERT
72	687020.677	6156852.276	58.151	-34.7133	143.0423	ERT
73	687020.704	6156849.814	57.934	-34.7133	143.0423	ERT
74	687020.730	6156847.351	57.716	-34.7133	143.0423	ERT

75	687020.701	6156844.755	57.513	-34.7134	143.0423	ERT
76	687020.671	6156842.158	57.310	-34.7134	143.0423	ERT
77	687020.735	6156839.786	57.127	-34.7134	143.0423	ERT
78	687020.798	6156837.413	56.944	-34.7134	143.0423	ERT
79	687020.843	6156834.741	56.747	-34.7135	143.0423	ERT
80	687020.887	6156832.069	56.549	-34.7135	143.0423	ERT
81	687020.805	6156829.600	56.465	-34.7135	143.0423	ERT
82	687020.722	6156827.131	56.381	-34.7135	143.0423	ERT
83	687020.711	6156824.760	56.217	-34.7135	143.0423	ERT
84	687020.699	6156822.388	56.052	-34.7136	143.0423	ERT
85	687020.699	6156819.928	56.002	-34.7136	143.0423	ERT
86	687020.699	6156817.468	55.951	-34.7136	143.0423	ERT
87	687020.690	6156814.918	55.911	-34.7136	143.0423	ERT
88	687020.680	6156812.368	55.871	-34.7137	143.0423	ERT
89	687020.654	6156809.899	55.804	-34.7137	143.0423	ERT
90	687020.627	6156807.430	55.736	-34.7137	143.0423	ERT
91	687020.584	6156804.828	55.646	-34.7137	143.0423	ERT
92	687020.541	6156802.226	55.555	-34.7137	143.0423	ERT
93	687020.527	6156799.657	55.555	-34.7138	143.0423	ERT
94	687020.513	6156797.088	55.555	-34.7138	143.0423	ERT
95	687020.486	6156794.698	55.560	-34.7138	143.0423	ERT
96	687020.458	6156792.307	55.564	-34.7138	143.0423	ERT